Experimental study on the spatial coherence and polarization of random optical fields

Juan Zhao

Submitted for the degree of Doctor of Philosophy

Heriot-Watt University

Institute of Photonics and Quantum Sciences

School of Engineering and Physical Sciences

October 2014

ABSTRACT

All optical fields are inherently of statistical nature undergoing random fluctuations. The underlying theory of fluctuating optical fields is known as coherence theory and partial polarization. This thesis describes the experimental study on the coherence and polarization measurements for statistical optical fields. Particular emphasis is placed on the full field visualization for coherence function and coherence matrix, and its application to the study of changes in random optical fields on propagation.

The thesis consists of 9 chapters including Chapter 1 devoted to introduction. Chapter 2 proposes a novel optical geometry for the full-field coherence visualization to study the coherence diffraction. The non-diffracting solutions for the coherence function and the coherence interference phenomena have been presented in Chapter 3 and Chapter 4, respectively. As the application, Chapter 5 presents the experimental demonstration of the coherence holography to synthesize the arbitrary spatial coherence function. To take the vector nature, Chapter 6 and Chapter 7 develop our optical geometry for the full-field visualization of coherence polarization matrix to study of the stochastic electromagnetic fields on propagation. The principle of coherence tensor holography is proposed in Chapter 8 and experimentally demonstrated for the first time. At last, conclusions and future works have been given.

ACKNOWLEDGEMENTS

I would like to express my sincere gratitude to my supervisor Dr. Wei Wang for his advice, guidance and encouragement over the last five years. I really cannot find words to acknowledge the support he offered when most needed. I am fortunate to have him as my advisor.

I am very grateful to my internal examiner Dr. Xianwen Kong and external examiner Dr. Michael Linde Jakobsen for their invaluable suggestions.

I wish also to thank Prof. Dayong Wang from Beijing University of Technology who inspired me and introduced me to this interesting field.

I would like to show my gratitude to all my colleagues at the optical diagnostics group who were present during this time. I won't forget those useful discussions which made this work a lot easier. I would also like to thank all of the technicians in the mechanical engineering workshop for their help in making my experimental hardware and for their assistance.

Finally, I want to thank my family for all their love and support. Without their support and faith in me, I would not be the woman I am today. I love you all.

DEDICATION

To my father Mr. Ximin Zhao, my mother Mrs. Zhimian Zheng, and my brother Mr. Hui Zhao, thanks for always believing in me and encouraging me to do my best. Thank you for supporting me in all of my endeavours.

To my dear husband for his care, love, understanding, and patience during the busy times of my PhD. Thank you for always being there for me.

ACADEMIC REGISTRY
Research Thesis Submission

Name*:*	JUAN ZHAO		
School/PGI:	EPS / IPAQS		
Version: *(i.e. First, Resubmission, Final)*	FINAL	Degree Sought (Award **and** Subject area)	PhD Physics

Declaration

In accordance with the appropriate regulations I hereby submit my thesis and I declare that:

1) the thesis embodies the results of my own work and has been composed by myself
2) where appropriate, I have made acknowledgement of the work of others and have made reference to work carried out in collaboration with other persons
3) the thesis is the correct version of the thesis for submission and is the same version as any electronic versions submitted*.
4) my thesis for the award referred to, deposited in the Heriot-Watt University Library, should be made available for loan or photocopying and be available via the Institutional Repository, subject to such conditions as the Librarian may require
5) I understand that as a student of the University I am required to abide by the Regulations of the University and to conform to its discipline.

* *Please note that it is the responsibility of the candidate to ensure that the correct version of the thesis is submitted.*

Signature of Candidate*:*		Date:	

Submission

Submitted By *(name in capitals):*	
Signature of Individual Submitting:	
Date Submitted:	

For Completion in the Student Service Centre (SSC)

Received in the SSC by *(name in capitals):*			
Method of Submission *(Handed in to SSC; posted through internal/external mail):*			
E-thesis Submitted *(mandatory for final theses)*			
Signature:		Date:	

LIST OF PUBLICATIONS

Journal papers:

[1] **Juan Zhao** and Wei Wang, "Experimental study of spatial coherence diffraction based on full-field coherence visualization," J. Opt. Soc. Am. A, 31, 2217-2222(2014).……related to Chapter 2.

[2] **Juan Zhao**, Mitsuo Takeda and Wei Wang, "Generation of the coherence non-diffracting beam," (ready for submission)...…….....related to Chapter 3.

[3] **Juan Zhao** and Wei Wang, "Interference of the spatial coherence functions," (ready for submission).……...related to Chapter 4.

[4] **Juan Zhao** and Wei Wang, "Stokes parameters reconstruction for incoherent polarization sources by the vectorial van Cittert-Zernike theorem," (ready for submission)...…….....related to Chapter 6.

[5] **Juan Zhao** and Wei Wang, "Experimental study on the spatial evolution of the beam coherence-polarization matrix and the generalized Stokes parameters for random electromagnetic fields," (ready for submission).....related to Chapter 7.

[6] **Juan Zhao** and Wei Wang, "Polarization sensitivity 3-D coherence holography," (ready for submission).....…..related to Chapter 8.

Conference papers:

[1] Wei Wang, **Juan Zhao** and Mitsuo Takeda, "Recent progress in statistical information optics: Statistical information processing for optics," Proc. Of SPIE 9066, 906603 (2013)...…….....related to Chapter 2, 6 and 7.

[2] **Juan Zhao**, Mitsuo Takeda and Wei Wang, "A comparison of diffracting and non-diffracting coherence functions based on full-field spatial coherence visualization system," Proc. Of SPIE: The International Conference on Photonics and Optical Engineering and the Annual West China Photonics Conference 2014 (accepted)……...…related to Chapter 2 and 3.

[3] **Juan Zhao**, Chunyang Wang and Wei Wang, "Synthesis of spatial coherence function based on coherence holography," Proc. Of SPIE: The International Conference on Photonics and Optical Engineering and the Annual West China Photonics Conference 2014 (accepted)…….…..related to Chapter 5.

[4] **Juan Zhao**, Ailing Tian and Wei Wang, "Experimental demonstration of the van Cittert-Zernike theorem for random electromagnetic fields," Proc. Of SPIE: The International Conference on Photonics and Optical Engineering and the Annual West China Photonics Conference 2014 (accepted).related to Chapter 6.

CONTENTS

LIST OF FIGURES

ABBREVIATIONS

AP	aperture
BCPM	beam coherence-polarization matrix
BS	non-polarizing beam splitter
CCD	charge-coupled device
CH	coherence holography
CGH	computer generated hologram
CTH	coherence tensorholography
DF	density filter
FT	Fourier transform
FWHM	full width at half maximum
GG	ground glass
OCT	optical coherence tomography
OPD	optical path difference
PBS	polarizing beamsplitter
S	source
SOPD	synthetic optical path difference
SFS	spatial filter system
SLM	spatial light modulator
V-CH	vectorial coherence holography

NOMENCLATURE

a	radius
$\tilde{E}_{x,y}$	orthogonal components of the electric field
f	focal length
H	amplitude transmittance of the hologram
I	intensity distribution
J_0	first kind, 0^{th} order Bessel function
J_1	first kind, first order Bessel function
$\begin{bmatrix} J_{xx} & \tilde{J}_{xy} \\ \tilde{J}_{yx} & J_{yy} \end{bmatrix}$	Jones matrix
$M_{A,B}$	focal length ratio
$P(x,y,z)$	degree of polarization
S_0 , S_1, S_2, S_3	generalized Stokes parameters
$\tilde{U}$	complex amplitude
$\tilde{W}$	mutual intensity matrix, beam coherence-polarization matrix
Δz	optical path difference
Z	synthetic optical path difference
$\tilde{\Gamma}$	spatial coherence function
ρ	polar coordinate $0 \le \rho \le 1$
$\tilde{\mu}$	degree of coherence

Chapter 1

Introduction

1.1 Background and objectives

The coherence properties of light play an important role in determining the optical field. The basic wave propagation law for mutual coherence discovery by Wolf has laid a foundation to treat many important problems in statistical optics [1,2]. Since the coherence function obeys a pair of wave equations it can be envisaged that the wave phenomena appear in optical coherence function. One of the most important studies in the propagation of spatial coherence is the van Cittert-Zernike theorem which shows that even completely incoherent source can generate a partially coherent optical field in the process of its propagation. And the relationship between the spatial coherence function (mutual intensity) and the intensity distribution over the spatial incoherent light source is formed by Fourier transform integral. The van Cittert-Zernike theorem has prepared the ground for determination of the source far away from the observer [3,4]. It has succeeded in astronomy, and has great potentialities in fluoremetry, scattering measurement, etc.

It is well known that the real part of the coherence function is related to the fringe pattern observed in Young's double-slit experiment. However, this discrete measurement is time consuming and sometimes can be difficult to evaluate. In the absence of rapid and inexpensive measuring instruments, a lot of researches of spatial

coherence still remain in the theoretical simulation. As for the all-sided and particular investigation, direct intensity measurements are needed. In this thesis, we offer a direct route to mutual intensity function in which the full-field distribution of the space-shift-variant two-point correlation function can be obtained from a modified radial shearing interferometer. By using the spatial coherence visualization system we proposed, the mutual intensity function can be recorded in one go. It makes it possible for a continuous fast measurement, which offered us a chance to demonstrate the spatial coherence in laboratory.

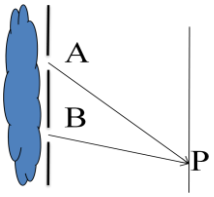

Figure 1-1 Young's two-point interference experiment.

There is another important property of light that is polarization. In the history of optics, the theory of coherence and the theory of polarization were regarded as two independent branches in optics. Coherence arises from correlation between fluctuations at two different space time points. Polarization, on the other hand, is a manifestation of fluctuating components of the electric field at a single point. For many years the subjects of coherence and polarization have been developed independently. When we discuss the coherence properties of the field, some simplified models have been used by treating the optical field as scalar fields by ignoring their polarization properties arising from the vector nature of the electromagnetic field. However all optical fields undergo random fluctuations. It affects all classical wave fields without exception even coherence function. Recently a unified theory of coherence and polarization of random electromagnetic beams has been introduced by Wolf [5]. The unified theory provides an elegant description about the changes in the state of polarization of a partially coherent electromagnetic beam on propagation. The coherence and polarization properties of random fields can be fully described by a 2×2 cross-spectral density matrix (for quasi-monochromatic field, the cross-spectral density matrix reduce to a mutual intensity matrix or a beam

coherence polarization matrix) and 4 generalized Stokes parameters [6,7]. However, in the absence of rapid and inexpensive measuring instruments, a lot of researches of unified theory of coherence and polarization still remain in the theoretical simulation. In this thesis, we would like to experimentally demonstrate the unified theory of coherence and polarization of random electromagnetic beams by an optical experiment, which may be regarded as a tensor version of van Cittert-Zernike theorem.

Finally, we introduce a new technique of unconventional holography, called coherence holography [8]. As a theoretical application, coherence plays fundamental role in holography and interferometry, and control of coherence is essential in an illumination system for microscopy and lithography. In this thesis, we introduce the synthesis and analysis of a spatial coherence function based on coherence holography.

1.2 Thesis structure

This thesis is organised as follows.

In chapter 1, we give a briefly introduce of background of this field, and the motivation of the thesis.

In chapter 2, we present a novel interferometer for full-field spatial coherence visualization, and experimentally investigate the diffraction phenomena in the spatial coherence function. Coherence Airy pattern stemming from spatial coherence is been observed for the first time.

In chapter 3, we demonstrate a non-diffracting solution for the optical coherence function that is propagation-invariant. The full-field distribution of the non-diffracting coherence function has been studied theoretically and experimentally.

In chapter 4, we introduce the interference between spatial coherence functions and present some classic phenomena about interference in the format of coherence

function, such as: variation of intensity distribution, lack of class, principal maxima and secondary maxima in multi-aperture system, etc.

In chapter 5, we experimentally demonstrate three kinds of spatial coherence functions by using coherence holography, and study its propagation properties.

So far, we have studied the fluctuations characteristics of the coherence function in the scalar field. Next, we want to study the coherence functions in the vector field.

In chapter 6, we propose an optical system for measuring the mutual intensity matrix. And re-examine the van Cittert-Zernike theorem for electromagnetic field.

In chapter 7, we demonstrate an interferometric technique for characterizing the mutual intensity function of partially polarized, partially coherent optical beams. The beam coherence-polarization matrix and the generalized stokes parameters of random electromagnetic fields are determined experimentally.

In Chapter 8, we extend the scalar coherence holography to vectorial field, and introduce a tensor manner for coherence holography.

In Chapter 9, we make conclusions and discuss some future areas of work in the unified theory of coherence and polarization.

References

[1] J. W. Goodman, *Statistical Optics*, 1st edition (Wiley 2000).

[2] E. Wolf, *Introduction to the Theory of Coherence and Polarization of Light*, 1st edition (Cambridge University Press, 2007).

[3] P. H. van Cittert, “Die Wahrscheinliche Schwingungsverteilung in Einer von Einer Lichtquelle Direkt Oder Mittels Einer Linse Beleuchteten Ebene,” Physica 1, 201-210 (1934).

[4] F. Zernike, “The concept of degree of coherence and its application to optical problems,” Physica 5, 785-795 (1938).

[5] E. Wolf, “Unified theory of coherence and polarization of random electromagnetic beams,” Phys. Lett. A 312, 263-267 (2003).

[6] E. Wolf, “Polarization invariance in beam propagation,” Opt. Lett. 32, 3400-3401 (2007).

[7] F. Gori, M. Santarsiero, S. Vicalvi, R. Borghi and G. Guattari, “Beam coherence-polarization matrix,” J. Eur. Opt. Soc. A Pure Appl. Opt. 7, 941-951 (1998).

[8] M. Takeda, W. Wang, Z. Duan and Y. Miyamoto, "Coherence Holography," Opt. Express 23, 9629-9635 (2005).

Chapter 2

Diffraction of the Spatial Coherence Function

A novel optical geometry for the direct visualization of optical coherence function is proposed. The diffractions of partially coherent light by apertures with various forms are experimentally investigated and the full-field spatial coherence functions have been observed by using the proposed interferometric system. Similar to the well-known Airy disk stemming from optical diffraction, we studied the spatial coherence function near the coherence focal plan on the analogy of the Fraunhofer and Fresnel diffraction integrals. Following the conventional definitions for the optical resolutions in optical imaging system, the lateral and longitudinal resolutions for the spatial coherence imaging have been proposed.

2.1 Introduction

The statistical properties of light play an important role in determining the outcome of most optical experiments. It has long been recognized that correlations provide very convenient methods in describing the statistical properties of light [1-4]. In particular, the cross correlation between the fluctuating fields at different space time points, known as the coherence function, is a quantity of great interest. Dated back to 1930s, P. H. van Cittert and F. Zernike had proposed a Fourier transform relationship between the spatial coherence function and the intensity distribution over the spatial incoherent light source [5, 6]. More generally, the basic wave propagation law for

mutual coherence discovery by Wolf has laid a foundation to treat many important problems in statistical optics [4]. Recently, the concept of partial coherence theory has become increasingly important in optical research, and the propagation of partially coherent fields has been widely studied due to its theoretical importance and practical interest [7-13].

On the other hand, diffraction effect is a general characteristic of wave phenomena whenever a wave passes through an aperture or around an obstacle. Since the coherence function obeys a pair of wave equations, it can be envisaged that the diffraction phenomena also appears in the format of optical coherence function.

In this chapter, we investigated the full-field diffraction phenomena in spatial coherence function based on a novel interferometric system for spatial coherence visualization. Similar to the well-known Frauhofer diffraction pattern of a circular aperture, we observed an Airy disk-like pattern in the spatial coherence function, which serves as a direct experimental evidence for coherence diffraction. In formal analogy to the conventional definitions in optical system, the lateral and the longitudinal resolutions for coherence imaging have been first introduced from the experimental study of the detailed properties of the newly observed coherence focal spot.

2.2 A novel optical system for spatial coherence visualization

For the full-field coherence visualization, a schematic diagram of the proposed system is illustrated in Fig. 2-1. To generate a desired monochromatic spatially incoherent light source, a fast-spinning random phase mask (ground glass, GG) has been used to destroy the spatial coherence of the laser source. A radial sheering off-line interferometer is illuminated by this monochromatic, extended, spatially incoherent light source. The light emitted from the point source $P(x_o, y_o)$ is collimated by lens L_1 and is introduced into this interferometric system. The two telescope systems (L_2-L_3 and L_2-L_4) in two arms of the proposed interferometer share the same lens L_2, making the system compact. One beam (Arm A) reflected from

mirror M_1 is serving as a reference field. The other beam (Arm B) with different magnification reflected from a movable mirror M_2 is serving as a three-dimensionally displaced field. These two fields correlate with each other at the observation plane. Due to the fact that the lateral displacement is introduced by the radial shearing from the telescope systems with different magnifications and the longitudinal displacement is introduced by changing the optical path difference from the movable mirror, the interference fringes recorded by the CCD image sensor with pixel pitch of 5.2μm are the results of superposition of the two mutually displaced optical fields.

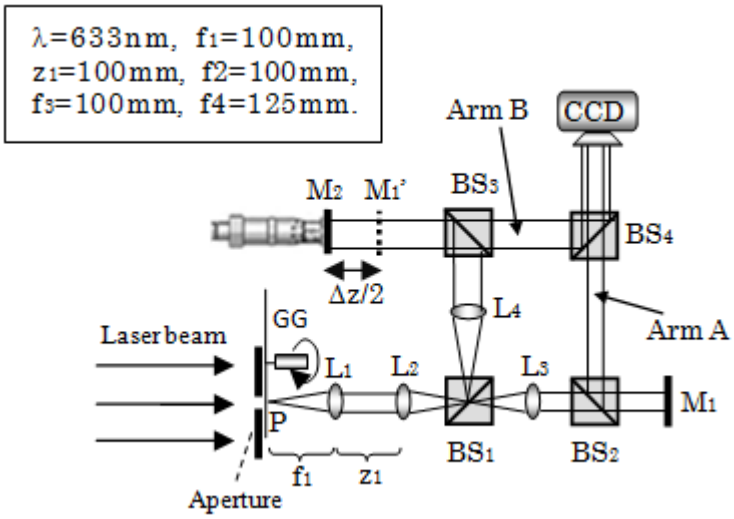

Figure 2-1 Schematic representation of the experimental setup for the full-field coherence visualization.

The distributions of the two optical fields from the two arms of the interferometric system can be calculated from Fresnel diffraction integrals. The point source $P(x_o, y_o)$ with its complex amplitude $\tilde{U}_o$ propagates through the arm A, and creates a field distribution $\tilde{U}_A$ on CCD plane,

$$\tilde{U}_A(x,y) = -\frac{\tilde{U}_o(x_o,y_o)}{j\lambda f_1 M_A}\exp[jk(z_1 + f_1 + f_2 + f_3 + z_2)]$$
$$\exp[\frac{j\pi}{\lambda f_1}(x_o^{\,2} + y_o^{\,2})(1 - \frac{z_1}{f_1} + \frac{f_2 + f_3}{M_A f_1} - \frac{z_2}{M_A^{\,2} f_1})]\exp[-\frac{2j\pi}{\lambda M_A f_1}(xx_o + yy_o)] \quad (2\text{-}1)$$

where z_1 is the optical path length from L_1 to L_2 plane, z_2 is the optical path length from L_3 to CCD plane and $M_A = f_3/f_2$ is the focal length ratio for the arm A. Similarly, the field distribution from the same point source propagating through the arm B is:

$$\begin{aligned}\tilde{U}_B(x,y) = -\frac{\tilde{U}_o(x_o,y_o)}{j\lambda f_1 M_B}\exp[jk(z_1 + f_1 + f_2 + z_2 + f_3 + \Delta z)] \\ \exp[\frac{j\pi}{\lambda f_1}(x_o{}^2 + y_o{}^2)(1 - \frac{z_1}{f_1} + \frac{f_2 + f_4}{M_B f_1} - \frac{z_2 + f_3 - f_4 + \Delta z}{M_B{}^2 f_1})] \\ \exp[-\frac{2j\pi}{\lambda M_B f_1}(xx_o + yy_o)],\end{aligned} \tag{2-2}$$

where Δz is an additional optical path difference introduced by the movable mirror M_2, and $M_B = f_4/f_2$ is the focal length ratio for the interferometric arm B.

The fields $\tilde{U}_A$ and $\tilde{U}_B$ from different arms of the interferometer are superimposed to form interference fringes on the CCD image sensor. Because each point source is completely incoherent to any other points on the source, the overall intensity on the image sensor is the sum of the fringe intensities obtained from all of the point sources. After some straightforward algebra, this intensity distribution becomes:

$$I = \iint_s \left|\tilde{U}_A + \tilde{U}_B\right|^2 dx_o dy_o = I_A + I_B + 2\,\mathrm{Re}\{\tilde{\Gamma}\}, \tag{2-3}$$

where $\mathrm{Re}\{\cdots\}$ denotes the real part, and I_A and I_B are the averaged light intensities through the interferometric arm A and arm B, respectively. The complex function $\tilde{\Gamma}$ in the last term of Eq. (2-3) will be recognized as the spatial coherence function,

$$\begin{aligned}\tilde{\Gamma}(x,y,Z) = \frac{\exp(jk\Delta z)}{\lambda^2 f_1{}^2 M_A M_B}\iint_S I_0(x_0,y_0)\exp[\frac{j\pi Z}{\lambda f_1{}^2}(x_0{}^2 + y_0{}^2)] \\ \exp[-\frac{2j\pi(M_A - M_B)}{\lambda f_1 M_A M_B}(xx_0 + yy_0)]dx_0 dy_0,\end{aligned} \tag{2-4}$$

with $Z(\Delta z)$ being the synthetic optical path difference (SOPD),

$$Z(\Delta z) = \frac{f_2(M_A - M_B)}{M_A M_B} - \frac{z_2 + f_3 - f_4 + \Delta z}{M_B{}^2} + \frac{z_2}{M_A{}^2}. \tag{2-5}$$

Equation (2-4) indicating the relation between the spatial coherence function $\tilde{\Gamma}$ and the source intensity distribution I_o can be understood as the particular example of the generalized van-Cittert Zernike theorem applied to our proposed optical system. Notice that the spatial coherence function in Eq. (2-4) is the Fourier transform of the product of the source intensity distribution and quadratic phase factor. This mathematical expression is similar to the well known Fresnel diffraction integral of the optical field used widely in Fourier optics [14] and can be regarded as the Fresnel diffraction of the spatial coherence function. Unlike previous work on the theoretical analysis for the diffraction of mutual coherence with $\Gamma(\Delta x, \Delta y, \Delta z)$ being six-dimensional function [7-11], the mutual coherence function in Eq. (2-4) is the three dimensional function in coordinate of (x, y, Z). It is the lateral sheering introduced by the two telescope systems with different magnifications and the longitudinal path delay introduced by the moving mirror that enables a simultaneous full-field visualization of the spatial coherence function. As shown in Section 4, the full-field coherence visualization by the proposed system has overcome the inherent limitation of the conventional coherence measurements by moving the two pinholes and introduced new opportunities to explore the optical coherence function in more details.

2.3 Detailed structures of the coherence difference patterns

Using the movable mirror, we are able to examine the spatial coherence evolution at different SOPD. In order to give a clear explanation for the full-field coherence diffraction, let's consider two special cases.

2.3.1 Lateral Coherence Function

Through an appropriate selection of the location for the movable mirror M_2, we are able to make the synthetic optical path difference $Z = 0$. The quadratic phase factors within the integrand in Eq. (2-4) disappear, leaving an exact Fourier transform relation:

$$\tilde{\Gamma}(x, y, 0) = \frac{\exp(jk\Delta z)}{\lambda^2 f_1^2 M_A M_B} \iint_S I_0(x_0, y_0) \exp[-\frac{2j\pi(M_A - M_B)}{\lambda f_1 M_A M_B}(xx_0 + yy_0)]dx_0 dy_0. \qquad (2\text{-}6)$$

The spatial coherence function in Eq. (2-6) expresses the well-known van Cittert-Zernike theorem, indicating the complex spatial coherence function proportional to the Fourier transform of the source intensity distribution. Similar to the conventional Fraunhofer Diffraction of the optical field [14], the plane with $Z = 0$ can be considered as the focal plane of the coherence diffraction, and the expression in Eq. (2-6) can be understood as the coherence Fraunhofer diffraction pattern.

Consider a circular monochromatic spatially incoherent light source with a uniform intensity, let the radius be a. For such a source, the coherence distribution at the coherence focal plane can be written as:

$$\tilde{\Gamma}(x, y, 0) = \frac{J_1[2\pi a(M_A - M_B)\sqrt{(x^2 + y^2)}/\lambda f_1 M_A M_B]}{2\pi a\lambda f(M_A - M_B)\sqrt{(x^2 + y^2)}}, \qquad (2\text{-}7)$$

where J_1 is a Bessel function of the first kind, first order. As expected for Frauhofer diffraction at a circular aperture, Eq. (2-7) provides the Airy formula of the spatial coherence function. From the locations of the zeroes of $J_1\{\cdots\}$, the central lobe of the coherence Fraunhofer diffraction pattern measured along the x or y axis, is given by:

$$D = 1.22\lambda f_1 M_A M_B / [a(M_A - M_B)]. \qquad (2\text{-}8)$$

2.3.2 Longitudinal Coherence Function

In what follows, we present another special case. If we put $x = y = 0$ in Eq. (2-4), the coherence function along the propagation axis is obtained:

$$\tilde{\Gamma}(0,0,Z) = \frac{\exp(jk\Delta z)}{\lambda^2 f_1^2 M_A M_B} \iint_S I_0(x_0, y_0) \exp[\frac{j\pi Z}{\lambda f_1^2}(x_0^2 + y_0^2)] dx_0 dy_0. \quad (2\text{-}9)$$

Therefore the proposed coherence visualization system could provide a very convenient approach for the experimental study of the longitudinal distribution of the spatial coherence function.

For the same circular source discussed above, the longitudinal coherence function along the optical axis reduces to:

$$\tilde{\Gamma}(0,0,Z) = \frac{2\pi \exp(jk\Delta z)}{\lambda^2 f_1^2 M_A M_B} \sin c(\frac{\pi a^2 Z}{2\lambda f_1^2}). \quad (2\text{-}10)$$

Note that the central interference fringes vanish first when:

$$Z = 2\lambda f_1^2 / a^2. \quad (2\text{-}11)$$

$\Delta l = 2Z$ is the width of main lobe (i.e. the distance between the first two zeros) along the optical axis.

2.4 Experiment

An experiment has been conducted to demonstrate the validity of the proposed system for study of the coherence diffraction. In our experiment, light from a He-Ne laser was first expanded and then collimated to illuminate a circular aperture. This circular pattern with a uniform intensity distribution was projected on a rapidly rotating ground glass to generate an extended, monochromatic, spatially incoherent

source. By moving the mirror M_2, we changed the optical path difference between the two interferometric arms and observed the coherence diffraction phenomena from the fringe visibility and fringe orientation.

2.4.1 Fresnel diffraction of spatial coherence function

Figure 2-2(a)-(c) provide the interferograms recorded at the different synthetic optical path difference. As shown in Fig. 2-2(a) for the desired coherence Fraunhofer diffraction, a set of concentric rings with a central spot of high fringe visibility and many peripheral lower fringe visibility rings are readily observed. By using Fourier fringes analysis [15], we can reconstruct the modulus distribution of the spatial coherence function as shown in Fig. 2-2(d). The resulting 3-D distribution for the coherence diffraction at the CCD plane in Fig. 2-2(g) has an identical structure to the Airy pattern in the format of the fringe contrast change.

By changing the optical path difference, we are able to observe the evolution for the coherence Fresnel diffraction. With the increase of SOPD, the curved carrier fringes have been observed due to the fact that the quadratic phase factor in Eq. (2-4) becomes more dominant. Fig. 2-2(b) shows the interferogram recorded at a typical location, $Z = 30mm$, where the central visibility of the fringes becomes zero. It should be noted that the disappearance of fringes contrast in central location of Fig. 2-2(b) is completely different from the results for the coherence vortex [16] since no phase singularity appears at the interferogram center. This phenomenon is similar to the well-known dark center of Fresnel diffraction patterns of optical field.

With the increase of SOPD, the central fringe visibility rises again as shown in Fig. 2-2(c) with its local fringe visibility lower than that shown in Fig. 2-2(a). All these demonstrated evolution for the coherence Fresnel diffraction can be easily observed from the 3-D view of the reconstructed amplitudes distribution for the spatial coherence function as shown in Fig. 2-2 (g)-(i).

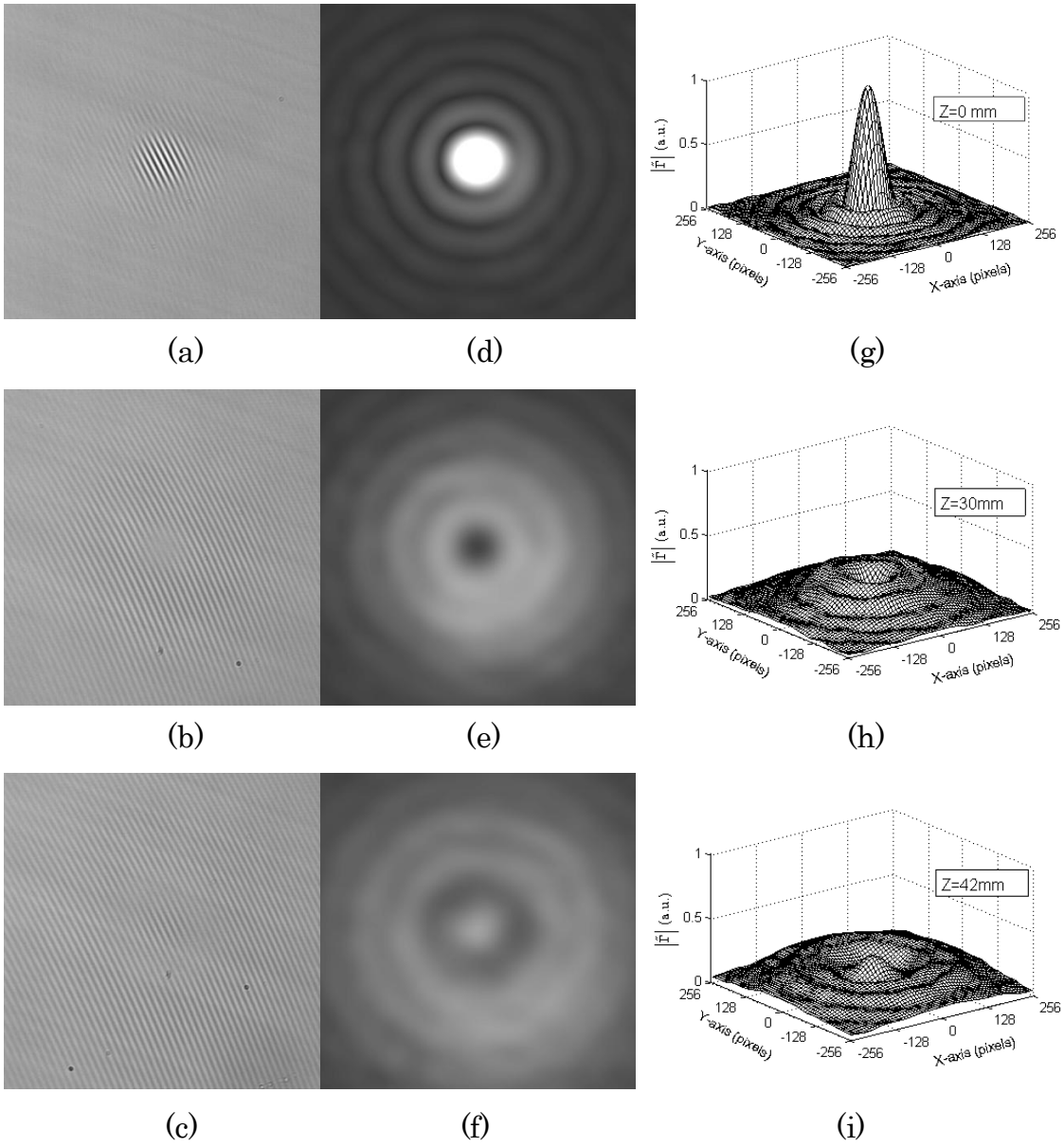

Figure 2-2 Left column: the interferograms recorded at different synthetic optical path differences $Z = 0, 30, 42mm$ respectively ; middle column: the distributions of the modulus of the spatial coherence functions reconstructed from the corresponding interferograms; right column: the 3D representations for the modulus of normalized spatial coherence function.

Here, it is also important to point out several concepts related to the coherence visualization system. In Fig. 2-2(d), the central area of the coherence Fraunhofer

diffraction pattern is related to the conventional definition for spatial coherence area [4, 14]. In the traditional optical imaging system, the diameter of the central Airy pattern (called Airy disk) has been widely used to provide the definition for the lateral resolution. This resolution depends on the wavelength in use and the Numerical Aperture (NA) of lens. For our proposed system, the diameter expressed in Eq. (2-8) can also be reasonably adopted as the lateral resolution for the coherence imaging system, which is related to the synthetic magnification $M_A M_B/(M_A - M_B)$ as well. In this measure, the lateral resolution of our system is about 0.54 mm.

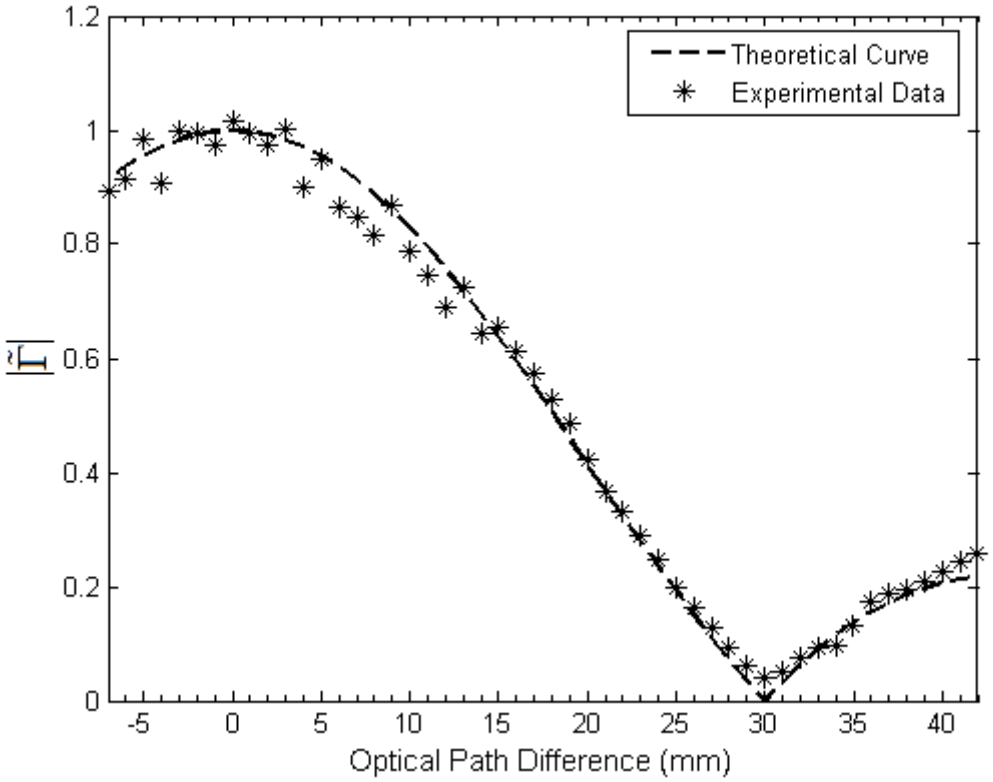

Figure 2-3 The normalized $\left|\tilde{\Gamma}(0,0,Z)\right|$ along the optical axis.

Figure 2-3 shows the distribution for the longitudinal spatial coherence function along the optical axis. The modulus of the spatial coherence function reaches its maximum at the coherence focal plan with $Z = 0$ and has its first minimum at the synthetic optical path difference $Z = 30mm$, where the central interference fringes vanish for the first time. In this measure, the coherence distance of the longitudinal spatial

coherence is 6cm, which is also the coherence length of the system. Similar to the depth of focus for the traditional optical imaging system, the coherence distance expressed in Eq. (2-11) can be regarded as the longitudinal resolution for spatial coherence imaging system.

2.4.2 3D Distribution of the coherence focal spot

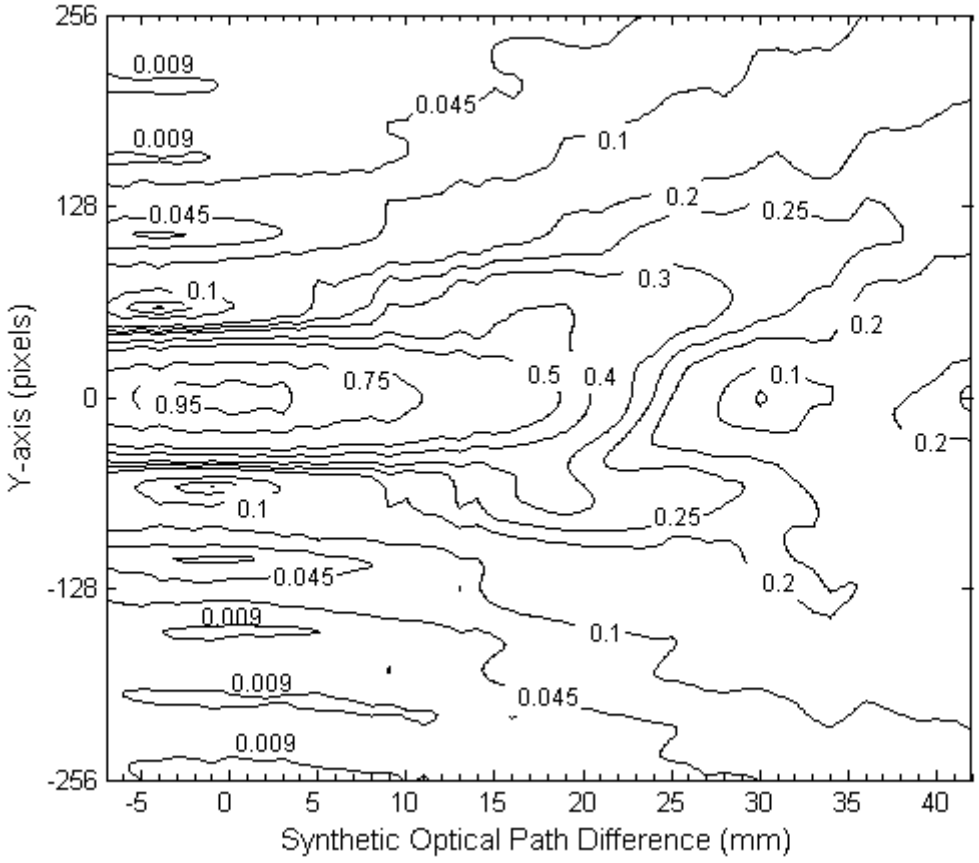

Figure 2-4 The contour lines of the normalized $\left|\tilde{\Gamma}(0,y,Z)\right|$ near the coherence focal plane.

In order to obtain a complete knowledge of the coherence diffraction, we have studied the full-field coherence distribution not only in the focal plane but also in the neighbourhood of this plane. The contour lines of the full-field distribution of coherence focal spot are showed in Fig. 2-4. As agreed with theoretical results [7],

this detailed structure of the coherence focal spot looks like an optical focus [17]. Notes that the capsule-like structure in Fig. 2-4 has a relative large value of the spatial coherence function, and any two fields within this region can be correlated easily. Therefore this capsule structure provides a direct experimental evidence for the spatial coherence volume. Without loss of generality, the contour line of the normalized modulus for the spatial coherence function equal to 0.5 provides the boundary for the spatial coherence volume.

It should also be noticed that the asymmetric coherence focal point observed in our experiment was caused by the off-axis interferometer. Although the introduction of the mirror tilt facilitates the coherence visualization through the fringe contrast, such mirror tilt also slightly changes the distribution of the spatial optical coherence function by breaking the central symmetry in the radial sheering interferometer.

This example for coherence diffraction is of great importance because many optical instruments have circular apertures. When the incident field is quasi-monochromatic partially incoherent, the effects of partial coherence on imaging system can be regarded as an imaging process of the optical coherence. When the diameter of the coherence Airy disk becomes larger than the resolving powering on detector, the partial coherence begins to have a visual impact on the image. Thus coherence diffraction sets a new fundamental resolution limit that is independent of the traditional optical image resolution stemming from the optical field diffraction.

2.5 Discussions

As an additional example to study the spatial coherence function by the proposed interferometric system, we have studied the Fraunhofer coherence diffraction generated by an incoherence source with different form. Consider a rectangular aperture with b and d being its length and width, respectively.

$$I_0(x_0, y_0) = rect(\frac{x_0}{b}, \frac{y_0}{d}). \tag{2-12}$$

If this rectangular aperture is illuminated by a quasi-monochromatic spatially incoherence light with a uniform intensity, the Fraunhofer diffraction for the spatial coherence function observed at the coherence focal plane is a Fourier transform of the incoherent source intensity. After inserting Eq. (2-12) into Eq. (2-4), we have

$$\tilde{\Gamma}(x,y,0) \propto bd\,\mathrm{sinc}\left[\frac{(M_A - M_B)bx}{\lambda f_1 M_A M_B}, \frac{(M_A - M_B)dy}{\lambda f_1 M_A M_B}\right]. \tag{2-13}$$

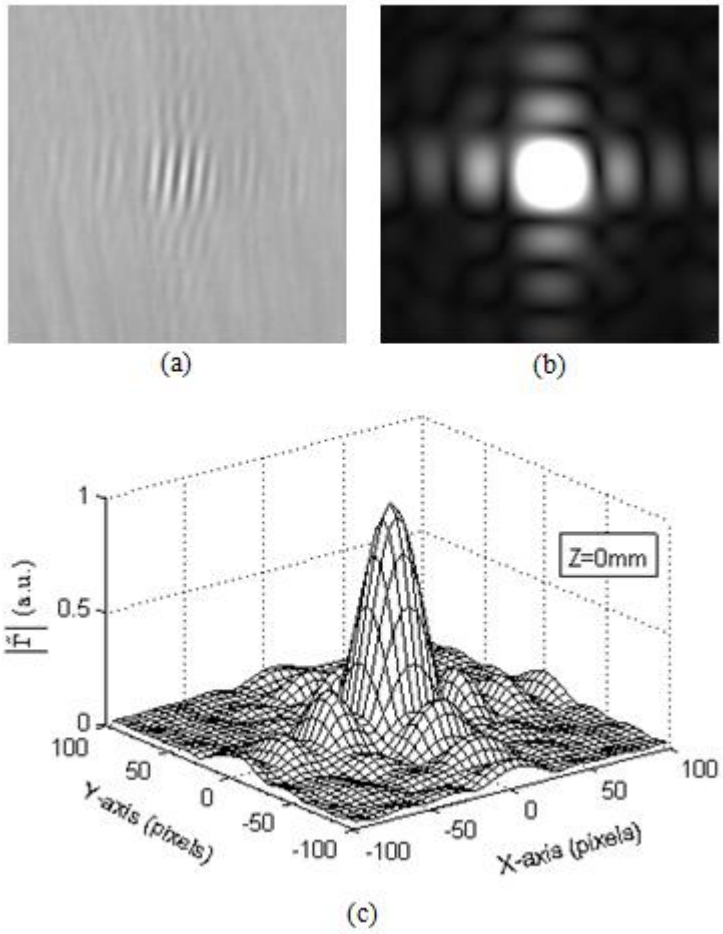

Figure 2-5 Spatial coherece patterns from a rectangular incoherent source. (a) the interferogram recorded at coherence focal plane; (b) the distribution of the modulus of the spatial coherence function; (c) the 3-D representation of the modulus for the normalized spatial coherence function.

Figure 2-5 shows the Fraunhofer diffraction of the spatial coherece created by a rectangular incoherent source when the interferogram has been recorded at the coherence focal plane, i.e. $Z = 0$. As shown in Fig. 2-5(b) for the modulus of the reconstructed spatial coherence function, the modulus rises to a maximum within each rectangle formed by pairs of consecutive dark lines; all these maxima are, however, only a small fraction of the central maximum, and decrease rapidly with increasing distance from the centre. Similar to the well-known Fraunhofer diffraction of a rectangular apertune for optical field [4,14], the resutls demonstrated in Fig. 2-5 provides another experimental demonstration for the spatial coherence diffraction from a rectangular incoherent source.

2.6 Summary

In summary, we have presented a novel interferometer for full-field spatial coherence visualization, and experimentally investigated the diffraction phenomena in the spatial coherence function. Compared with the conversional optical focal point, the behaviors of the newly observed coherence focus are essentially identical. The capsule structure of the central portion of the spatial coherence diffraction with high fringe contrast is particular interest because it provides a direct experimental demonstration of the spatial coherence volume. In analogy with conventional resolution definitions used in optical imaging system, the lateral size of spatial coherence Airy disk and the distance of the longitudinal coherence function can be referred to as the resolutions for coherence imaging. Furthermore, the proposed optical system enables direct observation of the full-field optical coherence distribution, and introduced new opportunity to explore other interesting phenomena in coherence function. Meanwhile, two proposed resolutions provide very useful criteria for choosing the light sources used in coherent system and defining the accuracy used in incoherent system.

References

[1] J. W. Goodman, *Statistical Optics*, 1st edition (Wiley 2000).

[2] M. J. Beran and G. B. Parrent, Jr., *Theory of Partial Coherence*, 2nd edition (Prentice Hall, Inc., 1964).

[3] E. Wolf, *Introduction to the Theory of Coherence and Polarization of Light*, 1st edition (Cambridge University Press, 2007).

[4] M. Born and E. Wolf, *Principles of Optics*, 6th edition, (Cambridge University, 1980).

[5] P. H. van Cittert, "Die Wahrscheinliche Schwingungsverteilung in Einer von Einer Lichtquelle Direkt Oder Mittels Einer Linse Beleuchteten Ebene," Physica 1, 201-210 (1934).

[6] F. Zernike, "The concept of degree of coherence and its application to optical problems," Physica 5, 785-795 (1938).

[7] G. B. Parrent, Jr., "On the propagation of mutual coherence," J. Opt. Soc. Am. 49, 787-789 (1959).

[8] G. B. Parrent, Jr., "Studies in the theory of partial coherence," Optica Acta, 6, 285-296 (2010).

[9] J. Rosen and A. Yariv, "Longitudinal partial coherence of optical radiation," Optics Commun., 117, 8-12 (1995).

[10] T. Asakura and I. Akamatsu, "Fresnel diffraction by a Circular Aperture Illuminated with Partially Coherent Light. I," Optica Acta 19, 749-763 (1972).

[11] H. Fujiwara, T. Asakura and K. Murata, "On the van Cittert-Zernike theorem," Opto-electronics, 4, 197-205 (1972).

[12] K. Tian and G. Barbastathis, "Coherence patterns originating from Incoherent volume sources," Opt. Lett., 29, 7-9, (2004).

[13] D. Mendlovic, G. Shabtay and A. W. Lohmann, "Synthesis of spatial coherence," Opt. Lett, 24, 361-363 (1999).

[14] J. W. Goodman, *Introduction to Fourier Optics*, 3rd edition, (Roberts and Company Publishers, 2005).

[15] M. Takeda, H. Ina and S. Kobayashi, "Fourier-transform method of fringe-pattern analysis for computer-based topography and interferometry," J. Opt. Soc. Am., 72, 156-160 (1982).

[16] W. Wang, Z. Duan, S. G. Hanson, Y. Miyamoto and M. Takeda, "Experimental study of coherence vortices: local properties of phase singularities in a spatial coherence function," Phys. Rev. Lett. 96, 073902 (2006).

[17] E. H. Linfoot and E. Wolf, "Phase distribution near focus in an aberration-free diffraction image," Proc. Phys. Soc. London B69, 823-832 (1956).

Chapter 3

Generation of the Non-diffracting Spatial Coherence Function

We demonstrate a non-diffracting solution for the optical coherence function that is propagation-invariant. Compared with the well-known diffraction of partially coherent light by an aperture, the transverse distribution of the non-diffracting coherence function generated by an incoherent circular slit source is unaltered by propagating in free space. The full-field distribution of the non-diffracting coherence function has been studied theoretically and experimentally.

3.1 Introduction

Diffraction is one of the universal phenomena. It affects all classical wave fields without exception. In an optical field, diffraction on a finite sized aperture also causes a fraction of the propagating energy to spread outside the central core of the Fraunhofer pattern into the outside rings or nodes. In many applications, diffraction phenomena may lead to adverse effects such as difficulties in detecting weak signals, channel crosstalk, changes in photo-detector responsivity, etc. It limits the development of some optical technology such as metrology, free-space communications, and optical lithography. However, there exists a particular kind of optical beam referred to as non-diffracting beam with its unique property of

unchanged transverse shape during the propagation [1-8]. Especially the J_0 beam as part of propagation-invariant waves in optical field has been employed to reduce the amount of the diffracted light for a long time.

In statistical optics, the propagation properties of optical coherence function have received a lot of attentions. Especially the diffraction of partially coherent light by an aperture described by the Van Cittert-Zernike theorem is undoubtedly one of the most important theorems of modern optics [9-14]. Similar to the well-known optical diffraction, the coherence function illuminated by a finite sized incoherent source also causes a coherence energy spreading, and the spot size of the diffractive coherence pattern is extended during its propagation resulting in a limited distance with high coherence. On the analogy of the non-diffracting optical beam, the complex coherence function should also have diffraction-free solutions. In recently, the J_0 correlated Schell-model sources caused great attention [15-25]. In this chapter, we experimentally demonstrate the J_0 coherence function and study its full-field distributions. The experimental results of the propagation behaviour of non-diffracting coherence function have been presented and compared with coherence diffraction phenomenon.

3.2 Principle

Let us provide, first, a general description of non-diffracting coherence function by referring to the Helmholtz equation is given by:

$$(\nabla_{(i)}{}^2 + \bar{k}^2)\tilde{\Gamma}(r_1, \mathrm{r}_2) = 0, (\mathrm{i} = 1 \mathrm{or} 2) \tag{3-1}$$

where ∇ is the Laplacian operator and $\bar{k} = 2\pi/\bar{\lambda}$. The mutual coherence function $\tilde{\Gamma}$ represents the cross correlation of light vibrations at point $r_{(i)}$ in space, $\nabla_{(i)}{}^2$ is the differential operation to be performed with respect to the point $r_{(i)}$. Without loss of generality, we will restrict our discussions to the case for the variation of location r_1

by keeping r_2 fixed. Thus, in cylindrical coordinates, the mutual coherence function $\tilde{\Gamma}(\rho_1,\rho_2;\phi_1,\phi_2;z_1,z_2)$ can be replaced by $\tilde{\Gamma}(\rho,\phi,z)$. And the generalized diffraction-free solution is

$$\tilde{\Gamma}(\rho,\phi,z)=\exp(j\beta_0 z)\sum_{m=-\infty}^{\infty}C_m J_m(\alpha_0\rho)\exp(jm\phi), \tag{3-2}$$

where $\alpha_0^2+\beta_0^2=k^2$, C_m are coefficients, and J_m is the mth order Bessel function of the first kind. Unlike the normal diffracting coherence function propagation accompanied by rapid decay of peak intensity, it is evident from Eq. (3-2) that each term has the same distribution $J_m^2(\alpha_0\rho)$ in every plane normal to the z axis with its half-width of the central peak proportional to α_0^{-1}.

Then, we re-examine the Van Cittert-Zernike theorem by reviewing it in an original formulation and extend the theorem to full-field propagation by referring to the Fresnel diffraction integral.

In partial coherence theory, the signal is realized as a complex coherence function. For the quasi-monochromatic signals, the spatial coherence between two points illuminated by an incoherent plane source is given by

$$\tilde{\Gamma}\approx\exp(-jkz)\int_0^{\infty}I(\rho)J_0(k\rho)\exp(-jkz\rho^2/2)\rho d\rho, \tag{3-3}$$

where J_0 is the 0th order Bessel function.

In what follows, we present special cases of the generalized coherence functions described by Eq. (3-3).

Let the incoherent source be a circular slit (ring-shaped) with a radius a, and take $\mathrm{I}(\rho)=1$ for simplicity, and then the coherence function (described by Eq. (3-3)) reduces to

$$\tilde{\Gamma} = 2\exp(-jkz)\,\mathrm{J}_0(ka)\exp(-jkza^2/2) \tag{3-4}$$

It should be noticed that, in practice, the electromagnetic fields associated with non-diffracting beams require an infinite amount of energy to propagate unaltered an arbitrarily long distance. Non-diffracting beams are not only unaffected by diffracting spreading, but also are capable of self-reconstructing. And a non-diffracting solution can be found when the equation is separable, that is, when it can be expressed as the product of a transverse and a longitudinal field. In Eq. (3-4), the propagation factor z is only in phase part, the transverse intensity distribution of the coherence function is contributed by J_0 function. On the analogy of the Eq. (3-2), among various types of non-diffracting solutions, the zeroth order Bessel function has the virtue of being the easiest to implement. The detailed properties of mathematical expression show that the transverse intensity of the coherence function propagates with the same spot size at different positions along the optical axis. The energy of the coherence function during the propagation z cannot spread outside the central core. Thus we got a non-diffracting coherence function finally.

One of the most common Fraunhofer diffraction patterns is produced by a circular aperture. In order to give a clear reference substance, we chose an incoherent circular aperture source with the same radius a, and also take $\mathrm{I}(\rho)=1$ for simplicity, and Eq. (3-3) reduces to

$$\tilde{\Gamma} = \exp(-jkz)\int_0^a \mathrm{J}_0(k\rho)\exp(-jkz\rho^2/2)\rho d\rho, \tag{3-5}$$

This coherence pattern has been investigated in Chapter 2. The spatially incoherent field illuminated by an extended circular source of uniform intensity distribution can be well characterized by the Airy function.

3.3 Experiment

To demonstrate the validity of the theory, experiments have been conducted based on the same optical geometry proposed in Chapter 2.

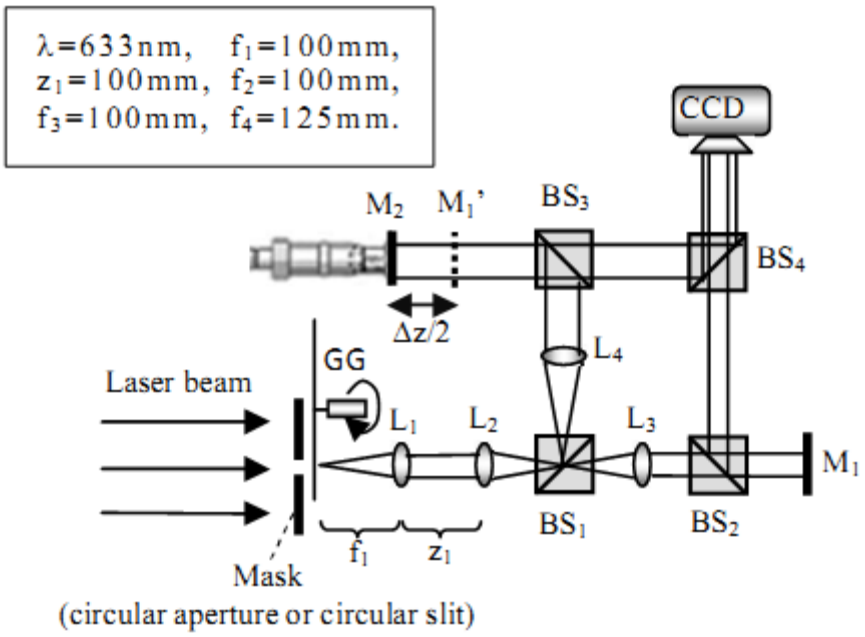

Figure 3-1 Schematic representation of the experimental setup. S (extended monochromatic spatially incoherent source); BS (Non-polarizing beam splitter); Focal length: f_1=100mm, f_2=100mm, f_3=100mm, f_4=125mm.

The experiment setup is shown in Fig. 3-1. In our experiment, light from a He-Ne laser was expanded and collimated to illuminate a circular slit (ring type). The patterns were projected on a rapidly rotating ground glass to serve as an extended quasi-monochromatic incoherent source. Ideally, each point on a ring source acts as a point source which the focusing lens transforms into a plane wave. By changing the synthetic optical path difference Z between the two arms, we observed the coherence diffraction phenomena from the fringes visibility.

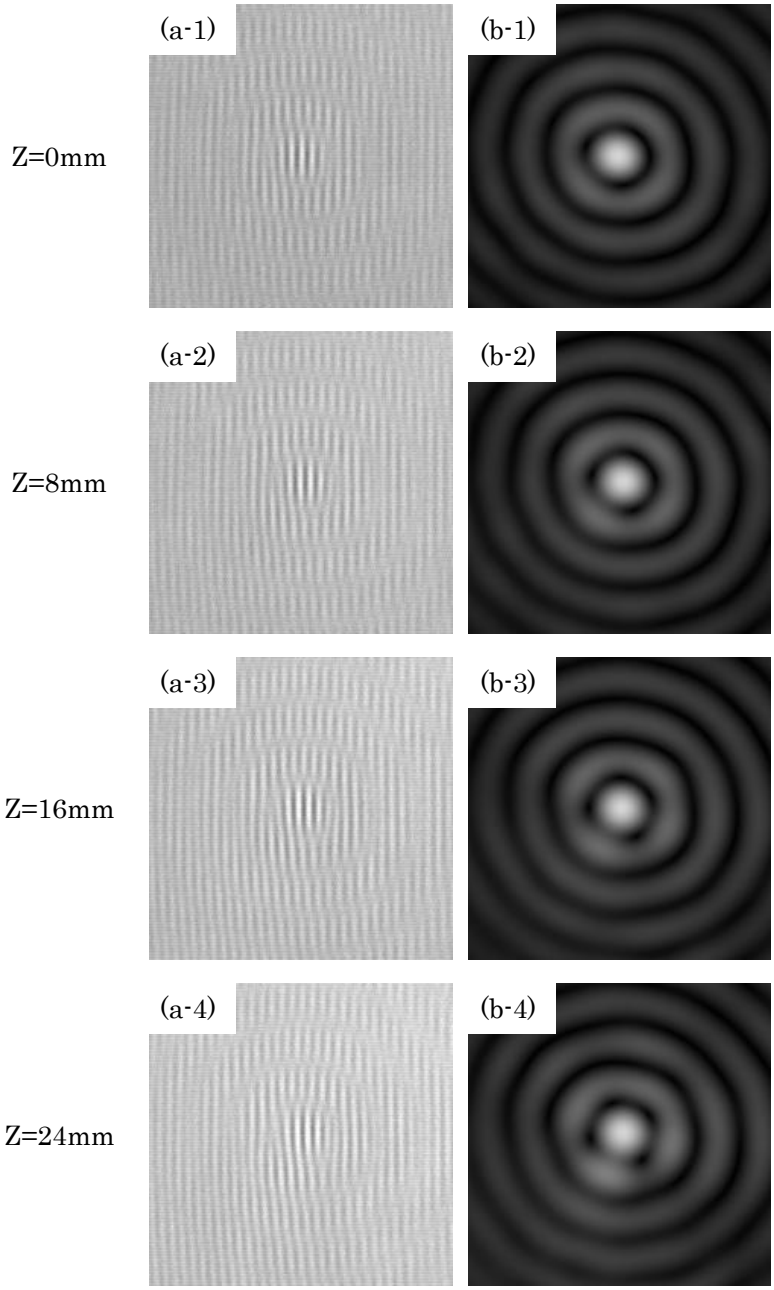

Figure 3-2 (a)The interferograms obtained from an incoherent circular slit source with various optical path differences ; (b) the normalized reconstructed coherence functions. The label number 1,2,3,4 represent different synthetic optical path differences $Z = 0, 8, 16, 24$ respectively.

Figure 3-2 is the coherence patterns from an incoherent circular slit source with an uniform intensity distribution. Figure 3-2 (a-1) is the interferogram recorded by the CCD camera at the coherence focal plane, $Z = 0$, where the complex coherence function is displayed through the fringe contrast. Figure 3-2 (b-1) is the normalized $\left|\tilde{\Gamma}(x, y, 0)\right|$ distribution after reconstruction [26]. As expected, the coherence function exhibits a Bessel function with a high contrast in the centre surrounded by concentric rings with neutral and low coherence. With the increase of radius, the fringe contrast decreases rapidly, and disappears at the first ring with zero fringe contrast. Figure 3-2 (a-2,3,4) is the interferograms for coherence diffraction at $Z = 8,16,24mm$ respectively and Figure 3-2 (b-2,3,4) is its normalized coherence distribution. In this case, the centres of these coherence function images demonstrate a high contrast spot, the size of these spots are the same. Thus the incoherent circular slit source is a coherence non-diffracting solution which has the capability of self-reconstructing even at arbitrarily position along the propagation direction.

In order to obtain a complete knowledge of the diffraction effect, the isophotes of full-field coherence distributions have been exhibited. Figure 3-3 is the contour map of the modulus of the coherence function that originates from a circular slit source along the optical axis. Following the definition of Rayleigh range, if we have a Gaussian-type coherence function with the same centre spot size (as shown in Fig 3-2(a), FWHM= 78μm, pixel size of CCD is 5.2μm) in the coherence focal plane, then we can calculate that the Rayleigh range is as small as 30mm. The isophotes of full-field coherence distributions show that the spatial coherence illuminated by an incoherent circular slit source has an constant intensity distribution as it propagates through space.

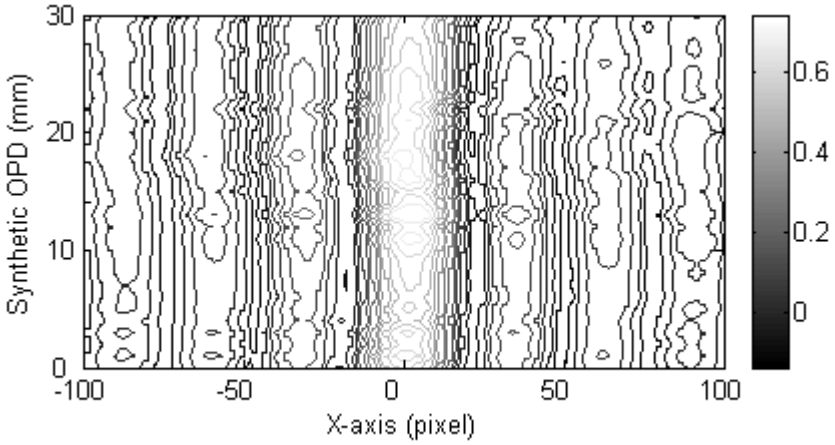

Figure 3-3 The contour lines of the normalized modulus of spatial coherence functions $\left|\tilde{\Gamma}(x,0,Z)\right|$ originate from a circular slit source along the optical axis.

For the sake of contrast, a parallel experiment has also been conducted which use a circular aperture source with the same diameter of the circular slit source.

The results of the incoherent circular aperture source are shown in Fig. 3-4. Figure 3-4 (a-1) is the fringes patterns recorded by the CCD camera at the coherence focal plane, $Z=0$; (a-2) is the interferograms for coherence diffraction at $Z=8mm$; (a-3) is the interferograms for coherence diffraction at $Z=16mm$; (a-4) is the interferograms for coherence diffraction at $Z=24mm$; Figure 3-4 (b-1,2,3,4) are the normalized coherence distribution after reconstruction. With the increase of synthetic optical path differences, the diameter of the first dark ring became larger, it can't maintain its original appearance.

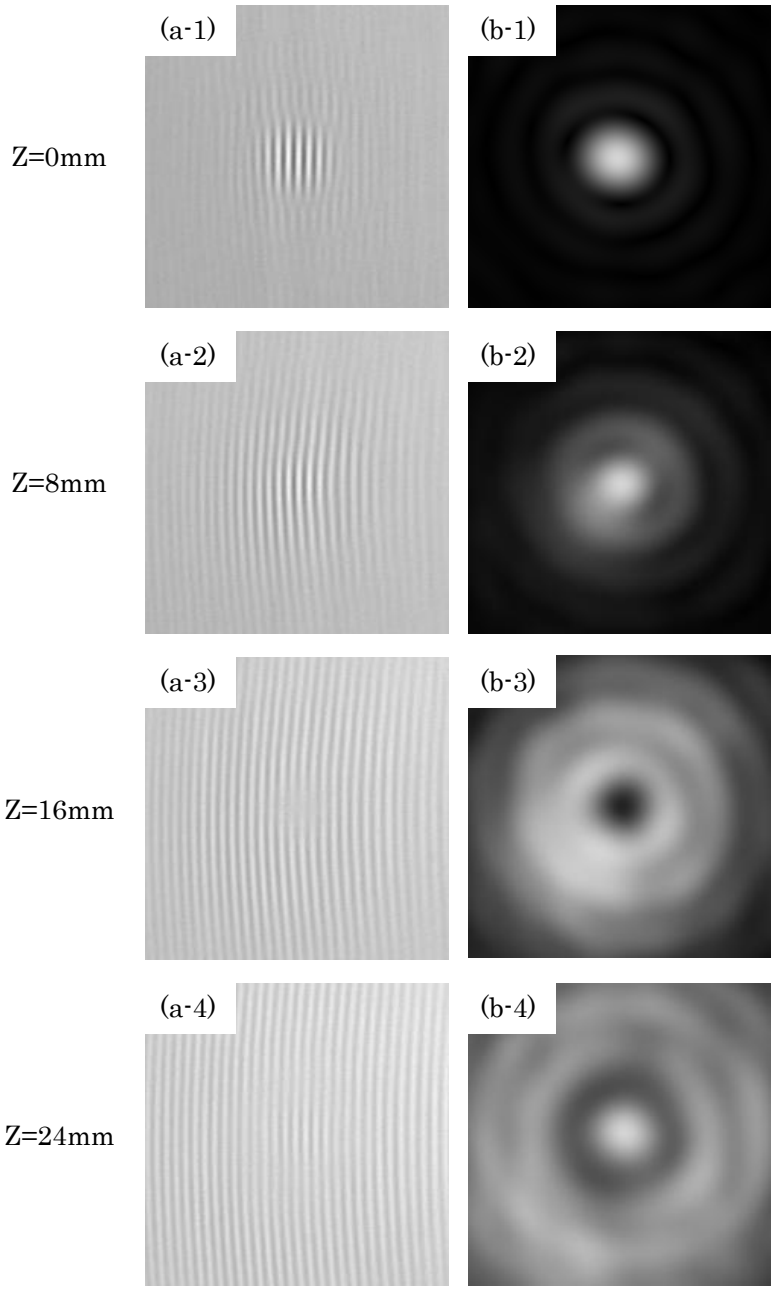

Figure 3-4 (a) the interferograms obtained from an incoherent circular aperture source with various optical path differences ; (b) the normalized reconstructed coherence functions. The label number 1,2,3,4 represent different optical path differences $Z = 0, 8, 16, 24$ respectively.

The contour lines in Fig. 3-5 show that spatical coherence in a space illuminated by an incoherent circular aperture source, has a non-constant intensity distribution as it propagates through space. A capsule-like structure can be easily observed which facilitates the concept of spatial coherence volume [12]. The coherence functions show a clearly divergent structure in propagation space. This is in marked contrast to the situation in the non-diffracting case shown in Fig. 3-3.

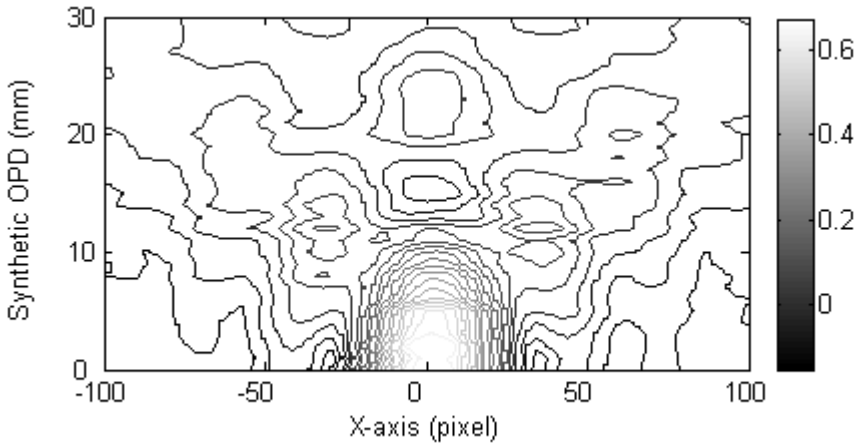

Figure 3-5 The contour lines of the normalized modulus of spatial coherence functions $\left|\tilde{\Gamma}(x,0,Z)\right|$ originate from a circular aperture source along the optical axis.

A quantitative comparison of the spreading of the central point energy of a circular slit beam and a circular aperture beam with the same diameter is shown in Fig. 3-6. The peak intensity of the coherence function from an incoherent circular slit source remains at a high value throughout the propagation. No measurable spreading of the central peak profile could be observed over a propagation distance of about 30mm. On the other hand, the peak intensity of the coherence function from an incoherent circular aperture source decreases and spreads rapidly. The former function have a consiferably longer coherence propagation distance than the latter before have a measurable spread.

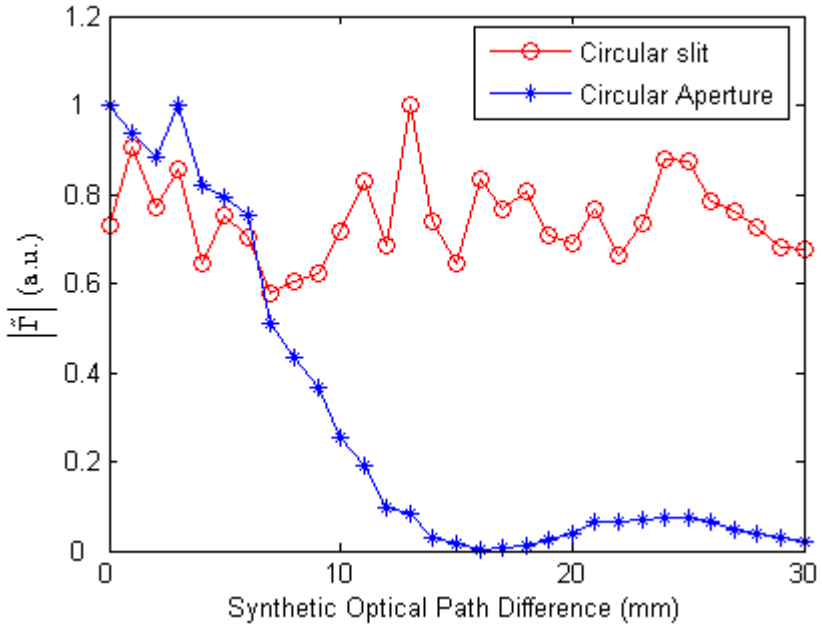

Figure 3-6 Longitudinal distributions of the normalized modulus of spatial coherence functions $\left|\tilde{\Gamma}(0,0,Z)\right|$ profile for the non-diffracting coherence function and the diffracting coherence function.

3.4 Summary

We present an experimental procedure for producing a non-diffracting coherence function. The coherence function generated by an incoherent circular slit source is formed by the 0^{th} order Bessel function. The 0^{th} order Bessel beam is the best known optical non-diffracting beam, and the 0^{th} order Bessel-type coherence function also remains unchanged under free-space propagation. To compare with the coherence diffraction function from an incoherent circular aperture source, the non-diffracting coherence function can propagates for a long distance without spreading and remains unchanged in its space structure. Therefore, the coherence function from the incoherent circular slit source does not suffer coherence diffraction effect during their propagation. For directly coherence visualization, we chose an off-axis interferometer. So the coherence function can be seen from the contrast of the interference fringes. If we use a coaxial system, then there will not be carrier fringes on CCD plane. We end up with a Bessel beam which has a uniform intensity distribution and a uniform

coherence distribution. In other words, we may generate a beam with first order correlation unchanged and second order correlation unchanged too.

References

[1] J. Durnin, J. J. Miceli, Jr. and J. H. Eberly, "Diffraction-free beam," Phys. Rev. Lett. 58, 1499-1501 (1987).

[2] J. Durnin, "Exact solutions for nondiffracting beams," J. Opt. Soc. Am. A 4, 651-654 (1987).

[3] R. Piestun and J. Shamir, "Generalized propagation-invariant wave fields," J. Opt. Soc. Am. A 15, 3039-3044 (1998).

[4] S. Chavez-Cerda, G. S. McDonald and G. H. C. New, "Nondiffracting beams: travelling, standing, rotating and spiral waves," Opt. Commun. 123, 225-233 (1996).

[5] C. A. Mcqueen, J. Arlt and K. D holakia, ''An experiment to study a 'nondiffracting' light beam,'' Am. J. Phys. 67, 912-915 (1999)

[6] C. Lopez-Mariscal and J. C. Gutierrez- Vega, "The generation of nondiffracting beams using inexpensive computer-generated holograms," Am. J. Phys. 75, 36-42 (2007)

[7] J. J. Miceli, J. Durnin and J. H. Eberly, "Comparison of Bessel and Gaussian beams," Opt. Lett. 13, 79-80 (1998)

[8] Z. Bouchal, J. Wagner and M. Chlup, "Self-reconstruction of a distorted nondiffracting beam," Opt. Commum, 151, 207-211 (1998)

[9] E. Wolf, "New theory of partial coherence in the space-frequency domain. Part I: spectra and cross spectra of steady-state sources," J.Opt. Soc. Am. 72, 343-351(1982)

[10] P. H. van Cittert, "Die Wahrscheinliche Schwingungsverteilung in Einer von Einer Lichtquelle Direkt Oder Mittels Einer Linse Beleuchteten Ebene," Physica 1, 201-210 (1934).

[11] F. Zernike, "The concept of degree of coherence and its application to optical problems," Physica 5, 785-795 (1938).

[12] M. Born and E. Wolf, *Principles of Optics*, 7th edition (Cambridge University 1985).

[13] J. W. Goodman, *Statistical Optics*, 1st edition (Wiley 2000).

[14] H. Fujiwara, T. Asakura and K. Murata, "On the Van Cittert-Zernike Theorem," Opto-electronics 4, 197-205 (1972).

[15] F. Gori, G. Guattari and C. Padovani, "Bessel–Gauss beams," Opt. Commun. 64, 491-495 (1987).

[16] J. Turunen, A. Vasara and A. T. Friberg, "Propagation invariance and self-imaging in variable-coherence optics," J. Opt. Soc.Am. A 8, 282-289 (1991).

[17] R. Simon, K. Sundar and N. Mukunda, "Twisted Gaussian Schell-model beams. I. Symmetry structure and normal-mode spectrum," J. Opt. Soc.Am. A 10, 2008-2016 (1993).

[18] M. W. Kowarz and G. S. Agarwal, "Bessel-beam representation for partially coherent fields," J. Opt. Soc. Am. A 12, 1324-1330 (1995).

[19] C. Palma and G. Cincotti, "Imaging of J0-correlated Bessel-Gauss beams," IEEE J. Quantum Electron. 33, 1032-1040 (1997).

[20] R. Borghi, "Superposition scheme for J0-correlated partially coherent sources," IEEE J. Quantum Electron. 35, 849-856 (1999).

[21] S. A. Ponomarenko, "A class of partially coherent beams carrying optical vortices," J. Opt. Soc. Am. A 18, 150-159 (2001).

[22] G. Gbur and T. D. Visser, "Can spatial coherence effects produce a local minimum of intensity at focus," Opt. Lett. 28, 1627-1629 (2003).

[23] J. Garnier, J.-P. Ayanides and O. Morice, "Propagation of partially coherent light with the Maxwell–Debye equation," J. Opt. Soc. Am. A 20, 1409-1417 (2003).

[24] L. Rao, X. Zheng, Z. Wang and P. Yei, "Generation of optical bottle beams through focusing J0-correlated Schell-model vortex beams," Opt. Commun. 281, 1358-1365 (2007).

[25] T. van Dijk, G. Gbur and T. D. Visser, "Shaping the focal intensity distribution using spatial coherence," J. Opt. Soc. Am. A 25, 575-581 (2008)

[26] M. Takeda, H. Ina and S. Kobayashi, "Fourier-transform method of fringe-pattern analysis for computer-based topography and interferometry," J. Opt. Soc. Am. 72, 156-160 (1982).

Chapter 4

Interference of the Spatial Coherence Functions

A single extended quasi-monochromatic light source can produce a special area in the observation plane over which the beams can be considered correlated. This area is referred to as the coherence area in which the field has a high spatial coherence. Here is a question: how does the spatial coherence function propagate while there are more extended sources? In this chapter, we will use a series of experiments to show how the spatial coherence functions are distributed in the observation plane, while there are two or more extended sources. The mathematical expression of interference of the spatial coherence function is introduced firstly. The interference of two extended quasi-monochromatic light sources is experimentally investigated; the phenomena of the interference of coherence function and missing class of the coherence function are demonstrated. Finally, we demonstrate an interference of multi-coherence functions.

4.1 Introduction

In superposition, waves are combined, and when waves combine they interfere. Since the optical coherence function satisfies the wave equations [1-3], it can be treated as a wave, so, when two or more coherence functions are superposed, this phenomenon can also be called as interference.

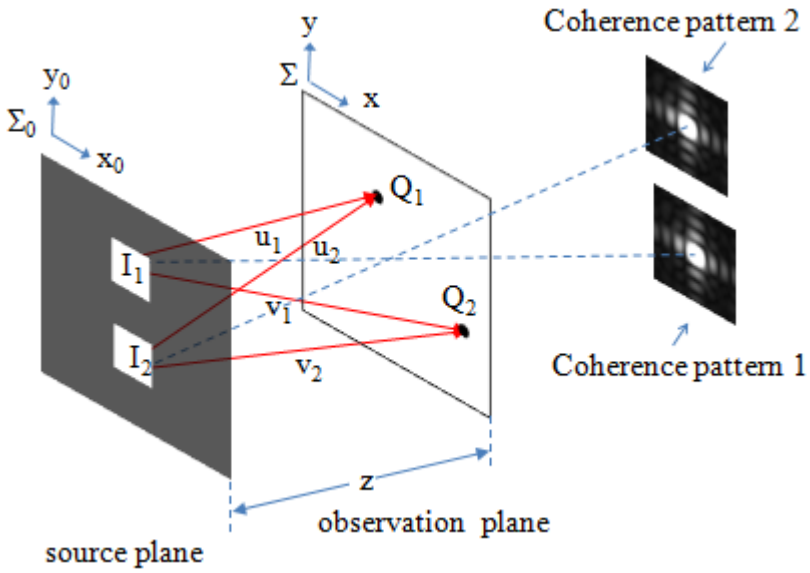

Figure 4-1 Schematic representation of the interference of the spatial coherence functions

We will begin our discussion of the interference between two spatial coherence functions (also called as coherence interference for short) by examining the combination of two spatial incoherent light sources. Figure 4-1 shows two extended quasi-monochromatic light source I_1 and I_2 (both of them have a same wavelength λ). The natures of the two sources are completely arbitrary. The spatial coherence exists when fluctuations measured at different observation point Q_1 and Q_2 (located by position vector $\vec{u}_1$, $\vec{u}_2$ and $\vec{v}_1$, $\vec{v}_2$) are correlated. Referring to the well-known Van Cittert-Zerinke theorem [4, 5], the coherence functions (originating from each incoherent source respectively) at the two points Q_1 and Q_2 on the observation plane are given by:

$$\Gamma_i(\Delta x,\Delta y)=\frac{\exp(-j\psi_i)}{(\bar{\lambda}z)^2}\int\int_{-\infty}^{\infty}I_i(x_o,y_o)\exp[\frac{2j\pi}{\bar{\lambda}z}(x_o\Delta x+y_o\Delta y)]dx_o dy_o,(\mathrm{i}=1\mathrm{or}\,2) \qquad (4\text{-}1)$$

where ψ_i is a quadratic phase factor

$$\psi_i = \frac{\pi}{\bar{\lambda} z}(u_i^2 - v_i^2). \tag{4-2}$$

The relationship between the coherence function of two points along the propagation axis and the intensity distribution over the source is described by the Fourier transform:

$$\Gamma_{1,2} = FT\{I_{1,2}\}. \tag{4-3}$$

Suppose that two light sources have a same rectangular distribution. Coherence patterns (on observation plane) originating from these two sources are shown in Fig.4-1. The interference of coherence function should be the superposition of the coherence pattern 1 and the coherence pattern 2. The principle of superposition guarantees that we may combine 'waves' algebraically to give other wave solutions. Obviously, Γ_1 and Γ_2 individually satisfy the linear differential equation, so, the interference of coherence function is defined to be

$$\Gamma_{total} = \Gamma_1 + \Gamma_2. \tag{4-4}$$

The superposition of coherence function may equal to the combination of each coherence functions.

From another standpoint, if consider the two sources as a single two-sub aperture source, $I_{total} = I_1 + I_2$, then, the coherence function of this single source is:

$$\Gamma_{total} = FT\{I_{total}\}. \tag{4-5}$$

According to fundamental principle of Fourier transform:

$$FT\{I_1 + I_2\} = FT\{I_1\} + FT\{I_2\}, \tag{4-6}$$

then, substitute Eq. (4-3) and Eq. (4-5) into Eq. (4-6), the coherence function of this two-aperture source is determined and equals Eq. (4-4). Therefore the coherence interference phenomenon can be observed when there are two or more extended sources.

4.2 Experiments and results

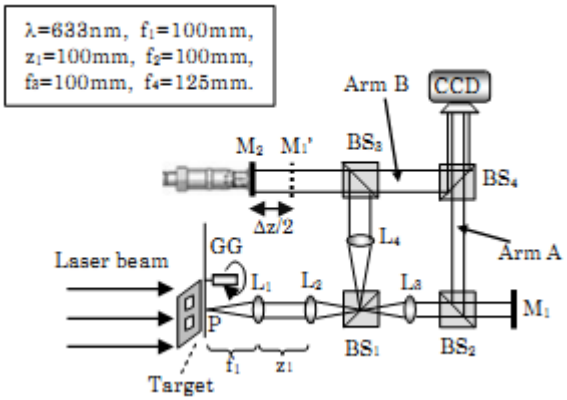

Figure 4-2 Experimental setup of the full-field spatial coherence visualization

The experiment setup is shown in Fig. 4-2. In our spatial coherence visualization system, light from a He-Ne laser was first expanded and then collimated to illuminate a target. The target used in our first experiment is a two-rectangle aperture I_1 and I_2, the distance between the two apertures is $2l$, the sizes of the rectangles are both $2a \times 2a$. The patterns were projected on a rapidly rotating ground glass to serve as an extended quasi-monochromatic incoherent source. We interfere two beams (from arm A and arm B) with different magnification and restore the coherence function by recording the visibility of interference fringes.

The intensity distribution on the CCD plane is given by

$$I_{CCD}(x,y) = I_A + I_B + 2\,\mathrm{Re}\{\tilde{\Gamma}_{total}(x,y,Z)\}, \tag{4-7}$$

where, $\mathrm{Re}\{\cdots\}$ denotes the real part, and I_A and I_B are the averaged intensity of the light through the interferometric arm A and arm B respectively. The function $\tilde{\Gamma}_{total}(x,y,Z)$ in the last term of Eq. (4-7) will be recognized as the coherence function:

$$\tilde{\Gamma}_{total}(x,y,Z)=\frac{\exp(jk\Delta z)}{\lambda^2 f_1^{\,2} M_A M_B}\iint_S [I_1(x_0,y_0)+I_2(x_0,y_0)] \exp[-\frac{2j\pi(M_A-M_B)}{\lambda f_1 M_A M_B}(xx_0+yy_0)]\exp[\frac{j\pi Z}{\lambda f_1^{\,2}}(x_0^{\,2}+y_0^{\,2})]dx_0dy_0, \tag{4-8}$$

where, $M_A=f_3/f_2$ is the focal length ratio for arm A , and $M_B=f_4/f_2$ is the focal length ratio for arm B, and $Z(\Delta z)$ is synthetic optical path difference (OPD) stemming from the path differences Δz between interferometric arm A and arm B,

$$Z(\Delta z)=\frac{f_2(M_A-M_B)}{M_A M_B}-\frac{z_2+f_3-f_4+\Delta z}{M_B^{\,2}}+\frac{z_2}{M_A^{\,2}}. \tag{4-9}$$

The intensity distribution of source 1 is

$$I_1=rect(\frac{x_0}{2a}+\frac{y_o}{2a})*\delta(x_0-l,y_0). \tag{4-10}$$

The intensity distribution of source 2 is

$$I_2=rect(\frac{x_0}{2a}+\frac{y_o}{2a})*\delta(x_0+l,y_0). \tag{4-11}$$

The coherence function can be recognized as the Fourier transform of the product of the source intensity distribution and quadratic phase factor.

Through an appropriate selection of Δz , we will make $Z=0$, the phase curvature disappears, leaving an exact Fourier transform relation:

$$\begin{aligned}\tilde{\Gamma}_{total}(x,y,0) &= FT\{rect(\frac{x_0}{2a}+\frac{y_o}{2a})*\delta(x_0-l,y_0)+rect(\frac{x_0}{2a}+\frac{y_o}{2a})*\delta(x_0+l,y_0)\} \\ &= 8a^2\cos(2\pi lf_x)\exp(-2\pi jf_y)\sin c(2af_x)\sin c(2af_y),\end{aligned} \tag{4-12}$$

where $f_x=\frac{(M_A-M_B)x}{\lambda f_1 M_A M_B}$, $f_y=\frac{(M_A-M_B)y}{\lambda f_1 M_A M_B}$.

And the spatial coherence function on the x-axis is given by

$$\tilde{\Gamma}_{total\_x}(x,0,0)=8a^2\cos(2\pi lf_x)\sin c(2af_x), \tag{4-13}$$

The cosine function is the interference term, and the sinc function is contributed by the coherence diffraction patterns originating from each aperture sources. Bright coherence interference fringes occur when $2\pi lf_x=m\pi$ (with m any integer); and zeros of envelope $\sin c(2af_x)$ occur when $2af_x=n\pi$ (with n a non-zero integer). A simple interpretation of the coherence interference is that it results from the interference of two coherence patterns originating from each single-aperture sources that overlap on the observing screen.

Experiments have been conducted. We adjust the path differences between the arms A and B, and located the distance as $Z=0$ where the interference fringes most clearly. The experimental results are shown in Fig. 4-3. There are two sets of fringes in Fig. 4-3. Pinstripes as the carrier fringes are produced by the Mach-Zehnder interferometer, used for coherence measurement. The second set of fringes can be seen after Fourier fringe analysis [6]. It is the distribution of coherence function (as shown in Fig. 4-3(b)), called as coherence interference fringes. In order to investigate the spatial coherence, we used extended light sources, so the coherence area in the observation plane is quite small, the dotted line in Fig. 4-3(c) is the envelope of the coherence area from a single aperture source, and the solid line is the result of coherence interference pattern.

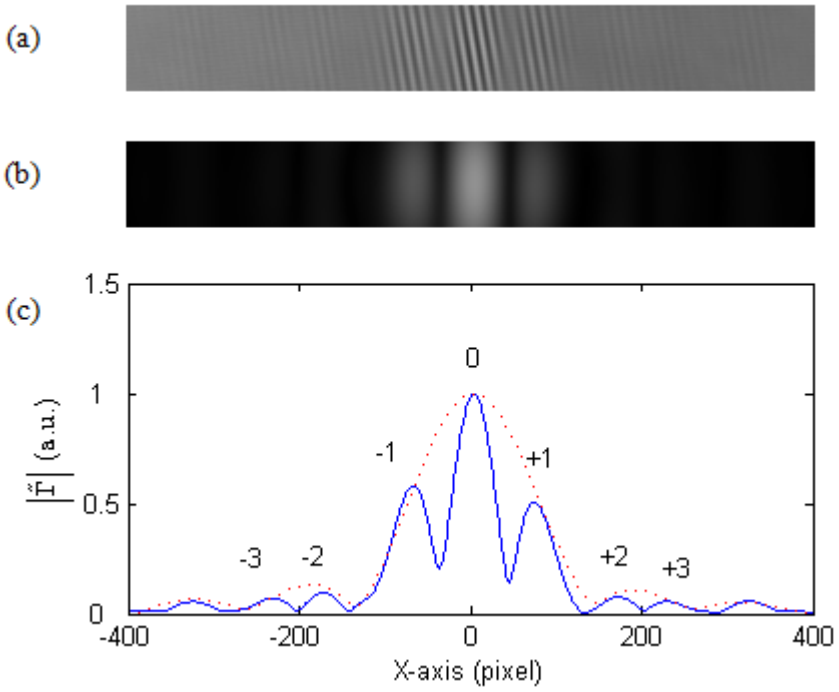

Figure 4-3 Interference of the spatial coherence functions from two apertures sources. (a) Interferograms obtained at $Z = 0$. (b) Normalized $\left|\tilde{\Gamma}(x,0,0)\right|$ after reconstruction [7]. (c) Curves of normalized $\left|\tilde{\Gamma}(x,0,0)\right|$ on the x-axis, where the dotted line is the coherence pattern from a single aperture source and solid line is coherence interference pattern of two-aperture source.

Next, we will investigate the propagation of the coherence interference pattern. According to the principle of independently propagating of light, light waves will continue to their original transmission regardless their overlapping. In other words, the propagation characters of the wave (propagation direction, speed, amplitude, phase, and polarization state) will not be affected the characters of the other wave. In the overlapping area, light vibration must obey the principle of wave superimposing. In vacuum, the principle of independently propagating of light and the principle of superposition is always established. These principles also apply to coherence interference.

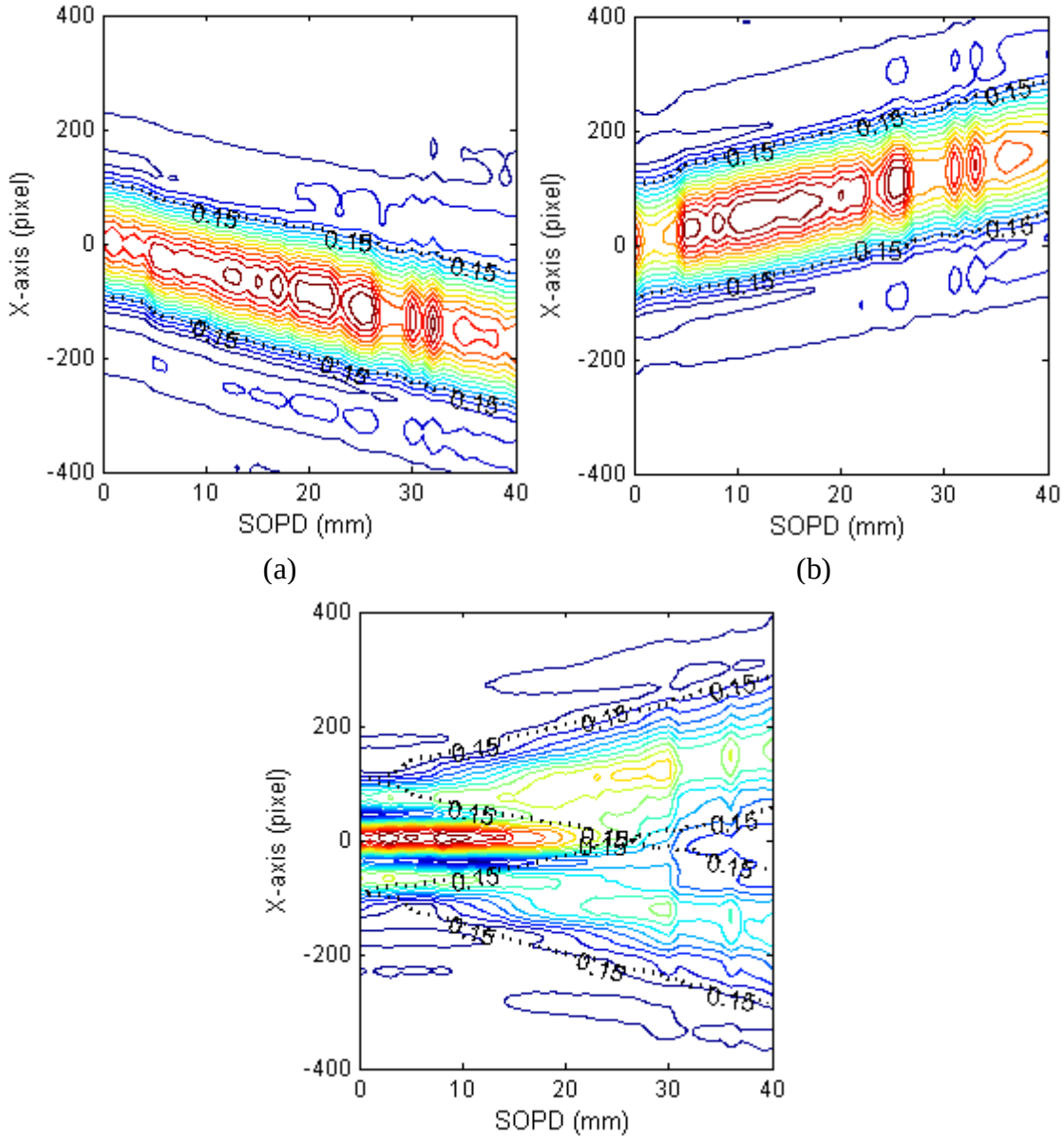

Figure 4-4 (a) Contour map of the spatial coherence originates from the left source; (b) contour map of the spatial coherence originates from the right source; (c) contour map of the spatial coherence originates from two-aperture source. Dotted lines are contour lines of coherence patterns from single aperture sources, with the value of 0.15; solid line is contour line of normalized $\left|\tilde{\Gamma}(x,0,Z)\right|$.

For simplicity, we give the following diagrams: Fig. 4-4 (a) shows the coherence function form left source, Fig. 4-4 (b) shows the coherence function from the right source and Fig. 4-4 (c) shows the interference of these two coherence functions. both of these two sources. Only within the superposition area (triangle region) we can observe interference fringes, and interference fringes are always parallel. From this experimental result, we can see two parallel dark fringes curve clearly within parallelogram wrapped by the dotted line. This superposition area is determined by both diffraction effect of each single aperture source and the distance between two sources.

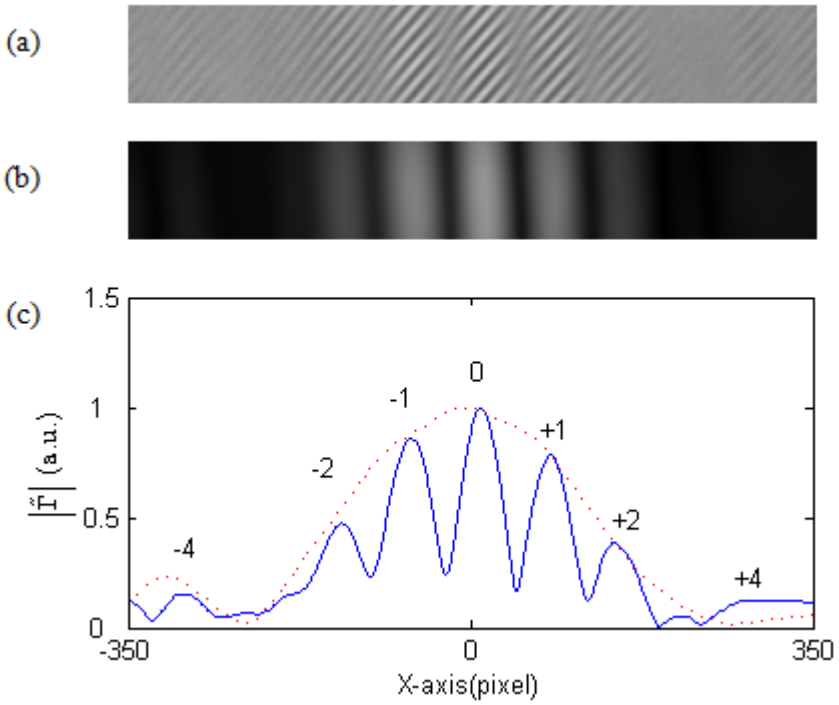

Figure 4-5 Interference of the spatial coherence function from two square apertures source, with spacing ratio of holes size and the distance between two holes is 1:3. (a) Interferograms obtained at $Z=0$. (b) Normalized $\left|\tilde{\Gamma}(x,0,0)\right|$ after reconstruction. (c) Curves of normalized $\left|\tilde{\Gamma}(x,0,0)\right|$ on the x-axis, where the dotted line is the coherence pattern from a single aperture source and solid line is coherence interference pattern of two-aperture source. Missing orders occur at ± 3.

Figure 4-5 introduce the missing order phenomenon. The missing orders in two-aperture coherence interference fringes occur when condition for interference term maximum coincides with a zero of the envelope. Notice that missing orders occur when the ratio of aperture spacing to aperture size is an integer $l:a=m$, and this integer m determines the order number of the first missing maximum. In Fig. 4-5, the spacing ratio of hole size and the distance between two holes is $1:3$. From Fig. 4-5-(c) we can see that the third class bright fringe missing.

It is interesting to re-examine Eq. (4-13). Consider a source that consists of more than two sub structures. Let's assume that there are N sub sources and all of these sub-sources have a same rectangular shape, with width $2a$ and separation l.

$$\begin{aligned}&\tilde{\Gamma}_{total\_x}(x,0,0)\\&=FT\{rect(\frac{x_0}{2a})\}(FT\{\delta(x_0)\}+FT\{\delta[x_0+l]\}+\ldots+FT\{\delta[x_0+(N-1)l]\})\\&=2a\sin c(2af_x)\frac{1-\exp(2\pi jNlf_x)}{1-\exp(2\pi jlf_x)}.\end{aligned} \tag{4-14}$$

Further simplification gives

$$\tilde{\Gamma}_{total\_x}(x,0,0)=2a\sin c(2af_x)\frac{\sin(N\gamma)}{\sin(\gamma)}, \tag{4-15}$$

where $\gamma=\pi lf_x$. The principle maxima occur when $\gamma=m\pi$, where the integer m refer to the Order Number. Secondary maxima occur when $\gamma=h\pi/2N$ with the odd-integer h.

Figure (4-6) illustrates the coherence interference fringes when N=4. Strong constructive coherence interference occurs at the principle maxima, with weaker secondary maxima in between. The N-aperture coherence pattern also includes an envelope $\sin c(2af_x)$. Between two adjacent principle maxima there will be $N-1$ points of minima intensity. The two minima on either side of a principle maximum are

separated by twice the distance of the others. Between the other minima the $\left|\tilde{\Gamma}\right|$ rises again, but the secondary maxima are much smaller than the principle maxima.

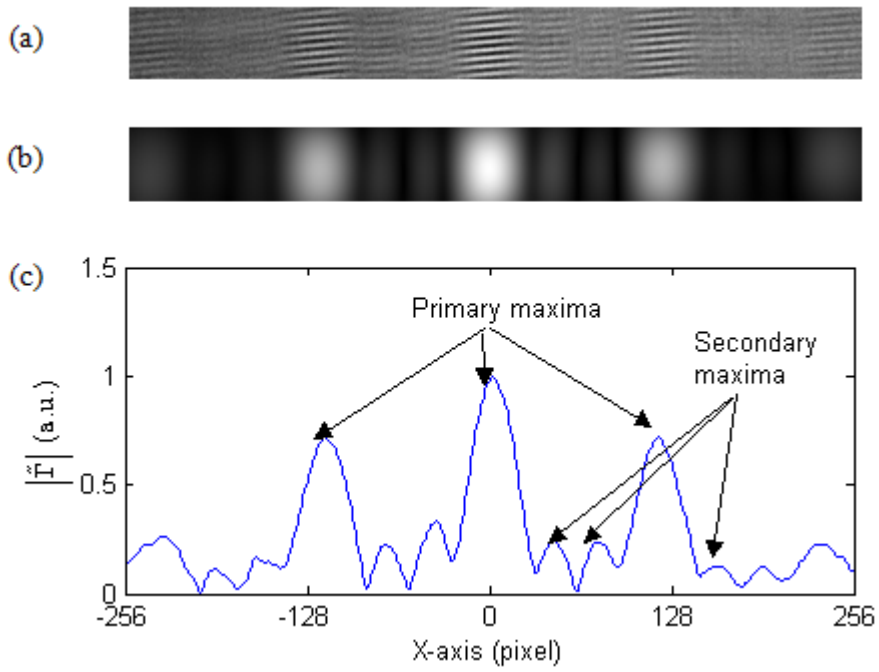

Figure 4-6 Interference of the spatial coherence function from four square apertures sources. (a) Interferograms obtained at $Z=0$. (b) The normalized $\left|\tilde{\Gamma}(x,0,0)\right|$ after reconstruction. (c) Curves of normalized $\left|\tilde{\Gamma}(x,0,0)\right|$ on the x-axis.

4.3 Summary

We introduced various phenomena of interference of spatial coherence functions. Interference fringes of the spatial coherence functions occurs in the region where two or more coherence functions are superposed. In the superposition area, interference fringes of spatial coherence function are parallel. The coherence interference patterns show some similar characters with optical interference, such as: variation of intensity distribution, lack of class, principal maxima and secondary maxima in multi-aperture system, etc.

Reference

[1] M. Born and E. Wolf, *Principles of Optics*, 6th edition (Cambridge University 1980).

[2] J. W. Goodman, *Statistical Optics*, 1st edition (Wiley 2000).

[3] E. Wolf, *Introduction to the Theory of Coherence and Polarization of Light*, 1st edition (Cambridge University Press 2007).

[4] P. H. van Cittert, "Die Wahrscheinliche Schwingungsverteilung in Einer von Einer Lichtquelle Direkt Oder Mittels Einer Linse Beleuchteten Ebene," Physica, 1, 201-210 (1934).

[5] F. Zernike, "The concept of degree of coherence and its application to optical problems," Physica, 5, 785-795 (1938).

[6] M. Takeda, H. Ina and S. Kobayashi, "Fourier-transform method of fringe-pattern analysis for computer-based topography and interferometry," J. Opt. Soc. Am., 72, 156-160 (1982)

Chapter 5

Synthesis of Spatial Coherence Function based on Coherence Holography

Coherence Holography is an unconventional holography technique, where a computer generated hologram is illuminated by spatially incoherent light and the recorded object is reconstructed by the 3D distribution of a spatial coherence function [1-3]. Because of its unique capability of controlling and synthesizing spatial coherence of quasi-monochromatic optical fields in 3D space, coherence holography has been applied for spatial coherence tomography, profilometry, and for the generation of coherence vortices [4-12]. In this chapter, we experimentally demonstrate three particular spatial coherence functions by using coherence holography, and study the propagation characteristic of the coherence functions.

5.1 Backgrounds

In coherence holography, the hologram is recorded by using coherent light. The recording process of coherence holography is exactly same as conventional holography technique. Figure 5-1 shows a recording process of Fourier transform holography.

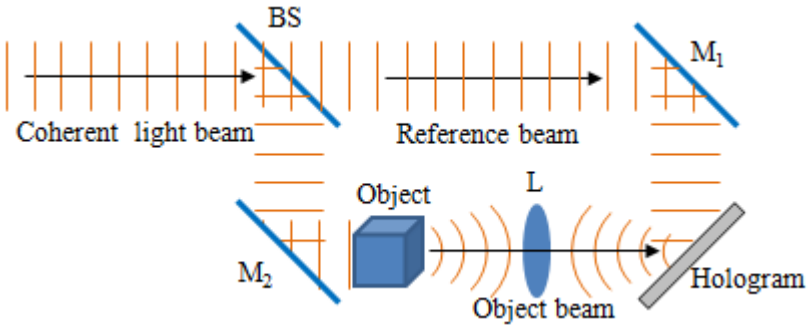

Figure 5-1 Geometry for recording of Fourier transform hologram.

The object field $\tilde{O}(f_x, f_y)$ on the hologram plate is given by the Fourier transform of the object wave $\tilde{o}(x_0, y_0) = |\tilde{o}(x_0, y_0)| \exp[j\varphi_0(x_0, y_0)]$, and the reference field $\tilde{R}(f_x, f_y) = \exp(if_x\theta_x + if_y\theta_y)$ is a plane wave. So the amplitude transmittance of the hologram can be written as

$$H(f_x, f_y) = \left|\tilde{O}(f_x, f_y) + \tilde{R}(f_x, f_y)\right|^2 = \left|\tilde{O}\right|^2 + \left|\tilde{R}\right|^2 + \tilde{O}\cdot\tilde{R}^* + \tilde{O}^*\cdot\tilde{R} \qquad (5\text{-}1)$$

where the asterisk denotes the complex conjugate.

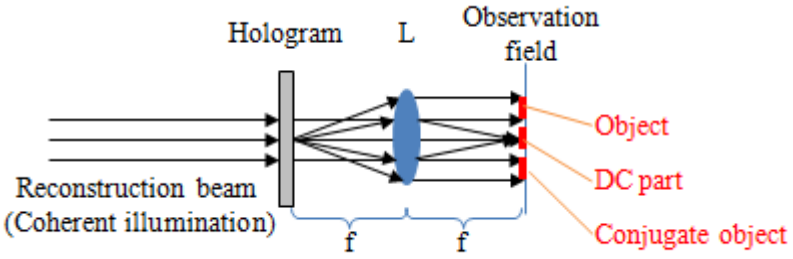

Figure 5-2 Reconstruction of conventional holography: optical image is reconstructed from a Fourier transform hologram with coherent illumination

If we illuminate the hologram $H(f_x, f_y)$ with coherent light, for example, a plane wave $\tilde{C}(f_x, f_y)$ illuminating the hologram at a correct angle, then the wave field

behind the hologram is $\tilde{U}_H(f_x, f_y) = H(f_x, f_y) \cdot \tilde{C}(f_x, f_y) \approx H(f_x, f_y)$, After Fourier transform, we find

$$\tilde{U}_F = FT\{\tilde{U}_H\} = (|\tilde{o}|^2 + 1) + \tilde{o} * \delta(x + \frac{\theta_x}{2\pi}, y + \frac{\theta_y}{2\pi}) + \tilde{o}^* * \delta(x - \frac{\theta_x}{2\pi}, y - \frac{\theta_y}{2\pi}), \qquad (5\text{-}2)$$

where $FT\{\cdots\}$ denotes the Fourier transform.

The first term in Eq. (5-2) is DC part; the second term is the real object with a linear shift while the last term is the conjugate object. Figure 5-2 shows the reconstruction of conventional Fourier transform holography.

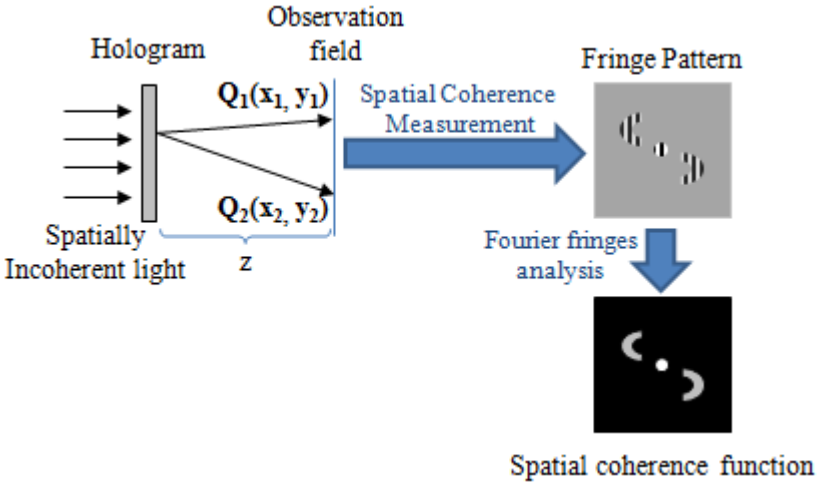

Figure 5-3 Reconstruction of coherence holography: coherence image is reconstructed from a Fourier transform hologram with incoherent illumination.

When the hologram $H(f_x, f_y)$ is illuminated with an incoherent light source, the intensity distribution behind the hologram is given by $I(f_x, f_y) = |H(f_x, f_y)|^2$. The mutual intensity of the observation field can be calculated from the van Cittert – Zernike theorem [13-15]:

$$\Gamma(x_1,x_2;y_1,y_2;z)=\frac{1}{(\lambda z)^2}\exp\{j\frac{\pi}{\lambda z}[(x_2{}^2-x_1{}^2)+(y_2{}^2-y_1{}^2)]\}$$
$$\iint\left|H(f_x,f_y)\right|^2\exp\{j\frac{2\pi}{\lambda z}[f_x(x_1-x_2)+f_y(y_1-y_2)]\}df_xdf_y \quad . \tag{5-3}$$

If we substitute from Eq. (5-1) into Eq. (5-3), then

$$\Gamma=\Gamma_{DC}+\Gamma_{Object}*\delta(x_1-x_2+\frac{\theta_x}{2\pi},y_1-y_2+\frac{\theta_y}{2\pi})$$
$$+\Gamma^*_{Object}*\delta(x_1-x_2-\frac{\theta_x}{2\pi},y_1-y_2-\frac{\theta_y}{2\pi}), \tag{5-4}$$

where the DC term and object term are given by

$$\Gamma_{DC}=\frac{1}{(\lambda z)^2}\exp\{j\frac{\pi}{\lambda z}[(x_2{}^2-x_1{}^2)+(y_2{}^2-y_1{}^2)]\}$$
$$\iint(\left|\tilde{O}\right|^4+4\left|\tilde{O}\right|^2+1)\exp\{j\frac{2\pi}{\lambda z}[f_x(x_1-x_2)+f_y(y_1-y_2)]\}df_xdf_y \tag{5-5}$$

$$\Gamma_{Object}=\frac{1}{(\lambda z)^2}\tilde{o}^2(\frac{x_1-x_2}{\lambda z},\frac{y_1-y_2}{\lambda z})\exp\{j\frac{\pi}{\lambda z}[(x_2{}^2-x_1{}^2)+(y_2{}^2-y_1{}^2)]\} \tag{5-6}$$

Similar to Eq. (5-2), the reconstruction of coherence holography also contains three parts: DC part, real image and conjugate image. The mathematical expression of the real image is given by Eq. (5-6). The mutual intensity $\Gamma_{Object}(x_1,x_2;y_1,y_2;z)$ has a similar distribution to the optical field $\tilde{o}(x_0,y_0)$.

The reconstruction process of coherence holography is completely different from conventional holography. Unlike conventional holography, the reconstructed image of the coherence holography is in the form of coherence function, which cannot be observed by naked eye. Under the help of spatial coherence measurement, such as Young's double-pinhole setup and spatial coherence visualization system, the coherence image can be observed from the contrast of interference fringes.

5.2 Experiments and results

5.2.1 Generation of coherence hologram

The coherence hologram used in our experiment is a computer generated Fourier transform hologram [Appendix A]. As seen in Eq. (5-1), two DC terms $|\tilde{O}|^2$ and $|\tilde{R}|^2$ denote the intensity of the object beam and the intensity of the reference beam, respectively. Both of them become unwanted autocorrelation image. Here, we simplified the construction of the hologram in order to limit the total energy of DC part. Thus the amplitude transmittance of the hologram reduce to

$$H(f_x, f_y) = \tilde{O} \cdot \exp(-if_x\theta_x - if_y\theta_y) + \tilde{O}^* \exp(if_x\theta_x + if_y\theta_y) + C \qquad (5\text{-}7)$$

where C denotes constant. $\tilde{O}(f_x, f_y)$ is the Fourier transform of a gray scale image.

(i) 2D hologram

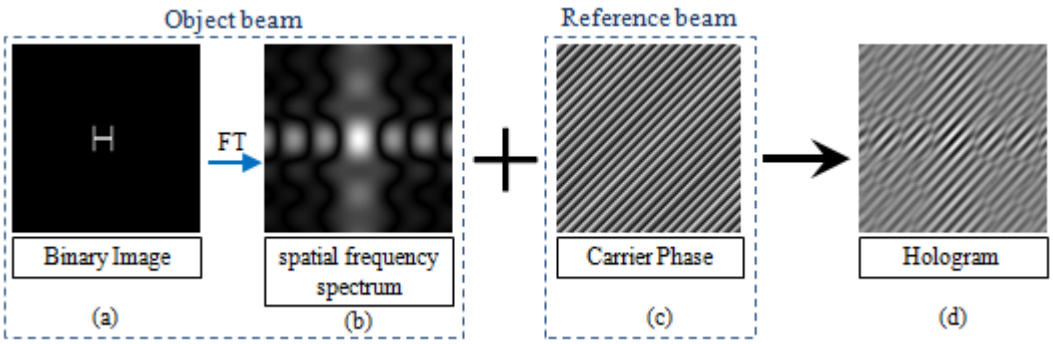

Figure 5-4 Generation of the 2D hologram. (a) Binary object; (b) Fourier transform of the object. (c) Phase distribution of reference beam on the hologram plane; (d) Generated hologram.

Consider a 2D binary image Letter H named $o_H(x, y)$, the optical field on the hologram is given by

$$H_H = FT\{o_H\} \cdot \exp(-if_x\theta_x - if_y\theta_y) + FT\{o_H\}^* \exp(if_x\theta_x + if_y\theta_y) + C \qquad (5\text{-}8)$$

A conceptual diagram of the generation of the hologram is show in Fig. 5-4. It can be seen from Fig.5-4(c), the fringes in the hologram stem from the carrier fringes, and its shape is modulated by the spatial frequency spectrum of the object.

(ii) 3D hologram

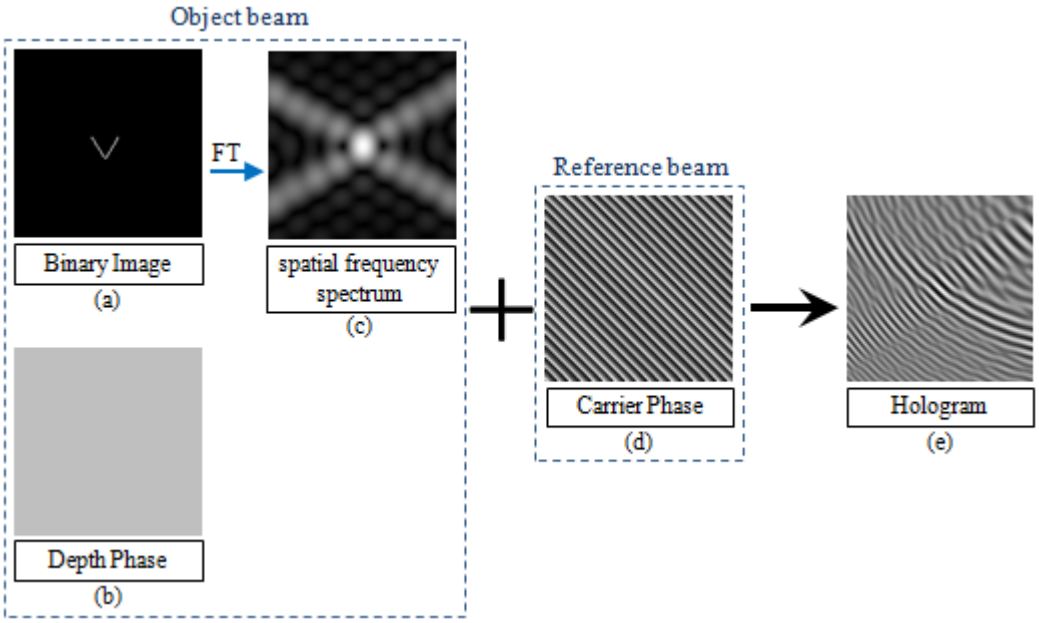

Figure 5-5 Generation of the 3D hologram. (a) Amplitude distribution of the 3D object; (b)Phase distribution of the 3D object; (c) Fourier transform of the amplitude of object. (d) Phase distribution of reference beam on the hologram plane; (e) Generated hologram.

Consider a 3D object Letter V, the amplitude distribution on the projection plane is a binary image $o_V(x,y)$, and the depth of the letter V is Δl. Thus the optical field on the hologram is given by

$$H_V = FT\{o_V\}\exp[-\frac{2j\pi}{\lambda\Delta l}(f_x^{\,2} + f_y^{\,2})]\cdot\exp(-if_x\theta_x - if_y\theta_y) \\ +FT\{o_V\}^*\exp[\frac{2j\pi}{\lambda\Delta l}(f_x^{\,2} + f_y^{\,2})]\exp(if_x\theta_x + if_y\theta_y) + C \tag{5-9}$$

Figure 5-5 shows the generation of the 3D hologram. Similar to Fig.5-4(c), the shape of the hologram in Fig.5-5 (e) is also modulated by the spatial frequency spectrums of corresponding object. Compare with 2D case, the fringes in 3D hologram is not straight, that is because of the quadratic Fresnel phase stem from the axial focal shift by depth Δl .

(iii) Phase hologram

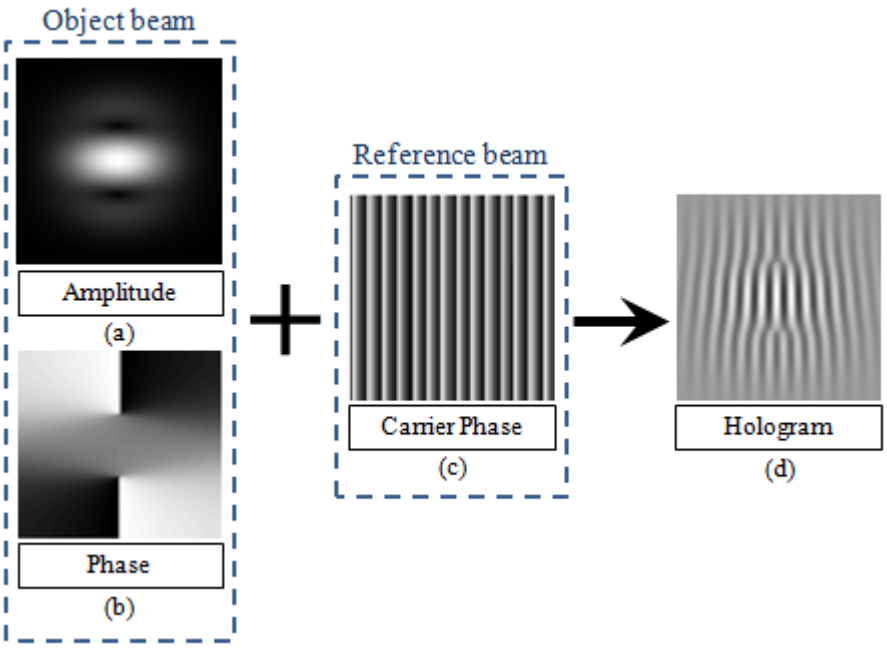

Figure 5-6 Generation of the phase hologram. (a) Amplitude distribution of the object; (b)Phase distribution of the object; (d) Phase distribution of reference beam on the hologram plane; (e) Generated hologram.

Figure 5-6 shows a phase hologram. The amplitude of the object is shown in Fig. 5-6(a) and the phase of the object is shown is Fig. 5-6(b). By using Eq. (5-7), we generate a hologram as seen in Fig. 5-6(d).

5.2.2 Experimental setup for coherence holography

For the purpose of synthesis of some special spatial coherence functions, experiments have been conducted based on the coherence holography technique. The experiment setup is shown in Fig. 5-7.

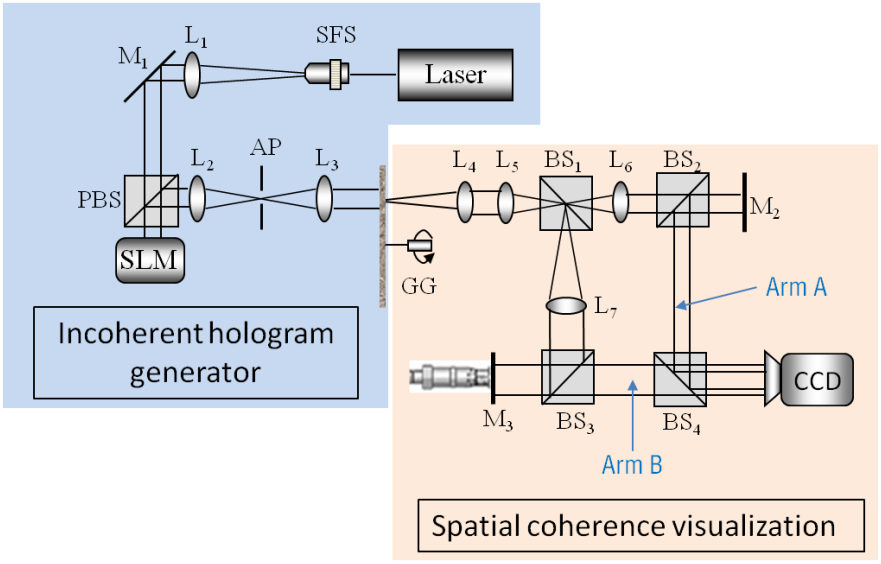

Figure 5-7 Experimental setup for coherence holography. SFS (spatial filter system); PBS (polarizing beam splitter); SLM (Liquid crystal spatial light modulator); AP (aperture); GG (ground glass); BS (Non-polarizing beam splitter). Focal length: f1=150mm, f2=100mm, f3=100mm, f4=100mm. f5=100mm, f6=100mm, f7=125mm

Our system is functionally divided into two parts. Before the rotating ground glass (GG) is an incoherent hologram generator, where a computer-generated hologram is firstly loaded by a spatial light modulator (SLM), secondly filtered by a low-pass 4-F system (L2 and L3) and finally projected into the ground glass. Here we have an incoherent source on the ground glass's back surface. After the ground glass is our spatial coherence visualization system which provide a direct observation for reconstruction of incoherent hologram.

The complex spatial coherence function on the CCD plane is given by

$$\tilde{\Gamma}(\xi,\eta,Z)=\frac{\exp(jk\Delta z)}{\lambda^2 f_4^{\,2} M_A M_B}\iint_S H(f_x,f_y)\exp[\frac{j\pi Z}{\lambda f_4^{\,2}}(f_x^{\,2}+f_y^{\,2})] \exp[-\frac{2j\pi(M_A-M_B)}{\lambda f_4 M_A M_B}(\xi f_x+\eta f_y)]df_x df_y, \quad (5\text{-}10)$$

where Δz is an additional optical path difference introduced by the movable mirror M3, $M_A = f_6/f_5$ is the focal length ratio for the arm A. $M_B = f_7/f_5$ is the focal length ratio for the arm B . $Z(\Delta z)$ is the synthetic optical path difference (SOPD).

$$Z(\Delta z)=\frac{f_5(M_A-M_B)}{M_A M_B}-\frac{z_2+f_6-f_7+\Delta z}{M_B^{\,2}}+\frac{z_2}{M_A^{\,2}}. \quad (5\text{-}11)$$

where z_2 is the optical path length from L_3 to CCD plane.

For simplicity we rewrite Eq. (5-10) as

$$\tilde{\Gamma}(\xi,\eta,Z)\doteq\iint_S H(f_x,f_y)\exp[\frac{j\pi Z}{\lambda f_4^{\,2}}(f_x^{\,2}+f_y^{\,2})]\exp[-2j\pi\alpha(\xi f_x+\eta f_y)]df_x df_y, \quad (5\text{-}12)$$

where $\alpha=\frac{M_A-M_B}{\lambda f_4 M_A M_B}$. Eq. (5-12) can be recognized as a Fourier transformer when the synthetic optical path difference $Z=0$.

5.2.3 Reconstruction of coherence hologram

(i) Reconstruction of 2D coherence hologram

In 2D coherence holography experiment, reconstructed hologram is recorded at coherence focal plane; where the synthetic optical path differences (SOPD) equal to zero.

If we substitute from Eq. (5-8) and $Z=0$ into Eq. (5-12), then the reconstructed coherence hologram is given by

$$\begin{aligned}\tilde{\Gamma}(\xi,\eta,0)=&\frac{1}{\alpha^2}o_H(\frac{\xi}{\alpha}+\frac{\eta}{\alpha})*\delta(\alpha\xi+\frac{\theta_x}{2\pi},\alpha\eta+\frac{\theta_y}{2\pi})\\&+\frac{1}{\alpha^2}o_H(\frac{\xi}{\alpha}+\frac{\eta}{\alpha})^**\delta(\alpha\xi-\frac{\theta_x}{2\pi},\alpha\eta-\frac{\theta_y}{2\pi})+C'\end{aligned}, \tag{5-13}$$

where C' denotes constant coefficient. The first term in Eq.(5-13) represents real object, the second term represents conjugate object, and the last constant represents the DC part. Delta functions represent the shift stemming from the incident angle of the reference beam. Therefore, after reconstruction of coherence holography, the reconstructed image is kind of coherence function, and one of the reconstructed coherence functions has a same shape to the original object.

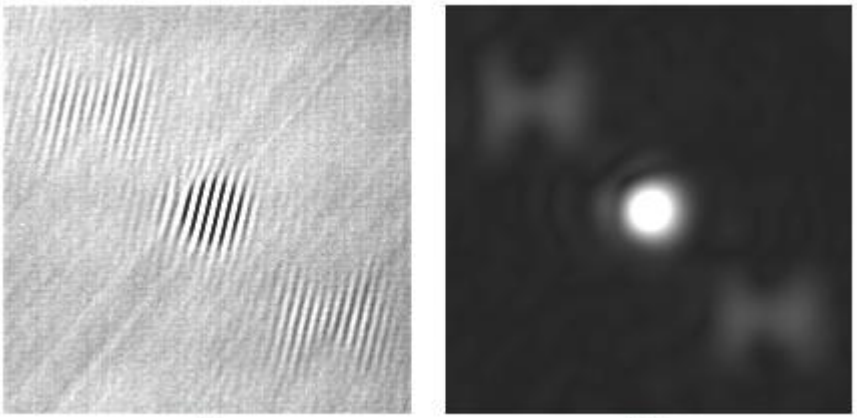

Figure 5-8 Reconstructed images in 2D coherence holography. (a) Interferogram recorded at coherence focal plane; (b) Distribution of the modulus of the spatial coherence function.

The experimental result is shown in Fig. 5-8. Figure 5-8(a) provides the interferogram recorded at the location where $Z=0$. It has an identical structure to the Letter 'H' in the format of the fringe contrast change. By using Fourier fringes analysis [16], we can reconstruct the modulus distribution of the spatial coherence function as shown in

Fig. 5-8(b). The real object lies in the second quadrant, the conjugate object lies in the fourth quadrant, and the bright spot in the middle of the picture denotes the DC part. As seen in Fig. 5-8, the object image Letter 'H' is been reconstructed in the form of coherence function.

(ii) Reconstruction of 3D coherence hologram

In 3D coherence holography experiment, there is quadratic phase factor in object field (as seen in Eq. (5-9)). If we substitute from Eq. (5-9) into Eq. (5-12), then the coherence function in the detector field is given by

$$\begin{aligned}\tilde{\Gamma}(\xi,\eta,Z) = &\iint_S FT\{o_V\}\cdot\exp[-\frac{2j\pi}{\lambda\Delta l}(f_x{}^2+f_y{}^2)]\cdot\exp(-if_x\theta_x-if_y\theta_y)\\ &\exp[\frac{j\pi Z}{\lambda f_4{}^2}(f_x{}^2+f_y{}^2)]\exp[-2j\pi\alpha(\xi f_x+\eta f_y)]df_xdf_y\\ &+\iint_S FT\{o_V\}^*\cdot\exp[\frac{2j\pi}{\lambda\Delta l}(f_x{}^2+f_y{}^2)]\exp(if_x\theta_x+if_y\theta_y) \quad .\\ &\exp[\frac{j\pi Z}{\lambda f_4{}^2}(f_x{}^2+f_y{}^2)]\exp[-2j\pi\alpha(\xi f_x+\eta f_y)]df_xdf_y,\\ &+\iint_S C\exp[\frac{j\pi Z}{\lambda f_4{}^2}(f_x{}^2+f_y{}^2)]\exp[-2j\pi\alpha(\xi f_x+\eta f_y)]df_xdf_y\end{aligned} \tag{5-14}$$

Through an appropriate selection of the location for the movable mirror M_3, we can make $Z=\frac{2f_4{}^2}{\Delta l}$. The quadratic phase factors within the first term of Eq. (5-14) could be compensated. And then, Eq.(5-14) reduces to

$$\begin{aligned}\tilde{\Gamma}(\xi,\eta,Z) = &\frac{1}{\alpha^2}o_V(\frac{\xi}{\alpha}+\frac{\eta}{\alpha})*\delta(\alpha\xi+\frac{\theta_x}{2\pi},\alpha\eta+\frac{\theta_y}{2\pi})\\ &+FT\left\{FT\{o_V\}^*\cdot\exp[\frac{4j\pi}{\lambda\Delta l}(f_x{}^2+f_y{}^2)]\right\}_{\xi,\eta}*\delta(\alpha\xi-\frac{\theta_x}{2\pi},\alpha\eta-\frac{\theta_y}{2\pi}),\\ &+C''\end{aligned} \tag{5-15}$$

where C'' denotes constant coefficient. The first term in Eq.(5-15) represents real object, the second term represents conjugate object with a quadratic phase factor, and

the last constant represents the DC part. Delta functions represent the shift stemming from the incident angle of the reference beam. Therefore, we find the reconstructed object only at $Z = \frac{2 f_4^{\,2}}{\Delta l}$. Compared to conventional holography, coherent holography provides a more simple way to reconstruct depth information (phase information) of the object.

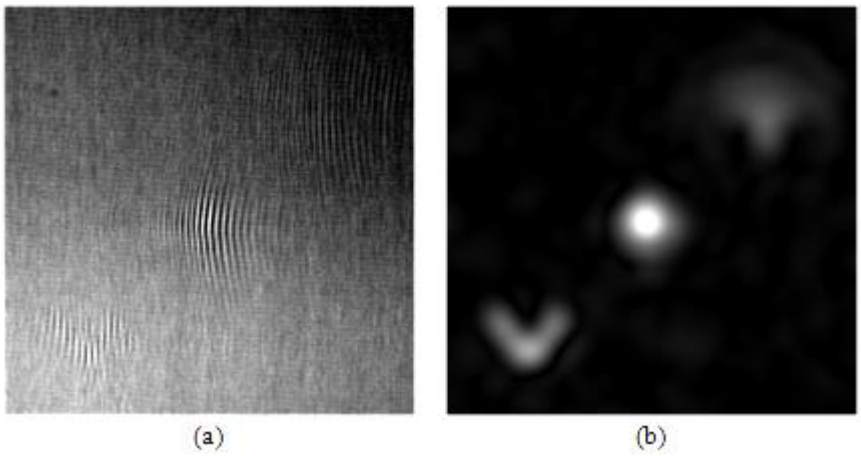

Figure 5-9 Reconstructed images in 3D coherence holography. (a) Interferogram recorded at coherence focal plane; (b) Distribution of the modulus of the spatial coherence function.

The experimental result is shown in Fig. 5-9. Figure 5-9(a) provides the interferogram recorded at the location where $Z = 0.5cm$. Because the interferogram is not recorded at coherence focal plane, so the fringes in the first quadrant and the middle spot are not straight anymore. The fringes in the third quadrant is straight that because the Fresnel phase factor stemming from SOPD and the quadratic phase factor stemming from object cancelled out, leaving a exactly Fourier transform relation. By using Fourier fringes analysis [16], we can reconstruct the modulus distribution of the spatial coherence function as shown in Fig. 5-9(b). The real object lies in the third quadrant; it has an identical structure to the Letter 'V'. The conjugate object lies in the first quadrant. The bright spot in the middle of the picture denotes the DC part.

(iii) Reconstruction of phase type coherence hologram

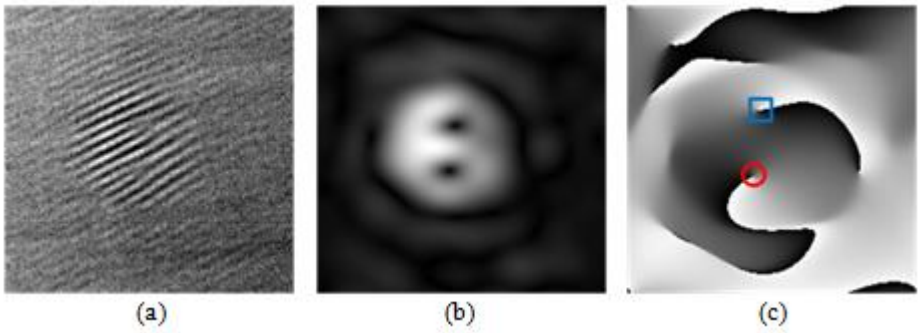

Figure 5-10 Reconstructed images in 2D coherence holography. (a) Interferogram recorded at coherence focal plane; (b) Distribution of the modulus of the spatial coherence function. (b) Phase of the spatial coherence function.

From the results of Experiment 2, we can see that the curvature of the interference fringes representing the phase information of the object. If the phase hologram used in the experiment comprises two phase singularities, then the reproduced image will exhibit two Y-shaped structures. Figure 5-10(a) provides the real object part of the recording interferogram. Two Y-shaped structures are coherence vortexes [6]. By using Fourier fringes analysis [16], we can reconstruct the distribution of the coherence function. The modulus distribution of the spatial coherence function is shown in Fig. 5-10(b). The phase of the spatial coherence function is shown in Fig. 5-10(c). It's also interesting to notice that there are two phase singularities exiting in the field marked by square and circular dot.

By changing the optical path difference, we are able to observe the evolution for the coherence vortexes. Figure 5-11 shows the propagation path of the coherence vortexes in free space. This spiral structure is widely used in fluid mechanics, especially Fujiwara effect.

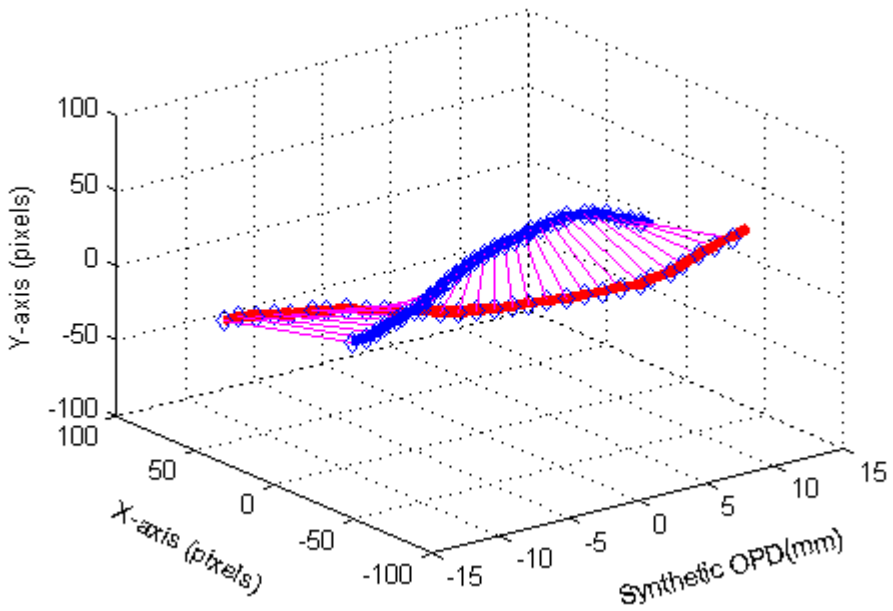

Figure 5-11 Propagation paths of the coherence vortexes in free space

5.3 Summary

In coherence holography, coherence function was treated as an information carrier; object information stored in hologram was restored in coherence function. Coherence holography is a technique that can control a spatial coherence function using an incoherent illuminated hologram. So, we can artificially synthesize spatial coherence functions by using corresponding holograms. In this chapter, we experimentally demonstrate three kinds of spatial coherence functions based on coherence visualization system, e.g., 2D coherence function from amplitude modulation hologram, 3D coherence function from 3D hologram, and coherence vortexes from phase type hologram. The simple experimental method we provided can be used to study the complex, un-straightforward spatial coherence function.

Reference

[1] M. Takeda, W. Wang, Z. Duan and Y. Miyamoto, "Coherence Holography," Opt. Express 23, 9629-9635 (2005)

[2] D. N. Naik, T. Ezawa, Y. Miyamoto and M. Takeda, “Phase-shift coherence holography,” Opt. Lett. 35(10), 1728–1730 (2010).

[3] D. N. Naik, T. Ezawa, Y. Miyamoto and M. Takeda, “3-D coherence holography using a modified Sagnac radial shearing interferometer with geometric phase shift,” Opt. Express 17(13), 10633–10641 (2009).

[4] W. Wang, H. Kozaki, J. Rosen and M. Takeda, "Synthesis of longitudinal coherence function by spatial modulation of an extended light source: a new interpretation and experimental verifications," Appl. Opt. 41, 1962-1971 (2002)

[5] J. Rosen and M. Takeda, “Longitudinal spatial coherence applied for surface profilometry,” Appl. Opt. 39(23), 4107–4111 (2000).

[6] W. Wang, Z. Duan, S. G. Hanson, Y. Miyamoto and M. Takeda, "Experimental study of coherence vortices: Local properties of phase singularities in a spatial coherence function," Phys. Rev. Lett. 96, 073902 (2006).

[7] Z. Duan, Y. Miyamoto and M. Takeda, "Dispersion-free optical coherence depth sensing with a spatial frequency comb generated by an angular spectrum modulator," Opt. Express 14, 12109-12121(2006).

[8] J. Rosen and G. Brooker, "Fluorescence incoherent color holography," Opt. Express 15, 2244-2250 (2007)

[9] J. Rosen and G. Brooker, “Digital spatially incoherent Fresnel holography,” Opt. Lett. 32(8), 912–914 (2007).

[10] R. Kelner and J. Rosen, “Spatially incoherent single channel digital Fourier holography,” Opt. Lett. 37(17), 3723–3725 (2012).

[11] D. N. Naik, T. Ezawa, R. K. Singh, Y. Miyamoto and M. Takeda, "Coherence holography by achromatic 3-D field correlation of generic thermal light with an imaging Sagnac shearing interferometer," Opt. Express 20(18), 19658–19669 (2012).

[12] D. N. Naik, G. Pedrini and W. Osten, "Recording of incoherent-object hologram as complex spatial coherence function using Sagnac radial shearing interferometer and a Pockels cell," Opt. Express 21, 3990-3995 (2013)

[13] M. Born and E. Wolf, *Principles of Optics*, 6th edition (Cambridge University 1980).

[14] P. H. van Cittert, "Die Wahrscheinliche Schwingungsverteilung in Einer von Einer Lichtquelle Direkt Oder Mittels Einer Linse Beleuchteten Ebene," Physica, 1, 201-210 (1934).

[15] F. Zernike, "The concept of degree of coherence and its application to optical problems," Physica, 5, 785-795 (1938).

[16] M. Takeda, H. Ina and S. Kobayashi, "Fourier-transform method of fringe-pattern analysis for computer-based topography and interferometry," J. Opt. Soc. Am., 72, 156-160 (1982)

Chapter 6

Experimental Demonstration of the van Cittert-Zernike Theorem for Random Electromagnetic Fields

In scalar coherence theory, the van Cittert-Zernike theorem plays an important role for studying the propagation processes of partially coherent fields [1-4]. For more general applications, the unified theory of coherence and polarization has recently been used to characterize the random electromagnetic fields [5-11]. Moreover the van Cittert-Zernike theorem has been extended for the vector field successfully [12-14]. In this chapter, we address this topic and introduce a novel optical device to demonstrate the vectorial van Cittert-Zernike theorem. The experimental results show that the mutual intensity matrix of the electromagnetic field produced by a polarized incoherent source increases on propagation whereas the degree of the polarization remains unchanged.

6.1 Introduction

In the history of optics, the subjects of coherence and polarization have been developed independently. Coherence arises from correlation between fluctuations at two or more points in space. Polarization, on the other hand, is a manifestation of fluctuating components of the electric filed at a single point. When we discuss the

coherence properties of the field, some simplified models have been used by treating the optical field as scalar fields, thus ignoring their polarization properties arising from the vector nature of the electromagnetic field. Recently, a unification of the phenomena of coherence and polarization by taking the vector nature into account for a broad class of vectors fields has been developed and attracted a lot of interests [5]. A proper description of the polarization properties of random electromagnetic waves relies on the concept of the cross-spectral density matrix which makes it possible to predict the changes in the state of polarization of a partially coherent electromagnetic beam as the waves on propagate. We are interested here in quasi-monochromatic beam. In the simplest situation, the 2×2 mutual intensity matrix (also known as the beam coherence polarization matrix), is sufficient to yield a complete account of the second-order statistical properties of the quasi-monochromatic field [15,16]. In the past few years, a lot of work has been done to describe an extension of the van Cittert-Zernike theorem in terms of the 2×2 matrix to examine coherence and polarization properties of the field generated by a partially polarized incoherent electromagnetic field [12-14]. In this chapter, we would like to demonstrate the unified theory of coherence and polarization of random electromagnetic beams by an optical experiment, which may be regarded as a tensor version of van Cittert-Zernike theorem.

6.2 Principle

6.2.1 The van Cittert-Zernike theorem for electromagnetic filed

Consider a stochastic stationary electromagnetic field. We assume that the field is a beam, which propagates close to the z-axis into free space, as shown in Fig. 6-1. A partially polarized, spatial incoherent, quasi-monochromatic source is located in the plane z=0. W describes the correlation of signals received at any two different points in space. The superscripts (0) and (z) on the symbol $\vec{\vec{W}}$ denote the beam on the source plan z=0 and the beam propagating after a distance z, respectively. Let $\tilde{E}_{\alpha}^{(0)}(x_0, y_0)$ and $\tilde{E}_{\alpha}^{(z)}(x, y)$ be the orthogonal components of the fluctuation electric field $(\alpha = x, y)$ at source plane $z = 0$ and any transverse plane $z > 0$, respectively. Under the paraxial

approximation and independent propagation of two polarization components of an electric vector field, the field in plane $\Sigma^{(z)}(x,y,z)$ is given by:

$$\tilde{E}_{\alpha}^{(z)}(x,y)=\frac{1}{\lambda z}\exp(j\frac{2\pi}{\lambda}z)\iint_{\Sigma_0}\tilde{E}_{\alpha}^{(0)}(x_0,y_0)\exp\{j\frac{\pi}{\lambda z}[(x_0-x)^2+(y_0-y)^2]\}dx_0dy_0. \quad (6\text{-}1)$$

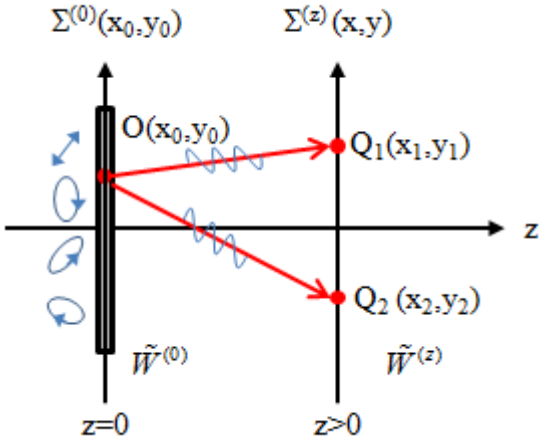

Figure 6-1 Illustration of the geometry for the vectorial van Cittert-Zernike theorem.

The second order statistical properties of the electromagnetic field are conveniently described by a 2×2 mutual intensity matrix $\tilde{W}$ [5]. $\tilde{W}^{(z)}$ denotes the mutual intensity matrix of the observation field $z=constant$. We assume that the optical field to be quasi-monochromatic. And the corresponding mutual intensity matrix of the electric field is reduced to:

$$\tilde{W}^{(z)}(x_1,x_2;y_1,y_2;z)=\begin{bmatrix}\tilde{W}_{xx}^{(z)}(x_1,x_2;y_1,y_2;z) & \tilde{W}_{xy}^{(z)}(x_1,x_2;y_1,y_2;z)\\ \tilde{W}_{yx}^{(z)}(x_1,x_2;y_1,y_2;z) & \tilde{W}_{yy}^{(z)}(x_1,x_2;y_1,y_2;z)\end{bmatrix}, \quad (6\text{-}2)$$

where

$$\tilde{W}_{\alpha\beta}^{(z)}(x_1,x_2;y_1,y_2;z)=\left\langle E_{\alpha}^{(z)*}(x_1,y_1,z)E_{\beta}^{(z)}(x_2,y_2,z)\right\rangle. \quad \alpha,\beta=x,y \quad (6\text{-}3)$$

Here and in the following, α and β denote the subscripts x or y. $\tilde{E}_x$ and $\tilde{E}_y$ are the components of the complex electric field vector in the x- or y- direction, respectively. The asterisk denotes the complex conjugate, and the angular bracket indicates a time average. The superscripts (0) and (z) on the symbol $\tilde{W}$ and $\tilde{E}$ denote the beam on the source plan $z=0$ and the beam propagating after a distance z, respectively.

If we substitute from Eq. (6-1) into Eq. (6-3), then

$$\tilde{W}_{\alpha\beta}^{(z)}(x_1,x_2;y_1,y_2;z)=\frac{1}{(\lambda z)^2}\exp\{j\frac{\pi}{\lambda z}[(x_2{}^2-x_1{}^2)+(y_2{}^2-y_1{}^2)]\}$$
$$\iint_{\Sigma_0}\tilde{E}_\alpha^{(0)*}(x_0,y_0)\tilde{E}_\beta^{(0)}(x_0,y_0)\exp\{j\frac{2\pi}{\lambda z}[x_0(x_1-x_2)+y_0(y_1-y_2)]\}dx_0dy_0 \quad . \qquad (6\text{-}4)$$

$\tilde{W}^{(0)}$ and $\tilde{W}^{(z)}$ denote the mutual intensity matrix of the source field $z=0$ and the observation field $z=constant$, respectively.

Consider the spatially incoherent source, the mutual intensity matrix $\tilde{W}^{(0)}$ becomes the Jones matrix:

$$\tilde{W}^{(0)}=\tilde{J}^{(0)}\equiv\begin{bmatrix}J_{xx}^{(0)} & \tilde{J}_{xy}^{(0)}\\ \tilde{J}_{yx}^{(0)} & J_{yy}^{(0)}\end{bmatrix}=\begin{bmatrix}\left\langle E_x^{(0)*}(x_0,y_0)E_x^{(0)}(x_0,y_0)\right\rangle & \left\langle E_x^{(0)*}(x_0,y_0)E_y^{(0)}(x_0,y_0)\right\rangle\\ \left\langle E_y^{(0)*}(x_0,y_0)E_x^{(0)}(x_0,y_0)\right\rangle & \left\langle E_y^{(0)*}(x_0,y_0)E_y^{(0)}(x_0,y_0)\right\rangle\end{bmatrix}. \quad (6\text{-}5)$$

By substituting Eq. (6-5) into Eq. (6-4), we obtain

$$\tilde{W}_{\alpha\beta}^{(z)}(x_1,x_2;y_1,y_2;z)=\frac{1}{(\lambda z)^2}\exp\{j\frac{\pi}{\lambda z}[(x_2{}^2-x_1{}^2)+(y_2{}^2-y_1{}^2)]\}$$
$$\iint_{\Sigma^{(0)}}\tilde{J}_{\alpha\beta}^{(0)}\exp\{j\frac{2\pi}{\lambda z}[x_0(x_1-x_2)+y_0(y_1-y_2)]\}dx_0dy_0 \quad . \qquad (6\text{-}6)$$

Equation (6-6) represents every element the vector generation of the van Cittert-Zernike theorem. For the whole field of the beam, the mutual intensity matrix of the

electromagnetic field from an incoherent monochromatic source is equal to the Fourier transforms of the Jones matrix of the source:

$$\tilde{W}^{(z)}(x_1,x_2;y_1,y_2;z)=\frac{1}{(\lambda z)^2}\exp\{j\frac{\pi}{\lambda z}[({x_2}^2-{x_1}^2)+({y_2}^2-{y_1}^2)]\}\\ \iint_{\Sigma^{(0)}}\tilde{J}^{(0)}\exp\{j\frac{2\pi}{\lambda z}[x_0(x_1-x_2)+y_0(y_1-y_2)]\}dx_0dy_0 \tag{6-7}$$

6.2.2 The spectral degree of coherence

Consider the observation plane $\Sigma^{(z)}$, when $x_1=x_2$ and $y_1=y_2$, the diagonal elements in Eq. (6-2) change to

$$S_\alpha^{(z)}(x_1,y_1,z)=W_{\alpha\alpha}^{(z)}(x_1,x_2;y_1,y_2;z)\delta(x_1-x_2,y_1-y_2)=\left\langle\left|E_\alpha^{(z)}(x_1,y_1,z)\right|^2\right\rangle. \tag{6-8}$$

$S_\alpha^{(z)}(x_1,y_1,z)$ represent the intensities of the components of the electric field at point Q_1 [5].

The intensity of the whole field of the beam is given by [9]

$$\begin{aligned}S^{(z)}(x_1,y_1,z)&=Tr[\tilde{W}^{(z)}(x_1,x_2;y_1,y_2;z)\delta(x_1-x_2,y_1-y_2)]\\&=S_\alpha^{(z)}(x_1,y_1,z)+S_\beta^{(z)}(x_1,y_1,z)\end{aligned}, \tag{6-9}$$

where Tr denotes the trace of the matrix.

And the degree of coherence of each element in $\tilde{W}$ is defined as the correlation coefficients $\tilde{\mu}_{\alpha\beta}$ which represents the correlation between the component $\tilde{E}_\alpha(x_1,y_1)$ at the point $Q_1(x_1,y_1)$ and the component $\tilde{E}_\beta(x_2,y_2)$ at the point $Q_2(x_2,y_2)$ [7].

$$\tilde{\mu}_{\alpha\beta}^{(z)}(x_1,x_2;y_1,y_2;z)=\frac{\tilde{W}_{\alpha\beta}^{(z)}(x_1,x_2;y_1,y_2;z)}{\sqrt{S_{\alpha}^{(z)}(x_1,y_1,z)}\sqrt{S_{\beta}^{(z)}(x_2,y_2,z)}}. \tag{6-10}$$

The mutual degree of coherence of the electric field of the beam at the two points $Q_1(x_1,y_1)$ and $Q_2(x_2,y_2)$, is defined by

$$\tilde{\mu}^{(z)}(x_1,x_2;y_1,y_2;z)=\frac{Tr\tilde{W}^{(z)}(x_1,x_2;y_1,y_2;z)}{\sqrt{S^{(z)}(x_1,y_1,z)}\sqrt{S^{(z)}(x_2,y_2,z)}}. \tag{6-11}$$

Consider the source plane $\Sigma^{(0)}(x_0,y_0)$, the diagonal elements in the Jones matrix Eq. (6-5) can be rewritten as

$$J_{\alpha\alpha}^{(0)}(x_0,y_0)=\left\langle\left|E_{\alpha}^{(0)}(x_0,y_0)\right|^2\right\rangle=S_{\alpha}^{(0)}(x_0,y_0). \tag{6-12}$$

The intensity of the source field is given by

$$S^{(0)}(x_0,y_0)=S_x^{(0)}(x_0,y_0)+S_y^{(0)}(x_0,y_0)=TrJ^{(0)}(x_0,y_0). \tag{6-13}$$

On substituting for the details of the correlation coefficients $\tilde{\mu}_{\alpha\beta}^{(z)}$ from Eqs. (6-6), (6-8) and (6-12) into Eq. (6-10), we find

$$\tilde{\mu}_{\alpha\beta}^{(z)}(x_1,x_2;y_1,y_2;z)=\frac{\iint_{\Sigma^{(0)}}\tilde{J}_{\alpha\beta}^{(0)}\exp\{j\frac{2\pi}{\lambda z}[x_0(x_1-x_2)+y_0(y_1-y_2)]\}dx_0dy_0}{\left(\iint_{\Sigma^{(0)}}S_{\alpha}^{(0)}dx_0dy_0\iint_{\Sigma^{(0)}}S_{\beta}^{(0)}dx_0dy_0\right)^{1/2}}. \tag{6-14}$$

According to the Cauchy–Schwarz inequality, it can be easily proved that

$$\left|\tilde{J}_{\alpha\beta}^{(0)}\right|^2\le S_{\alpha}^{(0)}S_{\beta}^{(0)}, \tag{6-15}$$

where $\tilde{J}_{\alpha\beta}^{(0)}$ represent the degree of the cross- correlation between the α-component at point Q_1 and the β-component at point Q_2. It is obvious that $0 \le \left|\tilde{\mu}_{\alpha\beta}^{(z)}\right| \le 1$.

Let us consider diagonal elements in Eq. (6-15),

$$\tilde{\mu}_{\alpha\alpha}^{(z)} = \frac{\iint_{\Sigma^{(0)}} S_{\alpha}^{(0)} \exp\{j\frac{2\pi}{\lambda z}[x_0(x_1-x_2)+y_0(y_1-y_2)]\}dx_0dy_0}{\iint_{\Sigma^{(0)}} S_{\alpha}^{(0)}dx_0dy_0}. \tag{6-16}$$

By substituting Eqs. (6-7), (6-9), (6-13) and (6-16) into Eq. (6-11), we find

$$\tilde{\mu}^{(z)} = \frac{\tilde{\mu}_{xx}^{(z)}\iint_{\Sigma^{(0)}} S_x^{(0)}dx_0dy_0 + \tilde{\mu}_{yy}^{(z)}\iint_{\Sigma^{(0)}} S_y^{(0)}dx_0dy_0}{\iint_{\Sigma^{(0)}}(S_x^{(0)}+S_y^{(0)})dx_0dy_0}. \tag{6-17}$$

From Eq.(6-17), we can summarize that, only when $\tilde{\mu}_{xx}^{(z)} = \tilde{\mu}_{yy}^{(z)} = 1$, the mutual degree of coherence $\tilde{\mu}^{(z)} = 1$. The electromagnetic field is completely coherent only when its components are both completely coherent.

6.2.3 The degree of polarization

The degree of polarization $P(x_1, y_1, z)$ at point $Q_1(x_1, y_1)$ is given by [5]

$$P(x_1,y_1,z) = \left(1 - \frac{4Det\tilde{W}(x_1,x_1;y_1,y_1;z)}{\left[Tr\tilde{W}(x_1,x_1;y_1,y_1;z)\right]^2}\right)^{1/2}. \tag{6-18}$$

According to Eq. (6-6), and let

$$I_{\alpha\beta} = \iint_{\Sigma^{(0)}} \tilde{J}_{\alpha\beta}^{(0)}dx_0dy_0. \tag{6-19}$$

Then, the degree of polarization $P(x_1, y_1, z)$ reduces to

$$P(x_1, y_1, z) = \left(1 - \frac{4(IxxIyy - |Ixy|^2)}{(Ixx + Iyy)^2}\right)^{1/2}. \qquad (6\text{-}20)$$

Equations (6-20) show that the degree of polarization of a completely incoherent electromagnetic field doesn't changed on their propagation [13].

6.3 Experiment

To demonstrate the vector van Cittert-Zernike theorem, an experiment has been conducted based on the coherence visualization system.

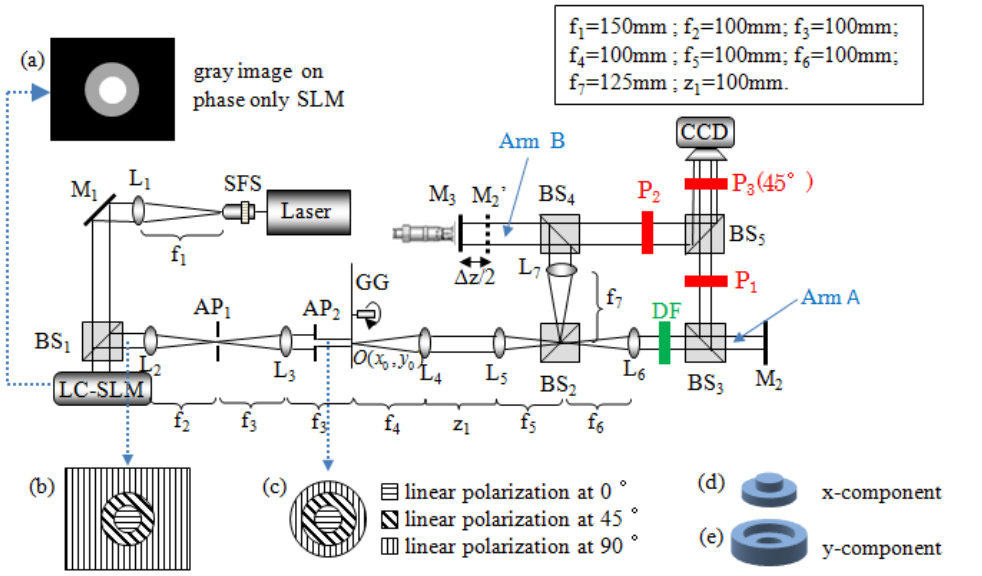

Figure 6-2 Schematic representation of the experimental setup for the measurement of the mutual intensity matrix from a monochromatic, spatially incoherent, polarized source.

The experiment setup is shown in Fig. 6-2. In our experiment, light from a He-Ne laser is first expanded by a spatial filter system (SFS) and then collimated by lens L_1 to illuminate the liquid crystal spatial light modulator (LC-SLM). The SLM using in our system is a phase modulating device, which can only change the polarization

properties of the incident beam whereas the intensity of the incident beam remains unchanged. The image we loaded in SLM is shown in Fig. 2-2(a). After SLM, we get a completely polarized beam with varied polarization and uniform intensity distribution, as shown in Fig. 2-2(b). By using the aperture AP_2, we can change the diameter of the incident laser beam (see Fig. 2-2(c)). And then, the circular beam is projected on a rapidly rotating ground glass (GG) to generate an extended, monochromatic, spatially incoherent, completed polarized source. Finally, a modified Mach-Zehnder interferometer is illuminated by this incoherent polarized source. Let polarizer P1 and P2 be chosen to transmit only x component and only y component of the incident beam, respectively. And let density filter (DF) be chosen to balance the intensities of the two optical fields at the opposite arms of the interferometer with different magnifications f_6/f_5 and f_7/f_5. The interference fringes recorded by the CCD image sensor are the results of superposition of the two mutually displaced optical fields. And the distributions of the mutual intensity matrix can be observed from the fringe visibility and fringe orientation.

The distributions of the two optical fields from the two arms of the interferometer can be calculated from Fresnel diffraction integrals. The point source $O(x_o, y_o)$ with its complex amplitude $\tilde{E}^{(0)}$ propagates through the arm A, and creates a field distribution $\tilde{E}^{(A)}$ on CCD plane

$$\begin{aligned}\tilde{E}_\alpha^{(A)}(x,y) = &-\frac{\tilde{E}_\alpha^{(0)}(x_o,y_o)}{j\lambda f_4 M_A}\exp[jk(z_1+f_4+f_5+f_6+z_2)] \\ &\exp[\frac{j\pi}{\lambda f_4}(x_o{}^2+y_o{}^2)(1-\frac{z_1}{f_4}+\frac{f_5+f_6}{M_A f_4}-\frac{z_2}{M_A{}^2 f_4})]\exp[-\frac{2j\pi}{\lambda M_A f_4}(xx_o+yy_o)],\end{aligned} \tag{6-21}$$

where z_1 is the optical path length from L_4 to L_5 plane, z_2 is the optical path length from L_6 to CCD plane and $M_A = f_6/f_5$ is the focal length ratio for the arm A. Similarly, the field distribution from the same point source propagating through the arm B is

$$\tilde{E}_{\alpha}^{(B)}(x,y) = -\frac{\tilde{E}_{\alpha}^{(0)}(x_o,y_o)}{j\lambda f_4 M_B}\exp[jk(z_1+f_4+f_5+f_6+z_2+\Delta z)]$$
$$\exp[\frac{j\pi}{\lambda f_4}({x_o}^2+{y_o}^2)(1-\frac{z_1}{f_4}+\frac{f_5+f_6}{M_B f_4}-\frac{z_2+f_6-f_7+\Delta z}{{M_B}^2 f_4})]\exp[-\frac{2j\pi}{\lambda M_B f_4}(xx_o+yy_o)], \quad (6\text{-}22)$$

where Δz is an additional optical path difference introduced by the movable mirror M_3, and $M_B = f_7/f_5$ is the focal length ratio for the arm B.

The fields $\tilde{E}^{(A)}$ and $\tilde{E}^{(B)}$ from different arms of the interferometer are superimposed to form interference fringes on the CCD image sensor. Because each point source is completely incoherent to any other points on the source, the overall intensity on the image sensor is the sum of the fringe intensities obtained from all of the point sources. After some straightforward algebra, this intensity distribution becomes:

$$I_{\alpha\beta} = \iint_s \left|\tilde{E}_{\alpha}^{(A)} + \tilde{E}_{\beta}^{(B)}\right|^2 dx_o dy_o = S_{\alpha}^{(A)} + S_{\beta}^{(B)} + 2\,\mathrm{Re}\{\tilde{W}_{\alpha\beta}\}, \quad (6\text{-}23)$$

where

$$S_{\alpha}^{(A)} = \iint_s \tilde{E}_{\alpha}^{*(A)}\tilde{E}_{\alpha}^{(A)}dx_o dy_o\ , \quad (6\text{-}24)$$

$$S_{\beta}^{(B)} = \iint_s \tilde{E}_{\beta}^{*(B)}\tilde{E}_{\beta}^{(B)}dx_o dy_o\ , \quad (6\text{-}25)$$

$$\tilde{W}_{\alpha\beta}(x,y,Z) = \iint_s \tilde{E}_{\alpha}^{*(A)}\tilde{E}_{\beta}^{(B)}dx_o dy_o\ . \quad (6\text{-}26)$$

$\mathrm{Re}\{\cdots\}$ denotes the real part, and $S_{\alpha}^{(A)}$ and $S_{\beta}^{(B)}$ are the averaged light intensities of the components of the electric field through the arm A and arm B, respectively. The complex function $\tilde{W}_{\alpha\beta}$ in the last term of Eq. (6-23) will be recognized as the mutual intensities of the electromagnetic field.

By substituting Eqs. (6-21) and (6-22) into Eq. (6-26), we obtain

$$\tilde{W}_{\alpha\beta}(x,y,Z)=\frac{\exp(jk\Delta z)}{\lambda^2 f_4{}^2 M_A M_B}\iint_S \tilde{E}_\alpha^{*(0)}\tilde{E}_\beta^{(0)}\exp[\frac{j\pi Z}{\lambda f_4{}^2}(x_0{}^2+y_0{}^2)] \exp[-\frac{2j\pi(M_A-M_B)}{\lambda f_4 M_A M_B}(xx_0+yy_0)]dx_0dy_0, \quad (6\text{-}27)$$

Z being the synthetic optical path difference:

$$Z=\frac{f_5(M_A-M_B)}{M_A M_B}-\frac{z_2+f_6-f_7+\Delta z}{M_B{}^2}+\frac{z_2}{M_A{}^2}. \quad (6\text{-}28)$$

Through an appropriate selection of the location for the movable mirror M3, we are able to make the synthetic optical path difference $Z=0$. The quadratic phase factors within the integrand in Eq. (6-4) disappear, leaving an exact Fourier transform relation:

$$\tilde{W}_{\alpha\beta}(x,y)=\frac{\exp(jk\Delta z)}{\lambda^2 f_4{}^2 M_A M_B}\iint_S \tilde{J}_{\alpha\beta}^{(0)}\exp[-\frac{2j\pi(M_A-M_B)}{\lambda f_4 M_A M_B}(xx_0+yy_0)]dx_0dy_0. \quad (6\text{-}29)$$

The spatial coherence function in Eq. (6-29) expresses the vector van Cittert-Zernike theorem, indicating the mutual intensity matrix proportional to the Fourier transforms of the source intensity distribution.

The results of our experiment are shown in Fig. 6-3. In the first group, Fig. 6-3(1) is the recorded interferograms at CCD plane, where $Z=0$, and the two polarizers P1 and P2 are both horizontal. By using Fourier fringes analysis [17], we can reconstruct the first element $\tilde{W}_{xx}$ in the mutual intensity matrix. The modulus distribution of $\tilde{W}_{xx}$ is shown in Fig. 6-3(2) and the phase distribution $\tilde{W}_{xx}$ is shown in Fig. 6-3(3). $\tilde{W}_{xx}$ has a similar structure to the first kind, first order Bessel function. That is because the x component of our source is formed by a stepped circular (see Fig. 6-2(d)). The fourth group in Fig. 6-3 is the results of $\tilde{W}_{yy}$, where $Z=0$, and the two polarizers P1 and P2 are both vertical. Fig. 6-3(11) has a set of concentric rings, which is the resultant of

the Fouries transform of a stepped ring source (see Fig. 6-2(e)). The results of anti-diagonal elements of the matrix are shown in the second and third group of Fig. 6-3, respectively. $\tilde{W}_{xy}$ and $\tilde{W}_{yx}$ have similar modulus distributions (as shown in Fig. 6-3(5) and (8)) and inverse phase distributions (as shown in Fig. 6-3(6) and (9)). The light emerges from a completely incoherent source becomes partially coherent on propagation, and the relationship between the mutual intensity matrix of observation field and the source is an identical Fourier transform.

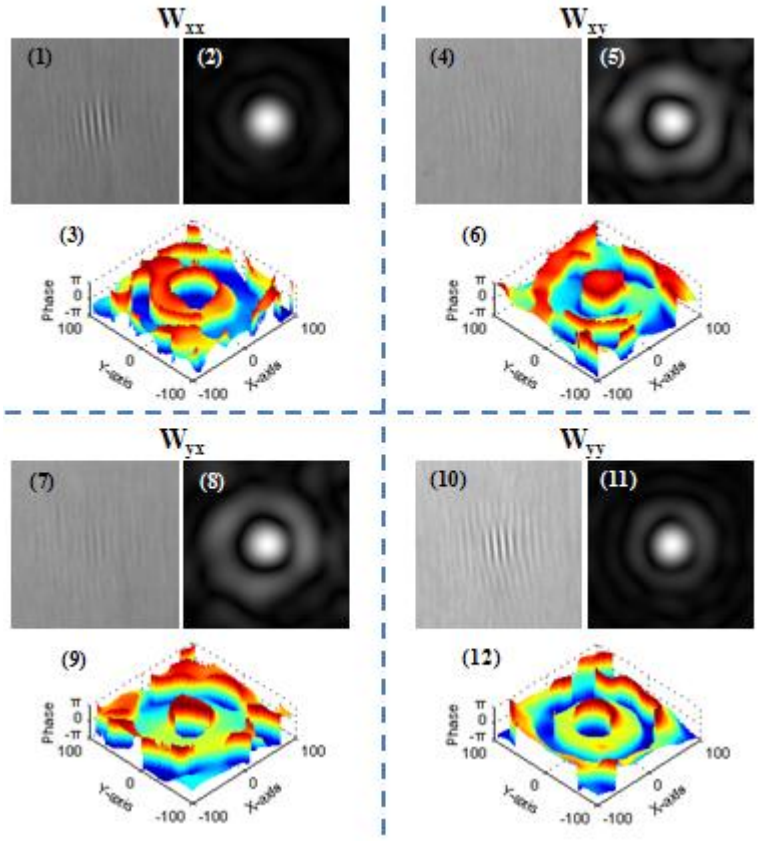

Figure 6-3 The recorded interferograms for each elements in mutual coherence matrix and the reconstructed mutual coherence intensity with their phase distributions. First group: (1), (2) and (3), corresponds $\tilde{W}_{xx}$; second group: (4), (5) and (6), corresponds $\tilde{W}_{xy}$; third group: (7), (8) and (9), corresponds $\tilde{W}_{yx}$ and fourth group: (10), (11) and (12), corresponds $\tilde{W}_{yy}$

From the reconstructed mutual intensity matrix, the degree of the polarization of the observation field can be obtained through Eq. (6-18). As shown in Fig. 6-4, the value of the degree of polarization approximately equal to 1, and the error is less than 4%. It means the degree of polarization of the electromagnetic beam doesn't change on their propagation.

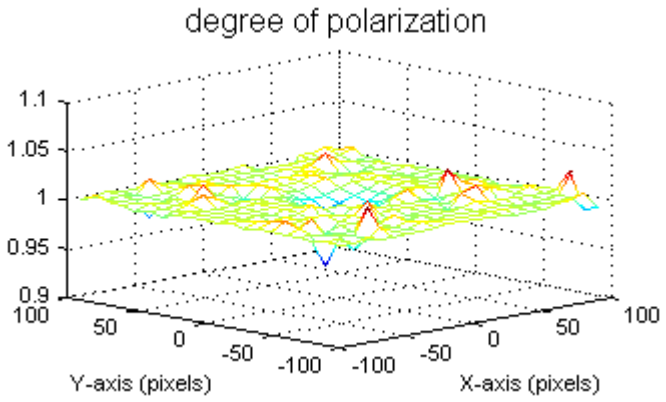

Figure 6-4 Degree of the polarization of the observation field

6.4 Discussion

If there is more than one source in the observation field or the field angle of two interference beam are completely different, off-diagonal elements of the beam coherence-polarization matrix ($\tilde{W}_{xy}$ and $\tilde{W}_{yx}$) are not conjugate. We should measure all of the four elements in the BCP matrix for a completely description.

Figure 6-5 illustrates the geometry for the vectorial van Cittert-Zernike theorem. The primary source S_1 with its complex amplitude $\tilde{E}_1^{(0)}$ propagates a distance z, and creates a field distribution $\tilde{E}_{S1}$ on secondary source plane; the primary source S_2 with its complex amplitude $\tilde{E}_2^{(0)}$ propagates a distance z, and creates a field distribution $\tilde{E}_{S2}$ on secondary source plane

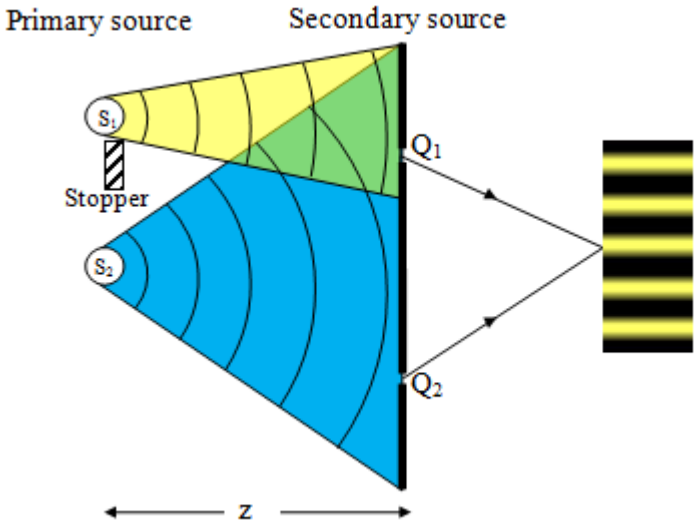

Figure 6-5 Schematic representation of the measurement of the spatial coherence function.

Taking into account all the contributions of the wavefields of the primary sources, the complex amplitude distribution at point Q1 is

$$\tilde{E}(Q_1)=\begin{bmatrix}\tilde{E}^{(x)}(Q_1)\\ \tilde{E}^{(y)}(Q_1)\end{bmatrix}=\begin{bmatrix}\tilde{E}^{(x)}_{S1}(Q_1)+\tilde{E}^{(x)}_{S2}(Q_1)\\ \tilde{E}^{(y)}_{S1}(Q_1)+\tilde{E}^{(y)}_{S2}(Q_1)\end{bmatrix}. \tag{6-30}$$

The complex amplitude distribution at point Q2 is

$$\tilde{E}(Q_2)=\begin{bmatrix}\tilde{E}^{(x)}(Q_2)\\ \tilde{E}^{(y)}(Q_2)\end{bmatrix}=\begin{bmatrix}\tilde{E}^{(x)}_{S2}(Q_2)\\ \tilde{E}^{(y)}_{S2}(Q_2)\end{bmatrix}. \tag{6-31}$$

The beam coherence-polarization (BCP) matrix is defined as

$$\begin{bmatrix}\tilde{W}_{xx}(Q_1,Q_2) & \tilde{W}_{xy}(Q_1,Q_2)\\ \tilde{W}_{yx}(Q_1,Q_2) & \tilde{W}_{yy}(Q_1,Q_2)\end{bmatrix}$$
$$=\begin{bmatrix}\left\langle \tilde{E}^{(x)*}_{S1}(Q_1)\tilde{E}^{(x)}_{S2}(Q_2)+\tilde{E}^{(x)*}_{S2}(Q_1)\tilde{E}^{(x)}_{S2}(Q_2)\right\rangle & \left\langle \tilde{E}^{(x)*}_{S1}(Q_1)\tilde{E}^{(y)}_{S2}(Q_2)+\tilde{E}^{(x)*}_{S2}(Q_1)\tilde{E}^{(y)}_{S2}(Q_2)\right\rangle\\ \left\langle \tilde{E}^{(y)*}_{S1}(Q_1)\tilde{E}^{(x)}_{S2}(Q_2)+\tilde{E}^{(y)*}_{S2}(Q_1)\tilde{E}^{(x)}_{S2}(Q_2)\right\rangle & \left\langle \tilde{E}^{(y)*}_{S1}(Q_1)\tilde{E}^{(y)}_{S2}(Q_2)+\tilde{E}^{(y)*}_{S2}(Q_1)\tilde{E}^{(y)}_{S2}(Q_2)\right\rangle\end{bmatrix} \tag{6-32}$$

Because the two sources S1 and S2 are independent with each other, Thus $\tilde{W}_{xy}(Q_1,Q_2) \neq \tilde{W}_{yx}^{*}(Q_1,Q_2)$. In this case, we have to calculate all of the elements in the BCP matrix for a completely description.

6.5 Summary

In this chapter, we re-examine the van Cittert-Zernike theorem for electromagnetic field. Same to the scalar van Cittert-Zernike theorem, each component in the mutual intensity matrix of the electromagnetic field from a spatially incoherent source is equal to the Fourier transform of corresponding intensity component of the source. And then, we have presented optical system for measuring the mutual intensity matrix. The experiment results show that the light emerges from a completely incoherent source becomes partially coherent on propagation, whereas the degree of polarization of the electromagnetic beam doesn't change during the propagation.

References

[1] P. H. van Cittert, "Die Wahrscheinliche Schwingungsverteilung in Einer von Einer Lichtquelle Direkt Oder Mittels Einer Linse Beleuchteten Ebene," Physica 1, 201-210 (1934).

[2] F. Zernike, "The concept of degree of coherence and its application to optical problems," Physica 5, 785-795 (1938).

[3] M. Born and E. Wolf, *Principles of Optics*, 6th edition (Cambridge University 1980).

[4] J. W. Goodman, *Introduction to Fourier Optics*, 3rd edition (Roberts and Company Publishers, 2005).

[5] E. Wolf, "Unified theory of coherence and polarization of random electromagnetic beams," Phys. Lett. A 312, 263-267 (2003).

[6] E. Wolf, *Introduction to the Theory of Coherence and Polarization of Light*, 1st edition (Cambridge University Press 2007).

[7] E. Wolf, "Polarization invariance in beam propagation," Opt. Lett. 32, 3400-3401 (2007).

[8] M. J. Beran and G. B. Parrent, Jr., *Theory of Partial Coherence*, 2nd edition (Prentice Hall, Inc., 1964).

[9] T. Shirai, E. Wolf, "Coherence and polarization of electromagnetic beams modulated by random phase screens and their changes on propagation in free space," J. Opt. Soc. A 21, 1907-1915 (2004).

[10] E. Wolf, "Correlation-induced changes in the degree of polarization, the degree of coherence, and the spectrum of random electromagnetic beams on propagation," Opt. Lett. 28, 1078-1080 (2003).

[11] Korottkova and E. Wolf, "Changes in the stated of polarization of a random electromagnetic beam on propagation," Opt. Commun 246, 35-43 (2005).

[12] T. Shirai, "Some consequences of the van Cittert-Zernike theorem for partially polarized stochastic electromagnetic fields," Opt. Lett. 34, 3761-3763 (2009).

[13] S. Ostrovsky, G. Martinez-Niconoff, Patricia Martinez-Vara and M. Olvera-Santanaria, "The van Cittert-Zernike theorem for electromagnetic fields," Opt. Express 17, 1746-1752 (2009).

[14] J. Tervo, T. Setala, J. Turunen and A. Friberg, "Van Cittert-Zernike theorem with Stokes parameters," Opt. Lett. 38, 2301-2303 (2013).

[15] F. Gori, M. Santarsiero, S. Vicalvi, R. Borghi and G. Guattari, "Beam coherence-polarization matrix," J. Eur. Opt. Soc. A Pure Appl. Opt. 7, 941-951 (1998).

[16] F. Gori, M. Santarsiero, R. Borghi and G. Piquero, "Use of the van Cittert-Zernike theorem for partially polarized sources," Opt. Lett. 25, 1291-1293 (2000).

[17] M. Takeda, H. Ina, and S. Kobayashi, "Fourier-transform method of fringe-pattern analysis for computer-based topography and interferometry," J. Opt. Soc. Am. 72, 156-160 (1982).

Chapter 7

Experimental Study on Beam Coherence-Polarization Matrix and Generalized Stokes Parameters for Random Electromagnetic Fields

With the help of a radial shearing interferometer in combination with polarizers, an experimental method has been proposed to determine the beam coherence-polarization matrix and the generalized Stokes parameters for random electromagnetic fields. The correlation-induced changes in stochastic electromagnetic beams on propagation are experimentally investigated by using the proposed interferometric system to provide important manifestation of the random fluctuations of optical fields for the first time.

7.1 Introduction

All optical fields undergo random fluctuations. The unified theory of coherence and polarization of random electromagnetic beams provides an elegant description about the changes in the state of polarization of a partially coherent electromagnetic beam on propagation [1-4]. For a quasi-monochromatic stochastic field, the usual treatment is based on a 2×2 beam coherence-polarization matrix (BCP matrix) whose elements have the form of mutual intensities $\tilde{W}(\mathbf{r}_1,\mathbf{r}_2)$ [5,6]. It is well known that the real part of the mutual intensity $\tilde{W}(\mathbf{r}_1,\mathbf{r}_2)$ is simply related to the fringe pattern observed in

Young's double-slit experiment by measurement of the fringe visibility and position for a large number of slit positions and separation [7]. Recently, a determination of the BCP matrix has been realized by using a set of polarizers and rotators in a modified version of Young's interferometer [8]. However, the mutual intensity function can sometimes be difficult to evaluate, so direct intensity measurements are preferred [9-11]. In the recent past, we offer a direct route to mutual intensity function in which the full-field distribution of the space-shift-variant two-point correlation function $\tilde{W}(\mathbf{r}_1,\mathbf{r}_2)$ can be obtained from a modified radial shearing interferometer. In this chapter, we improve our full-field spatial coherence visualization system for electromagnetic field. In this method, the mutual intensity of each BCP matrix element can be easily reconstructed from just a single image frame. And the generalized Stokes parameters can also be determined from the BCP matrix.

7.2 Definitions

For quasi-monochromatic electromagnetic fields, the BCP matrix is defined as

$$\tilde{W}(\mathbf{r}_1,\mathbf{r}_2)=\begin{bmatrix}\tilde{W}_{xx}(\mathbf{r}_1,\mathbf{r}_2) & \tilde{W}_{xy}(\mathbf{r}_1,\mathbf{r}_2)\\ \tilde{W}_{yx}(\mathbf{r}_1,\mathbf{r}_2) & \tilde{W}_{yy}(\mathbf{r}_1,\mathbf{r}_2)\end{bmatrix}=\begin{bmatrix}\left\langle \tilde{E}_x^{\,*}(\mathbf{r}_1)\tilde{E}_x(\mathbf{r}_2)\right\rangle & \left\langle \tilde{E}_x^{\,*}(\mathbf{r}_1)\tilde{E}_y(\mathbf{r}_2)\right\rangle\\ \left\langle \tilde{E}_y^{\,*}(\mathbf{r}_1)\tilde{E}_x(\mathbf{r}_2)\right\rangle & \left\langle \tilde{E}_y^{\,*}(\mathbf{r}_1)\tilde{E}_y(\mathbf{r}_2)\right\rangle\end{bmatrix}, \tag{7-1}$$

$\tilde{E}_x$ and $\tilde{E}_y$ are the components of the complex electric field vector in the x and y direction, respectively. (x_1,y_1,z_1) and (x_2,y_2,z_2) denote two different points Q_1 and Q_2, respectively. The asterisk denotes the complex conjugate, and the angular brackets indicate a time average.

The generalized Stokes parameters depend on the correlation of two spatial points. They are defined as

$$\tilde{S}_0(\mathbf{r}_1,\mathbf{r}_2)=\tilde{W}_{xx}(\mathbf{r}_1,\mathbf{r}_2)+\tilde{W}_{yy}(\mathbf{r}_1,\mathbf{r}_2), \tag{7-2a}$$

$$\tilde{S}_1(\mathbf{r}_1,\mathbf{r}_2)=\tilde{W}_{xx}(\mathbf{r}_1,\mathbf{r}_2)-\tilde{W}_{yy}(\mathbf{r}_1,\mathbf{r}_2), \tag{7-2b}$$

$$\tilde{S}_2(\mathbf{r}_1,\mathbf{r}_2)=\tilde{W}_{xy}(\mathbf{r}_1,\mathbf{r}_2)+\tilde{W}_{yx}(\mathbf{r}_1,\mathbf{r}_2), \tag{7-2c}$$

$$\tilde{S}_3(\mathbf{r}_1,\mathbf{r}_2) = i[\tilde{W}_{yx}(\mathbf{r}_1,\mathbf{r}_2) - \tilde{W}_{xy}(\mathbf{r}_1,\mathbf{r}_2)]. \tag{7-2d}$$

According to the spectral interference law [1,2] for random electromagnetic beams, the correlation function could be measured from the superposition of wave $\tilde{E}(x_1, y_1, z_1)$ and wave $\tilde{E}(x_2, y_2, z_2)$. For this reason we offer a spatial coherence visualization system based on interference technique.

7.3 Experiment

Our proposed 3-D mutual intensity measurement system is a simple combination of radius shearing interferometer and Michelson interferometer. The radius shearing interferometer, which introduces radially symmetric shear by interfering the wavefront with an expanded copy of itself, is an efficient instrument for lateral correlation measurement. The Michelson interferometer is a well-known instrument for longitudinal correlation measurement, e.g. Fourier spectroscopy.

The experiment setup is shown in Fig. 7-1. The incident light beam is split by Non-polarizing beam splitter BS_1 into two parts: the transmitted light beam, which will be called as beam *A*, have a Keplerian telescope (lens L_2 and L_3) with magnification ratio $f_3/f_2 = 1$; the reflected beam, which will be called as beam *B*, have a Keplerian telescope (lens L_2 and L_4) with magnification ratio $f_4/f_2 = 1.25$. Let polarizer P_1 and P_2 be chosen to transmit only x component and only y component of the incident beam, respectively. And let density filter DF be chosen to balance the intensities of the beam *A* and beam *B*. thus when the two beams recombine at the second beam splitter BS_2, a radial shear is introduces because of the different magnifications. Here the BS_2 is also the core device of the Michelson interferometer. A longitudinal motion of the movable Mirror M_3 produces an axial path difference Δz. The third polarizer P_3, which have a linear polarization at 45 °, helps to observe the interference fringes generated from the components $\tilde{E}_x$ and $\tilde{E}_y$. Finally, the interference of the two beams *A* and *B* occurs at CCD plane. The interferogram *I* obtained over the CCD plane might be a function of three parameters $(x, y, \Delta z)$. For consistent notation, the

corresponding mutual intensity function $\tilde{W}(x_1, x_2; y_1, y_2; z_1, z_2)$ may be replaced by $\tilde{W}(x, y, \Delta z)$ without confusion. By changing the directions of the polarizers P_1 and P_2, all the elements in the BCP matrix can be detected from our interferometer.

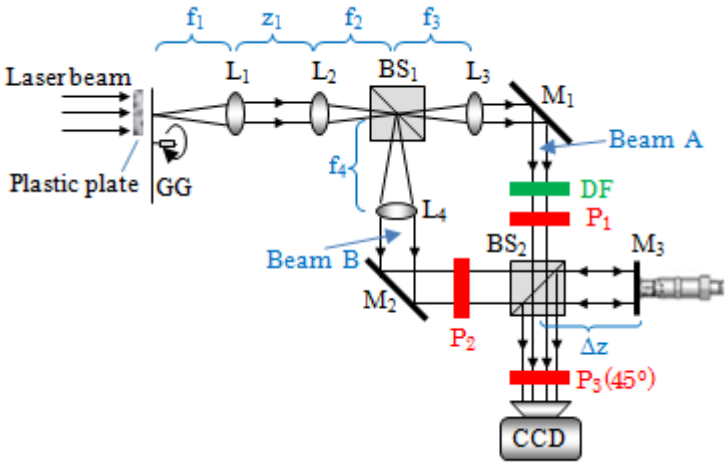

Figure 7-1 Schematic representation of the experimental setup for the full-field measurement of the BCP matrix from a quasi-monochromatic, partially polarized and partially coherent source. GG (ground glass); BS (Non-polarizing beam splitter); DF (density filter); P (linear polarizer); Focal length: f_1=100mm, z_1=100mm, f_2=100mm, f_3=100mm, f_4=125mm.

Figure 7-2 shows the experiment results when the optical path difference is $\Delta z = 5mm$. Figure 7-2(a) and (b) are the recorded interferograms I_{xx} and I_{yy} when the transmission axes of the linear polarizers P_1 and P_2 are both horizontal and vertical, respectively. Figure 7-2(c) is the interferogram I_{xy} recorded when P_1 is horizontal polarization and P_2 is vertical polarization. Oppositely, Fig. 7-2(d) is the interferogram I_{yx} recorded when P_1 is vertical polarization and P_2 is horizontal polarization. It is evident from the figures that the fringe visibility due to xx components is much bigger than the others. The source consists mainly of x polarization.

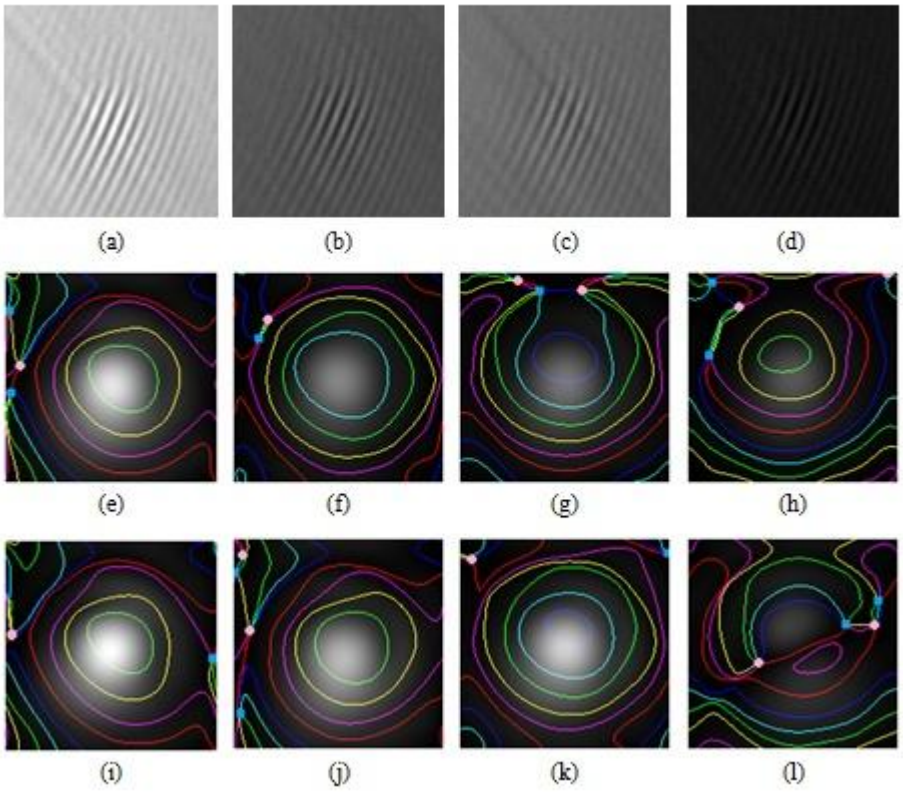

Figure 7-2 Top row: interferograms recorded at $\Delta z = 5mm$: (a) I_{xx}, (b) I_{xy}, (c) I_{yx}, (d) I_{yy}. Middle row: reconstructed mutual intensities with phase contour lines inserted. (e) $\tilde{W}_{xx}$, (f) $\tilde{W}_{xy}$, (g) $\tilde{W}_{yx}$, (h) $\tilde{W}_{yy}$. Bottom row: the generalized Stokes parameters: (i) S_0, (j) S_1, (k) S_2, (l) S_3.

By using Fourier fringes analysis [12], the distribution of the mutual intensity functions are reconstructed. The corresponding elements in BCP matrix have been given in Fig. 7-2(e)-(h): gray-scale pictures represent the amplitude of mutual intensity; color lines represent phase contour lines. It's also interesting to notice that there are many phase singularities exiting in the field marked by square and circular dot.

Using Eq. (7-3), the generalized Stokes parameters could be obtained from the elements of the BCP matrix. Fig. 7-2(i)-(l) show the amplitude of generalized Stokes parameters S_0, S_1, S_2 and S_3, respectively, with the phase contour lines inserted. It should be notice that the usual Stokes parameters (single point Stokes parameters) are

real functions which are calculated from light intensities. The generalized Stokes parameters are determined from the correlations of two points. They are complex functions which are form by complex mutual intensity functions. The two points Stokes parameter is not exactly calculated by algebraic addition of single point Stokes parameters, it's also modulated by the complex spatial coherence function of the two points. As seen in Fig. 7-2(i)-(l), all of the generalized Stokes parameters are complex functions.

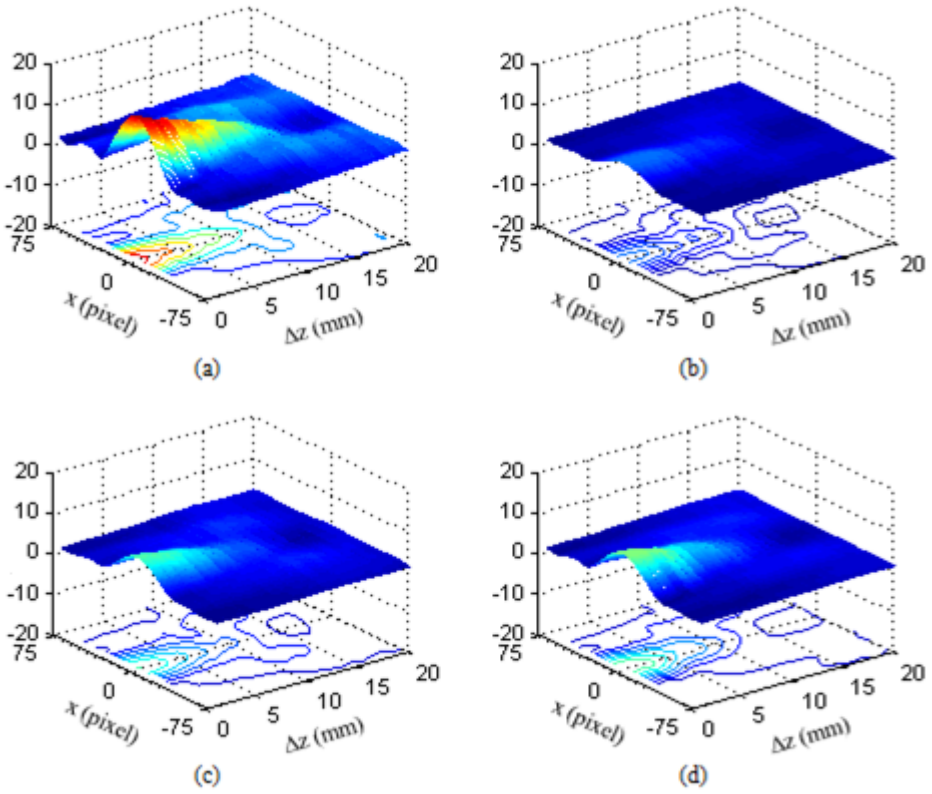

Figure 7-3 The 3-D distributions of the BCP matrix for electromagnetic field. (a)$\tilde{W}_{xx}$, (b)$\tilde{W}_{xy}$, (c)$\tilde{W}_{yx}$, (d)$\tilde{W}_{yy}$.

By changing the optical path differences, we are able to study the evolution of mutual intensity functions on propagation. The 3-D distributions for the mutual intensities in BCP matrix are showed in Fig. 7-3, which provide a full-field observation of propagation of BCP matrix.

From the reconstructed BCP matrix, the generalized Stokes parameters can also be obtained. The 3-D distributions of the generalized Stokes parameters for the electromagnetic field from a quasi-monochromatic partially polarized and partially coherent source is shown in Fig. 7-4.

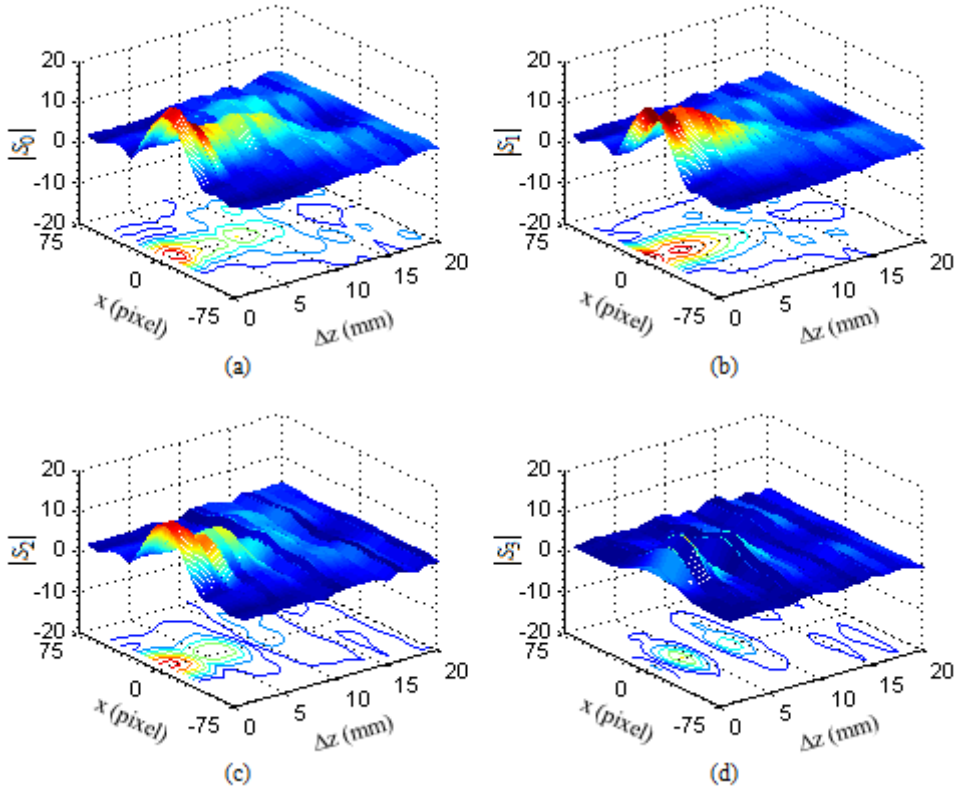

Figure 7-4 The generalized Stokes parameters for electromagnetic field.

It has been shown that the spatial and polarized information of electromagnetic field can efficiently be recorded in an interferogram and later be retrieved by a simple Fourier transformation. The interferogram literally comprises a frame of the 3-D spatial coherence function. By recording interferograms at different optical path differences, we can rebuild the 3-D distribution of the spatial coherence function. And then we are able to calculate the full-field BCP matrix and the full-field generalized Stokes parameters.

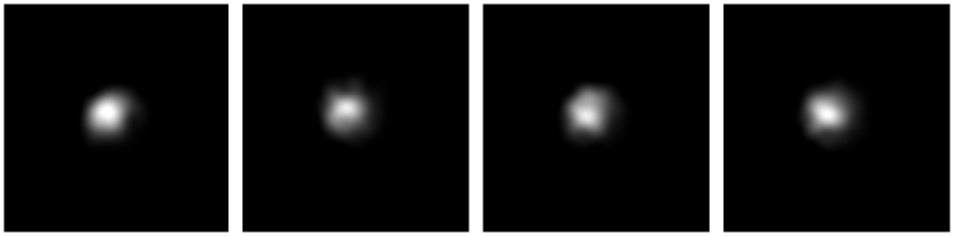

(a) (b) (c) (d)

Figure 7-5 The distributions of the reconstructed Jones matrix for the incoherent polarization source: (a) $J_{xx}^{(0)}$, (b) $J_{xy}^{(0)}$, (c) $J_{yx}^{(0)}$, (d) $J_{yy}^{(0)}$.

From the reconstructed mutual intensities, the Jones matrix $J^{(0)}$ can be obtained through an inverse Fourier transform based on the vectorial van Cittert-Zernike theorem. The polarization states of the incoherent source are given in Fig. 7-5.

7.4 Summary

In this chapter, we have demonstrated an interferometric technique for characterizing the mutual intensity function of partially polarized, partially coherent optical beams. The beam coherence-polarization matrix and the generalized stokes parameters of random electromagnetic fields have been determined experimentally. The proposed optical techniques offer a direct route for tensor coherence visualization and introduce new opportunities to explore other interesting phenomena in polarization and coherence of statistical optical fields.

References

[1] E. Wolf, "Unified theory of coherence and polarization of random electromagnetic beams," Phys. Lett. A 312, 263-267 (2003).

[2] E. Wolf, *Introduction to the Theory of Coherence and Polarization of Light*, 1st edition (Cambridge University Press, 2007).

[3] E. Wolf, "Polarization invariance in beam propagation," Opt. Lett. 32, 3400-3401 (2007).

[4] O. Korottkova and E. Wolf, "Changes in the stated of polarization of a random electromagnetic beam on propagation," Opt. Commun. 246, 35-43 (2005).

[5] F. Gori, M. Santarsiero, S. Vicalvi, R. Borghi and G. Guattari, "Beam coherence-polarization matrix," J. Eur. Opt. Soc. A Pure Appl. Opt. 7, 941-951 (1998).

[6] F. Gori, M. Santarsiero, R. Borghi and G. Piquero, "Use of the van Cittert-Zernike theorem for partially polarized sources," Opt. Lett. 25, 1291-1293 (2000).

[7] M. Born and E. Wolf, *Principles of Optics*, 6th edition, (Cambridge University 1980).

[8] B. Kanseri and H. C. Kandpal, "Experimental determination of electric cross-spectral density matrix and generalized Stokes parameters for a laser beam," Opt. Lett. 33, 2410-2412 (2008).

[9] C. Iaconis and I. A. Walmsley, "Direct measurement of the two-point field correlation function," Opt. Lett. 21, 1783-1785 (1996).

[10] D. Mendlovic, G. Shabtay and A. W. Lohmann, "Synthesis of spatial coherence," Opt. Lett. 24, 361-363 (1999).

[11] M. V. R. K. Murty, "A Compact Radial Shearing Interferometer Based on the Law of Refraction," Appl. Opt. 3, 853-857 (1964)

[12] M. Takeda, H. Ina and S. Kobayashi, "Fourier-transform method of fringe-pattern analysis for computer-based topography and interferometry," J. Opt. Soc. Am. 72, 156-160 (1982).

Chapter 8

Coherence tensor Holography

8.1 Introduction

Coherence Holography (CH) is an unconventional holography technique, where a computer generated hologram (CGH) is illuminated by spatially incoherent light and the recorded object is reconstructed by the 3-D distribution of a spatial coherence function [1-5]. The principle of coherence holography is based on the formal analogy between the diffraction integral and the formula of van Cittert-Zernike theorem [6-8]. Over the past few decades, the van Cittert-Zernike theorem has been extended to the vector field successfully [9-15]. The vectorial van Cittert-Zernike theorem prepared the ground for Vectorial Coherence Holography (V-CH) [16, 17] or Coherence Tensor Holography (CTH). In this chapter, we propose and experimentally demonstrate a compact optical system which extends coherence holography technique to vector field. We use two separate computer-generated holograms with different polarization states and reconstruct mutual intensity matrix at detector plane.

8.2 Principle

The principle of scalar coherence holography has been introduced in chapter 5. For convenience of explanation, I will continue following the same variables and expressions used in chapter 5.

In the vector field, we use two separate holograms, each of which is assigned to one of the orthogonal polarization components of the vector fields.

$$H_m = \tilde{O}_m \cdot \tilde{R}_m^{\ *} + \tilde{O}_m^{\ *} \cdot \tilde{R}_m + C_m \qquad (\text{Subscript}: m = x, y)\,. \tag{8-1}$$

Where $\tilde{O}_m$ is the m-component of the frequency spectrum of object $\tilde{o} = |\tilde{o}| \exp(i\phi)$

$$\tilde{O}(f_x, f_y) = FT\{\tilde{o}(x, y)\}\,. \tag{8-2}$$

According to the vectorial van Cittert-Zernike theorem we studied in Chapter 6. For the whole field of the beam, the mutual intensity matrix of the electromagnetic field from an incoherent monochromatic source is equal to the Fourier transforms of the Jones matrix of the source:

$$\begin{aligned}\tilde{W}^{(z)}(x_1, x_2; y_1, y_2; z) = \frac{1}{(\lambda z)^2} \exp\{j\frac{\pi}{\lambda z}[({x_2}^2 - {x_1}^2) + ({y_2}^2 - {y_1}^2)]\} \\ \iint_{\Sigma^{(0)}} \tilde{J}^{(0)} \exp\{j\frac{2\pi}{\lambda z}[x_0(x_1 - x_2) + y_0(y_1 - y_2)]\} dx_0 dy_0\end{aligned}\,. \tag{8-3}$$

We rewrite Eq.(8-3) as Eq.(8-4) for short,

$$\tilde{W}^{(z)} = FT\{\tilde{J}^{(0)}\}\,. \tag{8-4}$$

Consider that the reference beam has a plane wave front with an incident angle (θ, φ), the optical field of the reference beam can be written as

$$\tilde{R}(f_x, f_y) = \exp(-if_x\theta - if_y\varphi). \tag{8-5}$$

If we illuminate the holograms $\tilde{H}(f_x, f_y)$ with a random electromagnetic beam which has a planar wavefront 1, so the Jones matrix on the source field is given by

$$\tilde{J}^{(0)} = \begin{bmatrix} H_x & H_x + H_y \\ H_x + H_y & H_x \end{bmatrix}, \tag{8-6}$$

By substituting Eqs. (8-1), (8-2) and (8-5) into Eq. (8-4), we find

$$\tilde{W}_{xx}^{(z)} = o_x * \delta(\xi + \frac{\theta_x}{2\pi}, \xi + \frac{\varphi_x}{2\pi}) + o_x^* * \delta(\xi - \frac{\theta_x}{2\pi}, \xi - \frac{\varphi_x}{2\pi}) + C_x', \tag{8-7a}$$

$$\begin{aligned} \tilde{W}_{xy}^{(z)} = {} & o_x * \delta(\xi + \frac{\theta_x}{2\pi}, \xi + \frac{\varphi_x}{2\pi}) + o_x^* * \delta(\xi - \frac{\theta_x}{2\pi}, \xi - \frac{\varphi_x}{2\pi}) \\ & + o_y * \delta(\xi + \frac{\theta_y}{2\pi}, \xi + \frac{\varphi_y}{2\pi}) + o_y^* * \delta(\xi - \frac{\theta_y}{2\pi}, \xi - \frac{\varphi_y}{2\pi}) + C_{xy}' \end{aligned}, \tag{8-7b}$$

$$\begin{aligned} \tilde{W}_{yx}^{(z)} = {} & o_x * \delta(\xi + \frac{\theta_x}{2\pi}, \xi + \frac{\varphi_x}{2\pi}) + o_x^* * \delta(\xi - \frac{\theta_x}{2\pi}, \xi - \frac{\varphi_x}{2\pi}) \\ & + o_y * \delta(\xi + \frac{\theta_y}{2\pi}, \xi + \frac{\varphi_y}{2\pi}) + o_y^* * \delta(\xi - \frac{\theta_y}{2\pi}, \xi - \frac{\varphi_y}{2\pi}) + C_{yx}' \end{aligned}, \tag{8-7c}$$

$$\tilde{W}_{yy}^{(z)} = o_y * \delta(\xi + \frac{\theta_y}{2\pi}, \xi + \frac{\varphi_y}{2\pi}) + o_y^* * \delta(\xi - \frac{\theta_y}{2\pi}, \xi - \frac{\varphi_y}{2\pi}) + C_{yy}'. \tag{8-7d}$$

Diagonal elements of the beam coherence-polarization matrix ($\tilde{W}_{xx}$ and $\tilde{W}_{yy}$) can be regarded as self-correlation of polarization components, which are same as scalar coherence holography. Off-diagonal elements of the beam coherence-polarization matrix ($\tilde{W}_{xy}$ and $\tilde{W}_{yx}$) can be regarded as an addition of two scalar coherence holography.

8.3 Experiment

The two coherence holograms we used in our experiment are shown in Fig. 8-1. Left one is a 2D hologram generated from 2D letter ‘H’ (see Fig. 5-4); right one is a 3D hologram generated from 3D letter ‘V’ (see Fig. 5-5).

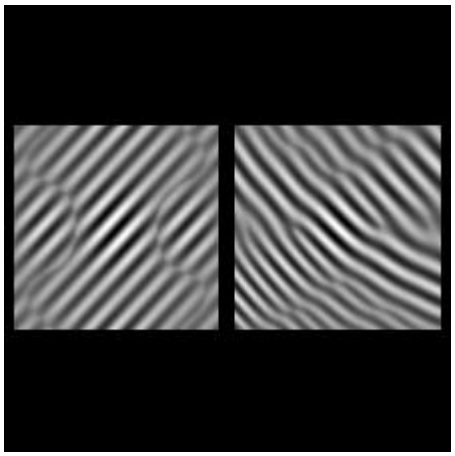

Figure 8-1 Holograms used in experiment, Left is a 2D hologram generated by binary object Letter 'H', called as Hologram H; Right is a 3D hologram generated by binary object Letter 'V' with a depth phase, called as Hologram V.

The experimental setup is shown in Fig. 8-2. Our system is functionally divided into two parts. Before the rotating ground glass (GG) is a triangular sagnac geometry is used to display two orthogonal polarization components onto the ground glass. Two computer-generated holograms are firstly loaded by a spatial light modulator (SLM), secondly filtered by a low-pass 4-F system (L2 and L3) and finally projected onto the ground glass. The polarizer P_1 has a linear polarization at 45 °. After the aperture AP_2, we have a hologram H at horizontal polarization and a hologram V at vertical polarization on the ground glass. After ground glass is a beam coherence-polarization matrix visualization system which has been introduced in Chapter 6 and 7. Let polarizer P_1 and P_2 be chosen to transmit only x component and only y component of the incident beam, respectively. A longitudinal motion of the movable Mirror M_4 produces an axial path difference. The polarizer P_4, which have a linear polarization at 45 °, helps to observe the interference fringes generated from the x component and y component.

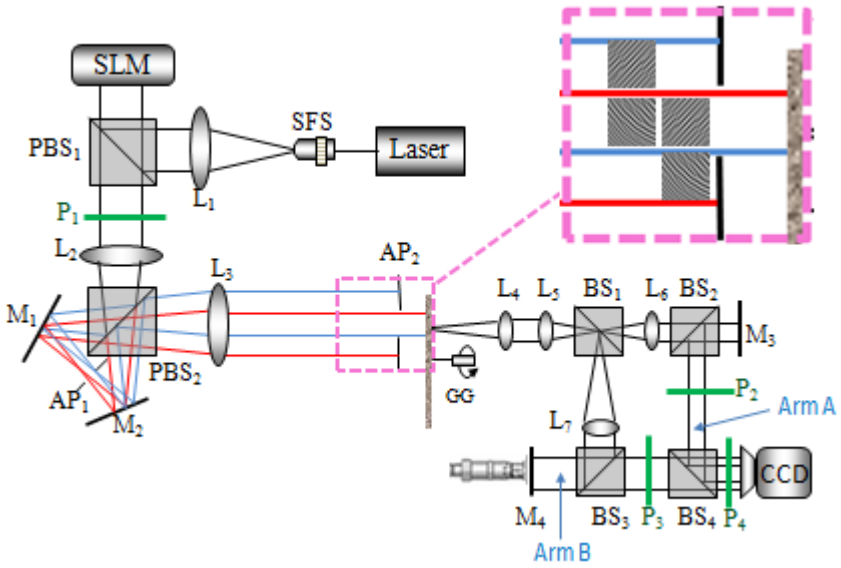

Figure 8-2 Experimental setup for coherence tensor holography. Triangular sagnac geometry used to display two orthogonal polarization components on the ground glass. And the radius shearing Mach-Zehnder interferometer is a 3-D spatial coherence visualization system. [Appendix B]

The experimental result is shown in Fig. 8-3(a) and (e) are related to $\tilde{W}_{xx}$. Because the hologram H is a 2D hologram, so its real image can be reconstructed at the location where $Z=0$. (a) has an identical structure to the Letter 'H' in the format of the fringe contrast. (d) and (h) are related to $\tilde{W}_{yy}$. Because the hologram V is a 3D hologram, so it's real image can be reconstructed at the location Fresnel phase factor stemming from SOPD and the quadratic phase factor stemming from object could be cancelled out. (h) has an identical structure to the Letter 'V'. (b) and (f) are related to $\tilde{W}_{xy}$; (c) and (g) are related to $\tilde{W}_{xy}$. These 2 groups of mutual intensity function show a clearly addition of x component and y component.

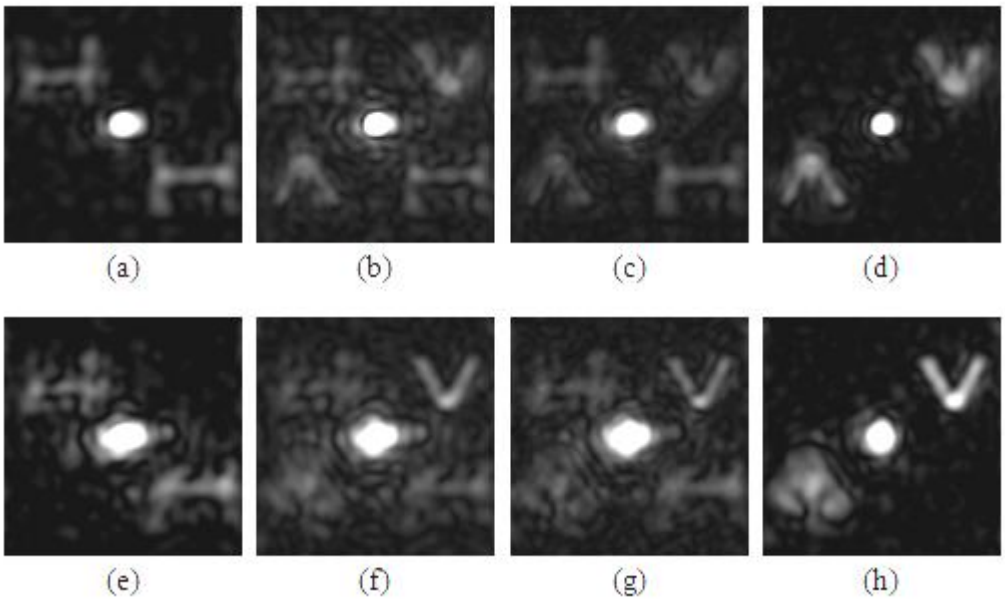

Figure 8-3 Reconstructed images [18] in coherence tensor holography. Top row: (a) the modulus of 4 elements in beam coherence-polarization matrix recorded at coherence focal plane, (a) $\tilde{W}_{xx}$; (b) $\tilde{W}_{xy}$; (c) $\tilde{W}_{yx}$; (d) $\tilde{W}_{yy}$. Bottom row: (b) the modulus of 4 elements in beam coherence-polarization matrix recorded at the location $Z = 1cm$, (e) $\tilde{W}_{xx}$; (f) $\tilde{W}_{xy}$; (g) $\tilde{W}_{yx}$; (h) $\tilde{W}_{yy}$.

8.4 Summary

We have extended coherence holography technique into vector domain. And the four elements in the beam coherence-polarization matrix are reconstructed. The experiment results show a high sensitivity both in polarization parameters and position parameters.

Reference

[1] M. Takeda, W. Wang, Z. Duan and Y. Miyamoto, "Coherence Holography," Opt. Express 23, 9629-9635 (2005)

[2] D. N. Naik, T. Ezawa, Y. Miyamoto and M. Takeda, “Phase-shift coherence holography,” Opt. Lett. 35(10), 1728–1730 (2010).

[3] D. N. Naik, T. Ezawa, Y. Miyamoto and M. Takeda, "3-D coherence holography using a modified Sagnac radial shearing interferometer with geometric phase shift," Opt. Express 17(13), 10633–10641 (2009).

[4] D. N. Naik, T. Ezawa, R. K. Singh, Y. Miyamoto and M. Takeda, "Coherence holography by achromatic 3-D field correlation of generic thermal light with an imaging Sagnac shearing interferometer," Opt. Express 20(18), 19658–19669 (2012).

[5] D. N. Naik, G. Pedrini and W. Osten, "Recording of incoherent-object hologram as complex spatial coherence function using Sagnac radial shearing interferometer and a Pockels cell," Opt. Express 21, 3990-3995 (2013)

[6] M. Born and E. Wolf, *Principles of Optics*, 6th edition (Cambridge University 1980).

[7] P. H. van Cittert, "Die Wahrscheinliche Schwingungsverteilung in Einer von Einer Lichtquelle Direkt Oder Mittels Einer Linse Beleuchteten Ebene," Physica, 1, 201-210 (1934).

[8] F. Zernike, "The concept of degree of coherence and its application to optical problems," Physica, 5, 785-795 (1938).

[9] E. Wolf, "Unified theory of coherence and polarization of random electromagnetic beams," Phys. Lett. A 312, 263-267 (2003).

[10] O. Korottkova and E. Wolf, "Changes in the stated of polarization of a random electromagnetic beam on propagation," Opt. Commun 246, 35-43 (2005).

[11] T. Shirai, "Some consequences of the van Cittert-Zernike theorem for partially polarized stochastic electromagnetic fields," Opt. Lett. 34, 3761-3763 (2009).

[12] S. Ostrovsky, G. Martinez-Niconoff, Patricia Martinez-Vara and M. Olvera-Santanaria, “The van Cittert-Zernike theorem for electromagnetic fields,” Opt. Express 17, 1746-1752 (2009).

[13] J. Tervo, T. Setala, J. Turunen and A. Friberg, “Van Cittert-Zernike theorem with Stokes parameters,” Opt. Lett. 38, 2301-2303 (2013).

[14] F. Gori, M. Santarsiero, S. Vicalvi, R. Borghi and G. Guattari, “Beam coherence-polarization matrix,” J. Eur. Opt. Soc. A Pure Appl. Opt. 7, 941-951 (1998).

[15] F. Gori, M. Santarsiero, R. Borghi and G. Piquero, “Use of the van Cittert-Zernike theorem for partially polarized sources,” Opt. Lett. 25, 1291-1293 (2000).

[16] R. K. Singh, D. N. Naik, H. Itou, Y. Miyamoto and M. Takeda, "Vectorial coherence holography," Opt. Express 19, 11558-11567 (2011)

[17] R. K. Singh, D. N. Naik, H. Itou, Y. Miyamoto and M. Takeda, "Stokes holography," Opt. Lett.37, 966-968 (2012)

[18] M. Takeda, H. Ina and S. Kobayashi, “Fourier-transform method of fringe-pattern analysis for computer-based topography and interferometry,” J. Opt. Soc. Am., 72, 156-160 (1982)

Chapter 9

Conclusions and future works

9.1 Conclusions

The most important contribution in this thesis is to offer a full-field spatial coherence measurement, where the interference fringes corresponding to the real part of the mutual intensity of a completely incoherent source can be directly recorded and from which the coherence function itself can be recovered computationally. That is, the full coherence function can be recorded in one go. Furthermore, the optical set-up makes it possible to consider the coherence function not only between points in one z-plane but also between points from two different planes, thereby effectively making it possible to record the full three-dimensional coherence function. This set-up and result is of course of great interest for situations where the coherence functions of completely incoherent sources needs to be determined experimentally. The results are useful for theoretical works.

Based on this technology, we carried out a lot of theoretical studies, such as coherence diffraction, resolutions for coherence imaging, coherence interference, experimental demonstrations for the van Cittert-Zernike theorem, coherence holography, etc. The experimental results are presented in Chapter 2, 3, 4 and 5.

In the next, we extended our knowledge into vector domain. In the vector case, we use the beam coherence-polarization matrix and generalized Stokes parameters to define the correlations of partially coherent partially polarized field. To achieve this aim, we modified the experimental setup, and re-exam the vectorial van Cittert-Zernike theorem in chapter 6. With the help of a radial shearing interferometer in combination with polarizers, the beam coherence-polarization matrix and the generalized Stokes parameters for random electromagnetic fields can be determined from a 4-step measurement. The experimental results are presented in Chapter 7. Similar to scalar case, the main purpose of studying coherence function is to describe the characteristics of sources. In Chapter 8, we extend the scalar coherence holographic technology, and introduce a tensor manner for coherence holography.

9.2 Future works

This thesis addresses several topics in the theory of stochastic optical fields. Some of the works described in this thesis indicate new research directions which the author wishes to investigate in the future.

9.2.1 Optical spatial coherence tomography

Optical coherence tomography (OCT) is a non-invasive imaging test that uses light waves to take cross-section images of optical scattering media [1]. The principle of OCT is low temporal coherence interferometry. The optical setup typically consists of a broad bandwidth light source. Depending on the small coherence length of the light source, optical coherence tomography has achieved sub-micrometer resolution.

Coherence properties of light can be used to determine structures of objects, whether it is temporal coherence or spatial coherence. In chapter 2, we have discussed the diffraction of the spatial coherence function. And the coherence volume from a spatially incoherent light source has also been given. From the experimental results we can conclude that a series of dark and bright fringes is only achieved when the path difference lies within the coherence length. That means our spatial coherence

visualization system can also provide a coherence gate which can be used in tomography. If we letting a low spatial coherence wave to interact with an object and then measuring the coherence properties of the scattered light, we will get the cross-section images of object. Some related work has been studied, such as Optical Vortex Metrology [2,3] and Fresnel Incoherent Correlation Holography [4-7].

9.2.2 Real-time coherence holography

In this thesis, we introduce the synthesis and analysis of a spatial coherence function based on coherence holography. The experimental results presented in the thesis are recorded by a prototype system. The author wishes to enhance resolution and make a real-time system in the future.

Reference

[1] D. Huang, E. A. Swanson, C. P. Lin, J. S. Schuman, W. G. Stinson, W. Chang, M. R. Hee, T. Flotte, K. Gregory, C. A. Puliafito and J. G. Fujimoto. “Optical coherence tomography, “ Science, 254, 1178–1181(1991).

[2] W. Wang, S. G. Hanson, Y. Miyamoto and M. Takeda, “Experimental Investigation of Local Properties and Statistics of Optical Vortices in Random Wave Fields,” Phys. Rev. Lett. 94, 103902 (2005)

[3] W. Wang, T. Yokozeki, R. Ishijima, A. Wada Y. Miyamoto, M. Takeda, and S. G. Hanson, "Optical vortex metrology for nanometric speckle displacement measurement," Opt. Express 14, 120-127 (2006)

[4] J. Rosen and G. Brooker. “Digital spatially incoherent Fresnel holography,” Opt. Lett. 32, 912–914 (2007).

[5] J. Rosen and G. Brooker. “Fluorescence incoherent color holography,” Opt. Express. 15, 2244–2250 (2007).

[6] J. Rosen and G. Brooker. “Non-scanning motionless fluorescence three-dimensional holographic microscopy,” Nature Photonics 2, 190 - 195 (2008).

[7] G. Brooker, N. Siegel, V. Wang and J. Rosen, “Optimal resolution in Fresnel incoherent correlation holographic fluorescence microscopy,” Opt. Express19 (6), 5047–5062 (2011).

Appendix A

Matlab code for computer generated Fourier transform hologram

```
clc;
clear;
close all;
%-------load object-------%
ob=imread('Psi.bmp');
ob=double(ob);
figure(1)
imshow(ob,[]);
%---------- carrier fx fy -------------%
ang_x=10; % degree
ang_y=10; % degree
for x=1:1000
   for y=1:1000
      C(x,y)=exp(i*x*ang_x*pi/180+i*y*ang_y*pi/180);
   end
end
figure(2);
imshow(C)
% ---------- Computer Generated Hologram  -----------------%
```

```
Object=zeros(1000,1000);
Object(476:1:525,476:1:525)=ob(:,:);
Object_ft=fftshift(fft2(Object));
%-------   complex number Object_ft=R*exp(i*Theta)   ----------%
%---------    Modulus of complex number     R     ----------%
%--------  Argument of a complex number  Theta   ----------%
R=abs(Object_ft);
figure(3)
imshow(abs(R),[])
Theta=angle(Object_ft);  %%% -pi(-3.14)::pi(3.14) %%%
Holo=real(R.*exp(i*Theta).*C)+20;
figure(4)
imshow(Holo,[])
imwrite(Holo/max(max(Holo)),'holo.bmp')
```

Appendix B

Photographs of a coherence tensor holography setup

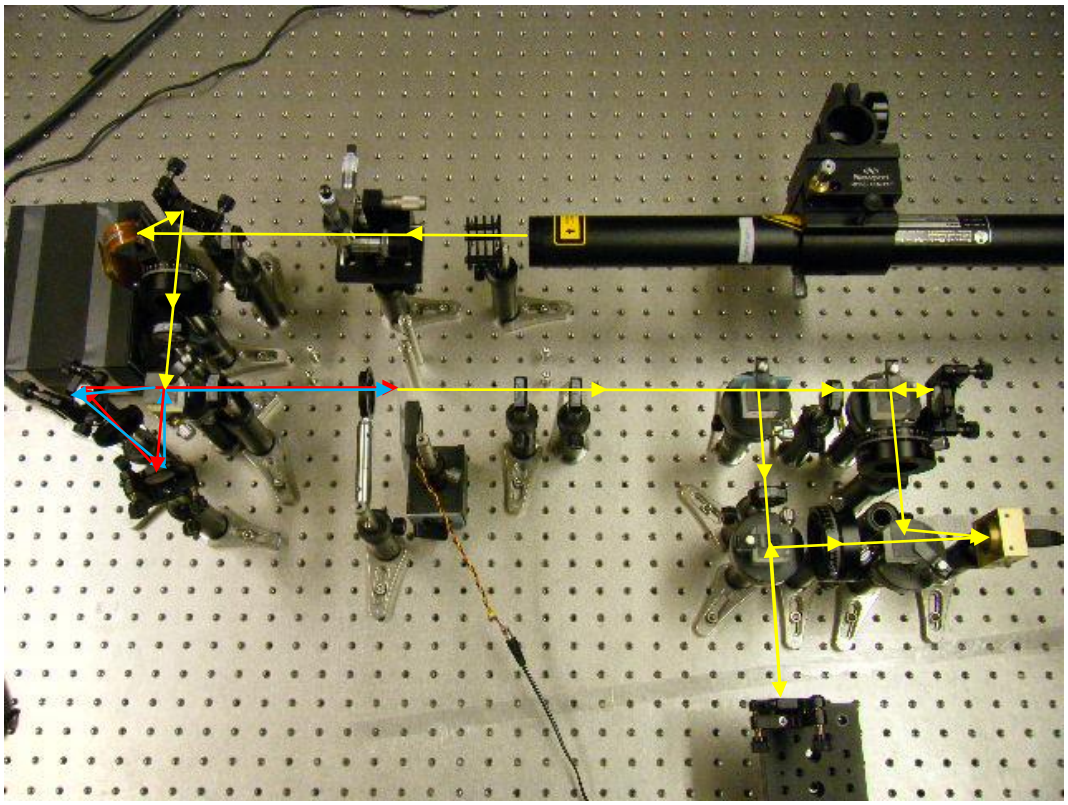

Figure B-1 Photograph of a coherence tensor holography setup.

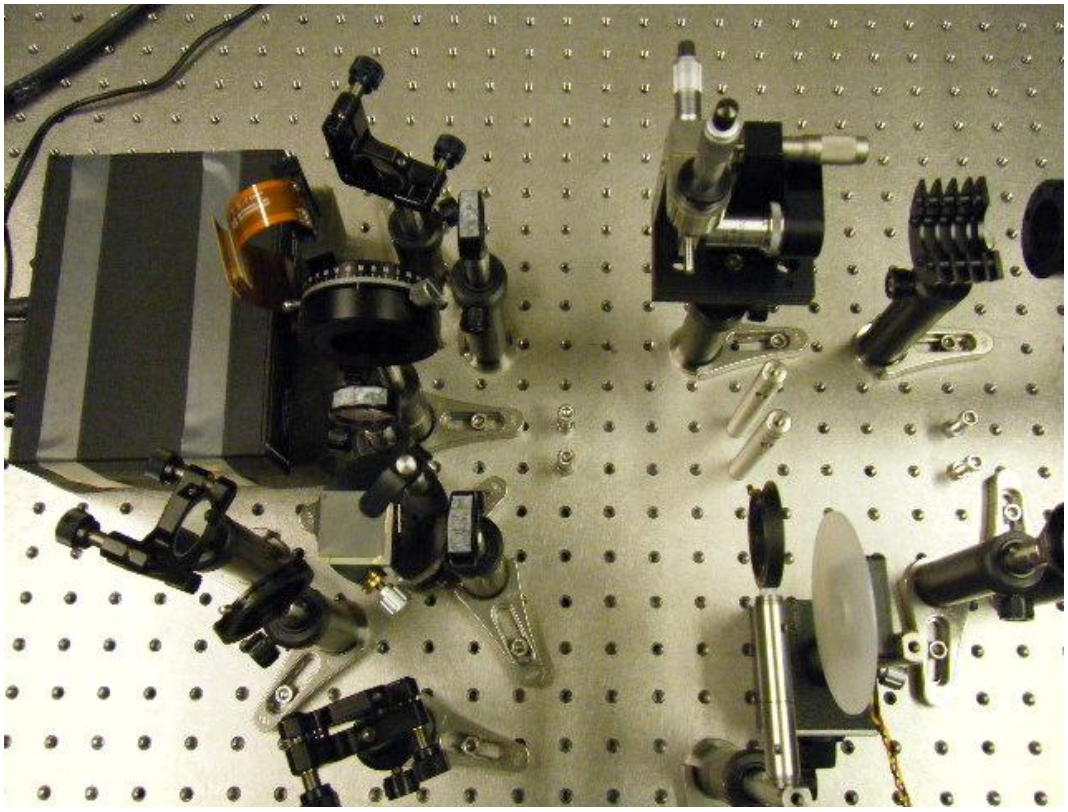

Figure B-2 Photograph of the incoherent hologram generator: triangular Sagnac geometry used to display two orthogonal polarization components on the ground glass.

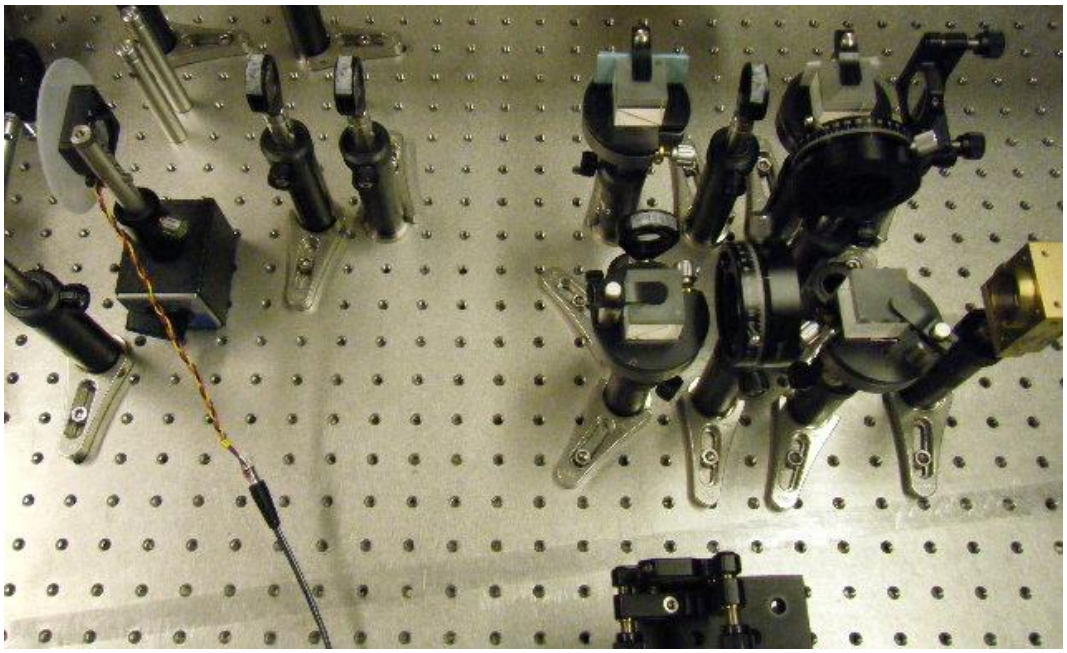

Figure B-3 Photograph of the spatial coherence visualization system.